Steady State Properties of Some Driven Diffusive Systems

Irina Mazilu

Dissertation submitted to the Faculty of the
Virginia Polytechnic Institute and State University
in partial fulfillment of the requirements for the degree of

Doctor of Philosophy
in
Physics

Beate Schmittmann, Chair
Royce K. P. Zia
David A. de Wolf
Tetsuro Mizutani
Brian Dennison

August 30, 2002
Blacksburg, Virginia

Keywords: driven diffusive systems, Monte Carlo simulations, small systems

Steady State Properties of Some Driven Diffusive Systems

Irina Mazilu

(ABSTRACT)

In an attempt to reach a better understanding of the properties and critical behavior of non-equilibrium systems, we investigate the steady state properties of three simple models, variations of the prototype, the driven Ising lattice gas. Our first system studied is the bilayer model, a stack of two driven Ising lattice gases allowed to interact. We study this model using a very simple analytic approximation, the high temperature expansion. Building on existing simulation data and field theory results, our goal is to test how faithfully the series expansion can reproduce the Monte Carlo phase diagram. We find that the agreement between our calculations and the already reported simulations results is remarkably good. Next, we investigate the critical behavior of a two-dimensional Ising lattice gas driven into a non-equilibrium steady state, subject to a local modification of the dynamics, namely, having anisotropic attempt frequencies for exchanges along different spatial directions. We employ both Monte Carlo simulation techniques and a high temperature expansion approximation and find the phase diagram of the system, perform a finite-size scaling study in order to determine the universality class of the model and compare our simulation results with the phase diagram obtained using the high temperature expansion. We conclude that the bias in the jump rates does not affect the universal critical properties of the system: the modified model is in the same universality class as the driven Ising lattice gas. Our last objective concerns a different inroad into the study of non-equilibrium steady states. Instead of investigating a non-equilibrium steady state via indirect observables, such as correlation functions and order parameters, we seek to compute the steady state probability distribution directly. This is feasible only for systems with a small number of degrees of freedom. We chose to study a one-dimensional version of the so-called two-temperature kinetic Ising model. We solve the master equation exactly for a 1×6 system, and compare the full configurational probability distribution with its equilibrium counterpart.

Dedication

To my dear parents, Maria and Gheorghe Maftei, for all their love and patience.

Acknowledgments

At the end of this incredible journey and the beginning of a new adventure, I would like to express my sincere gratitude to some very unique people that helped me reach this place.

This work would have never been completed without the constant help, encouragement and support of my advisor, Prof. Beate Schmittmann. Throughout the years she proved to be not only a great teacher and mentor, but also a very dear friend. What I learned from Dr. Schmittmann was not only high quality physics, but also a far more important lesson in work ethic, high professional standards, and a constant desire for improvement. Her kindness and welcoming attitude provided a great moral support and made things so much easier during my graduate years.

I also want to thank Prof. Royce Zia for teaching me a lesson in scientific curiosity and creativity. I enjoyed immensily the graduate classes taught by him, and I will always keep in mind the refreshing joy for physics and the freedom of thinking that he induced in his students.

My special thanks to Prof. John Ficenec for giving me a chance this summer to teach my first lecture and get a taste of what lies ahead of me. In this context, I want to also thank all the faculty I've been in contact with during these years, and from whom I learned the craft of teaching. A special mention to Amy Emerson, who encouraged me to not be afraid and try new things in the classroom, and also helped me land my first teaching job. Also, a warm thank you to Mr. Larry Bolling for always helping me with the demonstrations with an encouraging smile.

I thank Mrs. Chris Thomas for being such a wonderful help and so supportive during all these years. She showed me constantly that there is always time for being kind, and there is no greater achievement than to help someone in need. This valuable lesson in altruism and kindness will never be forgotten.

My sincere gratitude and appreciation to Prof. Ronald Reese who made me feel so

welcome at Washington&Lee , for all his encouragements and the nice conversations we had in the last couple of months.

I also want to thank my friend Kriton for being such a great moral support during this past year, for all our fun phone conversations and for always cheering me on and encouraging me not to give up. I hope that our friendship will resist the test of time and distance.

And last but not least, I thank my husband Dan for ten wonderful years together, for sharing everything, good and bad, for his constant encouragements and positive attitude, and for giving me the most precious gift of all: unconditional love. I thank him for making me laugh when I felt like crying, for putting up with my busy schedule and for being so wonderful in every respect. I hope that the future will be kind to us and we will share the rest of the adventure with the same joy and love as we did so far.

Contents

List of Figures

Chapter 1

Introduction

The study of systems far from thermal equilibrium is both challenging and rewarding. The reward comes from the fact that the vast majority of real life systems are non-equilibrium ones, so studying them gives us the opportunity to discover some answers, regarding the driving force of physical phenomena. The challenge is obvious. We step outside the comfort of the familiar Gibbs [1] framework for equilibrium systems, so we have to search for new avenues and tools in an effort to find the "Holy Grail" of this whole field, namely, the fundamental understanding and theoretical classification of non-equilibrium behavior.

Statistical mechanics constitutes the discipline which bridges the gap between the microscopic world of molecules, atoms and electrons and the macroscopic world of thermodynamics and the properties of materials. It teaches us how, knowing the quantitative properties of molecular interactions, we can predict the macroscopic behavior of the system. The foundation of equilibrium statistical mechanics rests upon Boltzmann's fundamental hypothesis [2]. If an isolated macroscopic system is ergodic [3], it will reach thermal equilibrium after a sufficiently long time. Then, every configuration (or microstate) available to the system can be found with equal probability. Of course, isolated systems are rather unrealistic, so the next step is to put the system in contact with a very large (infinite) heat reservoir. After a sufficiently long time, equilibration has occurred, meaning that the average net energy flux between the system and the thermal bath vanishes and both have reached the same temperature, T. Under these conditions, the probability for finding the system in a microstate σ is given by the canonical distribution:

$$P_{eq}(\sigma) = \frac{e^{-\beta H(\sigma)}}{Z}. \tag{1.1}$$

where $\beta = 1/k_B T$ is related to the inverse temperature via Boltzmann's constant k_B, and Z is the partition function which ensures the normalization of the probabilities. Thus, once we have specified a labeling of the microscopic configurations, $\{\sigma\}$, and we have determined the microscopic Hamiltonian $H(\sigma)$, i.e., the internal energy of each configuration so that the Boltzmann factor, $e^{-\beta H}$, is known, we can calculate, at least in principle, the partition function of the equilibrium system as well as arbitrary averages of time-independent observables. Of course, we can run into "technical difficulties" - in particular, some of the configurational sums may not be obtainable exactly, etc. - but the fundamental framework is well established.

Yet, systems in thermal equilibrium are the exception rather than the rule: If we look around us, the physical reality is overwhelmingly in a far-from-equilibrium state. Examples range from living cells to more complex biological organisms, or from weather patterns to ripples on water and sand. Looking for common features of these diverse systems, we note that they all consist of a huge number of particles (or, more generally, constituents), they are subject to external driving forces that prevent them from reaching thermal equilibrium, and finally, they are characterized by open boundaries so that there is a non-zero transport (of mass, energy, etc.) through the system.

The jump from the idealization of "thermal equilibrium" to the full, possibly turbulent dynamics of the real world is too far for our limited present knowledge of complex non-equilibrium systems, and we are therefore well advised to focus on the simplest generalizations of equilibrium systems, namely, *non-equilibrium steady states* (NESS). This particular category of systems is characterized by *time-independent* macroscopic behavior which can be achieved by applying a *uniform* driving force. We may view the external drive as a second bath, feeding energy into the system. As a consequence, we are now concerned with systems coupled to *two* reservoirs of energy in such a way that there is a constant energy flow through the system (e.g., a resistor in a steady state, gaining energy from a battery and losing it - at the same rate - to the atmosphere). If we look at the system alone, we can see that its energy is constant on the average: it is gaining as much energy from one reservoir as it is losing to the other. The system is in non-equilibrium, because there is a non-zero flux flowing through it; yet, after a sufficiently long time, it reaches a "steady state", with time-independent macroscopics. The fundamental problem is to find the associated stationary probability distribution, i.e., the generalization of the canonical distribution to this situation.

A good starting point for the study of these systems is the master equation which expresses the conservation of configurational probabilities. The *time-dependent* probability $P(\sigma, t)$ to find the system in configuration σ at time t changes only due to transitions into or out of σ, originating or ending in other configurations σ', in such a way that $\sum_\sigma P(\sigma, t) = 1$ for all times. Thus, we may write a balance (continuity)

equation: its right hand side consists of two sums: the first is a "gain" term, summing over all configurations from which configuration σ could possibly result, while the second is a "loss" sum, accounting for all configurations into which σ can evolve:

$$\frac{dP(\sigma,t)}{dt} = \sum_{\sigma'} \left\{ c\left[\sigma' \to \sigma\right] P(\sigma',t) - c\left[\sigma \to \sigma'\right] P(\sigma,t) \right\} \tag{1.2}$$

Here, $c\left[\sigma \to \sigma^{'}\right]$ denotes the transition rate (per unit time) from configuration σ into another configuration $\sigma^{'}$. These rates must be given, as part of defining a specific model. Our task is now to find the stationary solution of this equation, $P^{*}(\sigma) \equiv \lim_{t\to\infty} P(\sigma,t)$, for which the left hand side of Eqn.(1.2) vanishes:

$$0 = \frac{dP^{*}(\sigma)}{dt} = \sum_{\sigma'} \left\{ c\left[\sigma^{'} \to \sigma\right] P^{*}(\sigma^{'}) - c\left[\sigma \to \sigma^{'}\right] P^{*}(\sigma) \right\} \tag{1.3}$$

Of course, the steady state distribution $P^{*}(\sigma)$ will depend on the transition rates. Under rather generic conditions on the c's, it will be unique and therefore independent of initial conditions.

For a system in thermal equilibrium with a heat bath, we already know its steady state distribution, namely, $P_{eq}(\sigma)$ from Eqn.(1.1). As a result, we have to choose our rates carefully if we wish to model the dynamics of a system in its equilibrium state. The correct $P_{eq}(\sigma)$ results if the rates satisfy the detailed balance condition:

$$\frac{c\left[\sigma^{'} \to \sigma\right]}{c\left[\sigma \to \sigma^{'}\right]} = \frac{P_{eq}(\sigma)}{P_{eq}(\sigma^{'})} \tag{1.4}$$

We note briefly that this condition is necessary but not sufficient. Since $P_{eq}(\sigma) \propto \exp(-\beta H)$, we therefore choose our rates such that

$$\frac{c\left[\sigma^{'} \to \sigma\right]}{c\left[\sigma \to \sigma^{'}\right]} = \exp(\beta \Delta H) \tag{1.5}$$

where

$$\Delta H = H(\sigma^{'}) - H(\sigma) \tag{1.6}$$

A key feature of a system far from thermal equilibrium is the violation of detailed balance: its steady state distribution $P^{*}(\sigma)$ does not satisfy Eqn.(1.4).

A more intuitive way to discuss the detailed balance condition is to describe it in terms of the probability currents [4]. We consider a series of configurations $\sigma_1, \sigma_2, ..\sigma_n$, which

form a cycle: $1 \rightarrow 2.. \rightarrow n \rightarrow 1$. Next we define the products of the rates around the cycle as:

$$\begin{aligned} \Pi_+ &= c\left[\sigma_1 \rightarrow \sigma_2\right] c\left[\sigma_2 \rightarrow \sigma_3\right] ..c\left[\sigma_n \rightarrow \sigma_1\right] \\ \Pi_- &= c\left[\sigma_1 \rightarrow \sigma_n\right] c\left[\sigma_n \rightarrow \sigma_{n-1}\right] ..c\left[\sigma_2 \rightarrow \sigma_1\right] \end{aligned} \tag{1.7}$$

Detailed balance holds if

$$\Pi_+ = \Pi_- \tag{1.8}$$

for *all* cycles, which is equivalent to saying that the net probability current between any two configurations vanishes:

$$c\left[\sigma^{'} \rightarrow \sigma\right] P^*(\sigma^{'}) - c\left[\sigma \rightarrow \sigma^{'}\right] P^*(\sigma) = 0 \tag{1.9}$$

If the rates violate the detailed balance condition, then there will be non-trivial current loops:

$$c\left[\sigma^{'} \rightarrow \sigma\right] P^*(\sigma^{'}) - c\left[\sigma \rightarrow \sigma^{'}\right] P^*(\sigma) \neq 0 \tag{1.10}$$

This is a key characteristic of non-equilibrium steady states.

A very important concept in this context is the concept of universality. A vast amount of experience from equilibrium statistical mechanics has taught us that macroscopic long-distance, long-time properties are independent of numerous microscopic details, such as the precise form of interatomic interactions (as long as they remain short-ranged). Systems differing only in such irrelevant microscopic features are said to belong to the same universality class. If universality holds, then simple models, which are within the reach of a theoretical study, can be designed to understand and predict characteristics of much more complex systems belonging to the same universality class. In our work, we will start with a very simple model, *the driven lattice gas*, sometimes referred to as the "standard model", and we continue with variations of this model in an effort to find out if those variants, different from the original, maintain the same critical behavior, and therefore, belong to the same universality class. Thus, we hope to get a better understanding of what ultimately determines the key properties of non-equilibrium steady states.

1.1 The standard model

The Ising model was introduced by Lenz in 1925 [5, 6], in an attempt to understand the nature of phase transitions in ferromagnets. S.Katz, J.L Lebowitz and H. Spohn

[7] followed this philosophy and in a paper written in 1983 they introduced a very simple model for a non-equilibrium system, the "driven lattice gas" or "standard model". Their interest in the model was motivated, on the one hand, by its theoretical simplicity and, on the other hand, by the physics of fast ionic conductors. In this class of materials [8], one or more species of ions has a high mobility due to a large number of vacant or interstitial lattice sites; the ionic conductivity is strongly temperature-dependent, reminiscent of a phase transition. Katz, Lebowitz, and Spohn introduced a seemingly minor modification to the well-known Ising model: interpreting the Ising degrees of freedom as particles and holes which diffuse on a square lattice, they added a uniform "electric field" such that particles were preferentially driven in one direction. In conjunction with periodic boundary conditions, this drive induces a non-equilibrium steady state which showed such surprising properties that an avalanche of subsequent studies was spawned.

There are numerous reasons which make this model attractive to the theorist [9]:

- the dynamics is translationally invariant, and invariant under rotations in the subspace transverse to the drive;
- many of its equilibrium properties are well known, especially in two dimensions [10];
- for $d > 1$, where d is the dimension of the system, the system has non-trivial phases, both in and away from equilibrium;
- the model reduces to its equilibrium version, if the drive is turned off.

We now provide a brief description of the standard model. We start with the usual Ising lattice gas, defined on a d-dimensional hypercubic lattice with N sites. Each site i can be occupied or empty, which is reflected by a local occupation variable n_i, which can take only two values, 0 (for empty) or 1 (for occupied). The equivalent spin representation is easily obtained via $\sigma_i = 2n_i - 1$. Clearly, the local spin σ_i takes only the values ± 1. A complete set of $\{n_i\}$, with $i = 1, ..., N$ specifies a particular configuration σ. The number of particles is conserved, and we usually work with half-filled lattices, in order to be able to access the Ising critical point.

The next step is to define the microscopical Hamiltonian of the system:

$$H(\sigma) = -J_0 \sum_{\langle i,j \rangle} n_i n_j \tag{1.11}$$

with $J_0 > 0$ for attractive (ferromagnetic, in spin language), interactions, and $J_0 < 0$ for repulsive (antiferromagnetic) interactions. In the following, we will always assume $J_0 > 0$ unless otherwise specified. The sum runs over nearest-neighbor pairs of sites. The interaction of the system with its environment is represented by a coupling to a heat bath at temperature T.

At half density, and for $d > 1$, the Ising lattice gas exhibits the usual second order phase transition at a critical temperature T_c. For the two-dimensional case, T_c is known exactly: it takes the Onsager value [11]

$$T_c = T_{Ons} = 2.269...J/k_B \tag{1.12}$$

A number of critical properties (exponents, amplitude ratios and scaling functions) are universal and their values (functional forms) define the Ising universality class. In order to fall into the same universality class, a model must share the $s_i \rightarrow -s_i$ ("up-down") symmetry of the Ising Hamiltonian, be characterized by a scalar order parameter and possess sufficiently short-range interactions.

For a diffusive system, driven or not, particle number is conserved. Therefore Kawasaki dynamics [12] with the Metropolis rates [13] seems appropriate to describe the hopping of the particles to empty nearest-neighbor sites:

$$c(\vec{r}, \vec{r} + \vec{e}, \sigma) = \min\left(1, \exp\left(-\beta \Delta H\right)\right) \tag{1.13}$$

where ΔH is the change in the internal energy of the system after the particle-hole exchange, $\vec{r}$ is the position vector of the site and $\vec{e}$ is the unit vector of the lattice. These rates satisfy detailed balance with respect to the Boltzmann distribution. As a consequence, starting from some initial state, this dynamics should bring the system into the equilibrium state with stationary distribution given by Eqn.(1.1). This model is also known in the literature as Model B [14].

As mentioned above, S.Katz, J.L Lebowitz and H.Spohn [7] introduced a small modification to this model, namely a driving field E, uniform in both space and time. This drive acts along one of the lattice axes, and biases the jump rates: Particle-hole exchanges along (against) its direction are favored (suppressed), while exchanges in the transverse direction remain unaffected. Very important is the choice of boundary conditions. If "brick wall" boundary conditions are chosen, i.e., the particles are reflected at the boundaries, just like gas molecules bounce off the floor or the ceiling of a room, the system will eventually settle into an equilibrium state. Spatially inhomogeneous particle densities are established, indicating that translational invariance is lost. In order to restore translational invariance and, more importantly, to drive the

system into a *non-equilibrium steady state*, periodic boundary conditions are applied. As a consequence, the system carries a non-vanishing particle current.

The most natural extension of the equilibrium rates simply adds the (local) energy difference due to the bias to the change in configurational energy:

$$c(\vec{r}, \vec{r}+\vec{e}, \sigma) = \min\left(1, \exp\left(-\beta\left[\Delta H - bE\right]\right)\right) \tag{1.14}$$

where $b = 0, 1, -1$ for jumps transverse, along and against the field.

Monte Carlo simulations [7, 15] and field-theoretic studies [16, 17, 18] were performed, and the new model showed the following novel characteristics [7, 9].

Above the critical temperature (disordered phase):

- the system displays long range two-point correlations [19], decaying as r^{-d}, unlike its equilibrium counterpart which has short range (exponential) correlations;
- the structure factor exhibits a discontinuity singularity at the origin;
- non-trivial three-point correlations are present;
- its thermodynamics is shape-dependent [20].

At the critical temperature:

- the critical temperature increases with the strength of the drive;
- only one of the two lowest structure factors diverges;
- strong anisotropy occurs and two correlation lengths are defined;
- a new universality class is identified (new critical exponents found) [17, 18];
- anisotropic finite-size scaling is essential in order to obtain good data collapse [21].

Below the critical temperature:

- the system is in a phase segregated state, and only strips parallel to the drive are stable;

- interfaces are smooth in $d = 2$, in contrast to the equilibrium system [22, 23];
- with shifted periodic boundary conditions, the average internal energy depends on the orientation of the interfaces, and a sequence of splitting transitions occurs as the shift is varied.

Particularly puzzling is the fact that the critical temperature increases with the strength of the drive. One would expect that the reverse situation should happen, because the drive can be treated as an extra noise, overwhelming the nearest neighbor coupling whenever hops along the field are attempted. Later on, when we gain a deeper understanding of this new class of systems, we find arguments that explain this peculiar behavior of the model.

1.2 Variations of the standard model

The standard model generated a plethora of simple models, variations of the original. Some of them were obtained by modifying the driving field [24], others by changing the jump rates [25], or by adding an extra dimension [26]. Examples include repulsive interactions, random drives, quenched random impurities, multilayers and multispecies, etc. A complete review on the subject can be found in [9]. The interest in these novel systems is motivated by physical considerations. For example, the difficulty of imposing a uniform drive and periodic boundary conditions on a lattice led to investigating models with random drives and open boundaries. Also, driven multispecies lattices or multilayer systems are abundant in nature, and their practical applications motivate their study.

In this thesis, we study three of the variations of the standard model: *the two-dimensional driven diffusive lattice gas with anisotropic jump rates* , *the bilayer model* and *the two-temperature kinetic Ising model in one dimension.* Below we give a brief description of these three systems.

The first modification to the well-known standard model is to consider an anisotropy in the jump rates [25]: we introduce two different microscopic frequencies (inverse time scales) $\Gamma_{\parallel}$ and $\Gamma_{\perp}$ which control jumps in the parallel and perpendicular directions, respectively. In other words, we attempt more jumps in one of the directions. A measure of this bias is the following ratio:

$$\Gamma = \frac{\Gamma_{\parallel}}{\Gamma_{\perp}}. \tag{1.15}$$

We are interested in the critical behavior of this system as a function of Γ.

The second variation of the standard model is the bilayer model. It consists of two fully periodic $L \times L$ square driven Ising lattices arranged in a bilayer structure. For this case, the microscopic Hamiltonian of the system will include an extra term describing the interactions between layers, and we are interested in its properties as a function of this cross-layer coupling.

Our third model is a one dimensional version of the so-called two-temperature kinetic Ising model. Examples of "multi-temperature systems" are all around us, for example a water tank with an immersion heater. Imagine a set of sites arranged on a circle. Each site can be full or empty and it carries a spin variable. The spins are in contact with heat baths with *different* temperatures T_e and T_o on even and odd lattice sites, respectively. Due to the fact that the temperatures for the odd and even sites are different, there is a competition between the heat baths, each trying to drive the system towards equilibrium with the same Hamiltonian but at its own temperature [27]. As a result, energy flows from one sublattice to the other and the steady state is a nonequilibrium one. We solved this one dimensional model exactly and found the probability distribution for various small system sizes.

1.3 Techniques for studying NESS

Techniques for studying equilibrium and non-equilibrium systems can be divided into two broad categories. One adopts a microscopic approach, starting from the full, discrete lattice dynamics. This category includes exact solutions (possible only for small systems), Monte Carlo simulations, and high temperature expansion techniques. The other option is the mesoscopic approach, based on a coarse-grained description of the slow variables of the system, continuous in space and time. This involves Langevin equations, mean field theory (for systems away from criticality) and renormalized field theory (for critical properties). In this dissertation we are focusing on the microscopic approach, and we briefly mention some of the characteristics of each technique. Later, we will describe them at length.

1.3.1 Monte Carlo simulations

In studying non-equilibrium systems, Monte Carlo (MC) simulation techniques prove to be invaluable [7]. With the help of computer simulations, we can easily probe how

a well defined model is behaving under certain conditions. We can study its critical behavior, measure order parameters and fluctuations, etc. Computer simulations are often designed to check the accuracy of some approximation made in the analytical treatment of the model [28]. We will discuss in detail the steps involved when performing a Monte Carlo study, and the results obtained with this method for one of our models.

1.3.2 High temperature expansion technique

The high temperature expansion (HTE) technique [29] provides an alternate inroad towards a better understanding of these far from equilibrium systems. It is a simple analytic method, based directly on the microscopic dynamics, and can be used to estimate both correlations and the critical temperature. It can be easily extended to general rate functions, anisotropic interactions and higher dimensions. We compute the phase diagram for the previously mentioned models to the lowest order in β, and find remarkable qualitative agreement with the MC simulations, even at this relatively crude level of approximation.

1.3.3 Exact solutions for small systems

This method is within reach for small systems only, because it involves solving the master equation which becomes quite a challenge as the system size increases. Our main focus is a one dimensional non-equilibrium model, namely, the "two-temperature kinetic Ising model". We found the exact probability distribution for a number of system sizes, and in this dissertation we present one sample calculation and some relevant results for a 1×6 system.

1.4 Overview of the dissertation

In the next chapter, we study the bilayer model. We present a background view of the model and some new theoretical results obtained using the high temperature expansion technique. Using this simple approximation, we find the phase diagram of the model and match it, successfully, with the already known Monte Carlo simulation results. Also, we calculate other quantities such as the particle current and nearest-neighbor correlation functions. In chapter 3, we discuss in detail the two dimensional

driven lattice gas with anisotropic jump rates. We start with an extensive Monte Carlo study of the model and find the phase diagram. We continue with a finite-size scaling study, test the anisotropic scaling assumption [21] and find the critical exponents. On the analytic front, we employ again the high temperature expansion approximation in order to find the critical line of the system and compare it to the simulation results. Chapter 4 will be dedicated to the study of the one dimensional two-temperature kinetic model. We focus on a 1x6 system and find the exact solution for the probability distribution. Chapter 5 is a brief summary of our work and possible open research questions.

Chapter 2

Phase transitions in driven bilayer systems: a high temperature expansion approach

In this chapter, we begin by defining the microscopic model. Next, we briefly review the Monte Carlo simulation results [30] which were previously obtained for the bilayer model. We then turn to a description of the high temperature expansion technique and give some details of the calculations for this particular model. Finally, we discuss the phase diagram obtained using this very simple analytical method and compare it with the simulation data.

2.1 The bilayer model

Multilayer models were studied for a long time in equilibrium statistical mechanics for a multitude of reasons [31, 32]. One motivation was the desire to build a three-dimensional system by layering two-dimensional Ising lattices and allowing them to interact with one another. The study of equilibrium bilayer models proved useful in the description of real life systems, such as interacting solid surfaces or thin films [33]. The recent interest in the kinetics of intercalation, where foreign atoms diffuse into a layered host material [34], driven by electric fields or chemical potential gradients, extended the study of equilibrium bilayer systems towards the driven case. Initially, two driven two-dimensional Ising lattices were considered, one on top of the other, with no interlayer interactions, but with the possibility of particle jumps between

the layers [26]. A single transition was expected, from disorder to an ordered state characterized by two homogeneous layers, one with high and the other one with low density. Remarkably, however, two transitions were found, which we will describe in detail later. Intrigued by the rich and surprising behavior of the bilayer systems, we consider a stack of two driven Ising lattices and allow them to interact with one another. This model was already studied [30] with the help of simulation and field theory techniques [35], and we will complement and match some of these results using a simple analytic approach, the high temperature expansion approximation.

We start with a brief description of the model. A variation of the standard model, it consists of two fully periodic $L \times L$ square lattices arranged in a bilayer structure. We label the sites within each plane by their Cartesian coordinates x, y, and distinguish the two planes by a third coordinate, z, which takes only two values, e.g., 0 and 1. As usual, in order to describe a particular configuration, we define a set of occupation numbers $n(x, y, z)$, n being 0 for an empty site and 1 for an occupied site. We also can use the spin language notation $\sigma = 2n - 1$, with $\sigma = 1$ for a full cell and $\sigma = -1$ for an empty cell.

For the bilayer case, the microscopic Hamiltonian of the system includes an extra term describing the interactions between layers:

$$H = -J_0 \sum n(x, y, z)n(x', y', z) - J \sum n(x, y, z)n(x, y, z') \tag{2.1}$$

The first sum runs over all nearest neighbor sites (x, y, z) and (x', y', z) within a given plane, and the second sum reflects all cross-plane nearest neighbors, (x, y, z) and (x, y, z').

The first term of the Hamiltonian describes the usual two-dimensional Ising model with coupling J_0. The second term takes into account the interaction between different layers. Our analytic study is restricted to positive, fixed J_0, with J taking both positive and negative values (the choice of negative J's is motivated by the physics of intercalated materials [34]). A heat bath at temperature T is present, in order to model thermal fluctuations.

We drive the system out of equilibrium by applying an "electric" field E along the positive x-axis. This bias will induce preferential hopping along its direction, forcing the system into a non-equilibrium steady state with a net particle current. To describe the dynamics of this system at the microscopic level, including the bias, we allow only for nearest-neighbor exchanges. Adopting the usual Metropolis form, the rate for a particle jumping to a nearest-neighbor empty site, in configuration σ, is given by:

$$c(\vec{r}, \vec{r} + \vec{e}, \sigma) = \min\left(1, \exp\left(-\beta\left[\Delta H - bE\right]\right)\right) \tag{2.2}$$

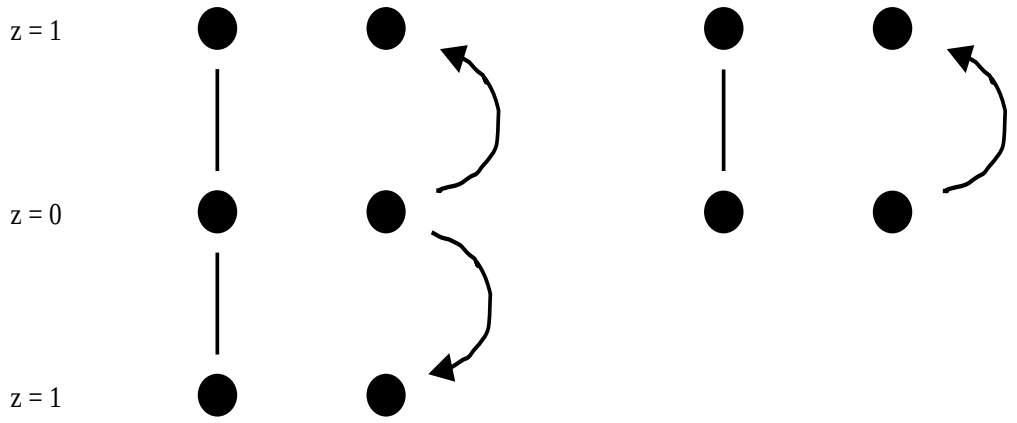

(a) Fully Periodic Boundary Conditions (b) Open Boundary

Figure 2.1: Different periodic boundary conditions

where $b = 0, 1$ or -1 for jumps transverse, along and against the field. Here, $\vec{r} = (x, y, z)$ is a vector which gives the position of one particular site on the lattice and $\vec{e}$ is a unit vector on the lattice.

A word on boundary conditions is in order. Within each plane, we retain periodic boundary conditions in the x- and y-directions throughout. In the z-direction, there are several possibilities: If we choose periodicity in z also, the site $(x, y, 0)$ is connected to site $(x, y, 1)$ via *two* bonds (Fig. 2.1.a) which enter into *both* the energetics *and* the dynamics (i.e., there are two channels for a particle to move from one layer to the other). Alternately, we can choose open boundary conditions in z and consider only a single bond between these two sites (Fig. 2.1.b). Mixtures of these two cases can also be constructed: one might choose periodic boundary conditions for the energetics, but allow only a single channel for particle moves, or vice versa. The first (second) "mixed" case is reducible to the case of open (periodic) boundary conditions, with J replaced by $2J$ ($J/2$).

2.2 Monte Carlo simulation results

The discovery of two phase transitions was reported in 1992 [26]: Monte Carlo simulations were performed for a system of two driven Ising layers with no interlayer interaction (i.e., $J = 0$), and under the influence of an infinite drive E. Decreasing T, it was found that the system first orders into two essentially identical layers, each in a phase-segregated state consisting of a (particle-rich) strip parallel to the field. This is called the *strip phase* (S). As the temperature is lowered even further, a second transition occurs, into a state characterized by two homogeneous layers at different particle densities. At $T = 0$, one layer will be full and the other one empty, so this state is called the *full-empty phase* (FE).

To put the puzzling presence of *two* transitions into a wider context, the next natural step was to introduce an interaction between the layers. Our study is based on the simulation results reported by Hill *et al* [30]. They investigated the phase diagram of this particular two-layer system at half filling, with fully periodic boundary conditions (periodicity in both energy and jumps). Their study was restricted to positive J_0, with several values of J/J_0 in the range $[-10, 10]$. Appropriate structure factors were chosen as order parameters (see [30] for details), and second-order transitions were identified using the fluctuations of these structure factors as functions of T. First order transitions were identified by observing hysteresis loops. For vanishing drive, i.e., the equilibrium case, the phase diagram in the T-J plane is symmetric. For positive J, when the temperature is lowered, the system orders into a strip phase (S), in order to minimize interfacial free energy. For negative J, at the same temperature, the system orders into a full-empty phase (FE), displaying homogeneous, opposite magnetization on the two planes. The two critical lines meet at a bicritical point $(T_{bc}, J = 0)$. A line of first order transitions extends from the bicritical point along the $J = 0$ axis down to $T = 0$, separating the S and FE phases. When the drive is turned on, the symmetry of the phase diagram is lost, and the most relevant new features are: the *lowering* of the critical temperature for large J and the *shift of the bicritical point* (and its attached line of first-order transitions) to higher values of T and negative interlayer coupling J (see Fig. 2.2). Thus, the S phase is observed to be stable in a finite window of negative interlayer coupling, so that two transitions must occur along the $J = 0$ axis. This discovery represents the most unexpected new characteristic of this driven diffusive system.

In a recent paper [36], Chng & Wang extended this phase diagram of the bilayer driven lattice gas, including *unequal intra-layer* attractive couplings. Their results showed that the bicritical point is shifted even further into the negative region of J, as the coupling transverse to the bias increases.

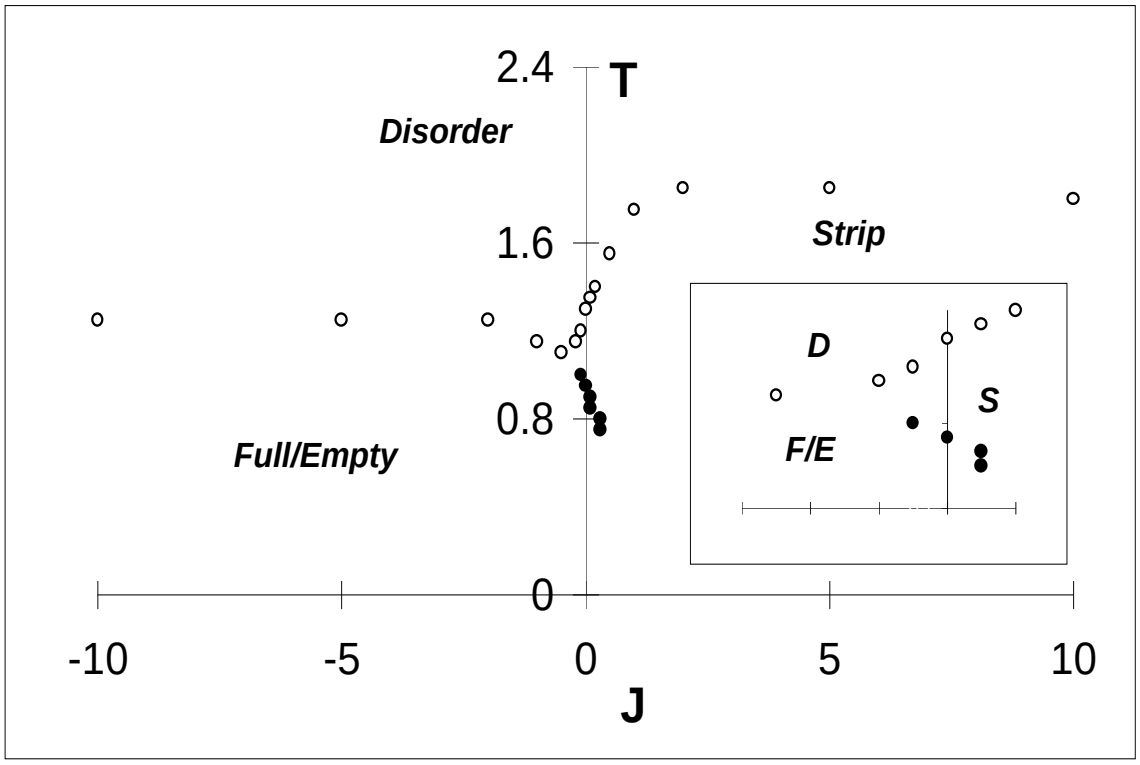

Figure 2.2: The phase diagram for the driven bilayer model obtained via computer simulations [30]. The plot is showing the presence of the two phases, S and FE and the shift of the bicritical point into the negative J region.

In order to explain [30] the novel characteristics of this model, some intuitive arguments were developed [30], based on the competition between suppression of short-range correlations [37] and enhancement of long-range ones [38] as a result of the bias. On one hand, the nearest-neighbor correlations are suppressed by the drive, which should lead to a lowering of the critical temperature. Yet, the drive changes the long-distance behavior of correlations, from an exponential to a power law decay, with positive (negative) amplitude for correlations parallel (transverse) to the drive. These anomalous long-range correlations play an important role, strongly favoring the S-phase, and hence increasing the critical temperature. The interplay between these two competing effects is very subtle, and either one can dominate depending on the region of the phase diagram.

In the following, we attempt to provide additional insights into these results, using a very simple approximation, namely, the high temperature expansion.

2.3 High temperature expansion technique

The motivation of our study comes from a need to look at the microscopic level dynamics for the multilayer system [30]. In order to estimate both correlations and the critical temperature, we employ this very straightforward analytic method, the high temperature approximation. In a paper published in 1988, Zhang *et al* [19] (ZWLV) investigated the two-point correlation functions for a two-dimensional system with infinite drive. Starting with the master equation, these authors argued that three-point correlations are negligible (while non-zero, they are numerically rather small) so as to arrive at a closed system of equations for the two-point correlations. To zeroth order in $\beta = 1/k_B T$, the solution is trivial. To first order in β, they studied the short-distance behavior of the solution *numerically*, by truncating the equations at a distance larger than a cutoff value. The results agree well with the simulation data. For the long-distance behavior, the equations were approximated by a Poisson problem with quadrupole symmetry. Again, there is a good agreement with the simulations, since the analytic solution captures the power law tail $1/r^2$.

Based on the approach by ZWLV *et al* [19], Schmittmann and Zia [39] generalized their analysis to include finite driving fields and solved the set of equations for the two-point correlation functions *exactly* by computing its Fourier transform, the structure factor S. Matching the series expansion of S to the expected critical singularity, the critical temperature was found. Given the fact that the phase diagram was calculated only to lowest order in β, *quantitative* agreement with the MC simulation cannot be expected, but, surprisingly, on a *qualitative* level, the computed critical temperature increased with the drive in the same manner as in the simulations.

A technical comment on the relation between "high temperature" and "finite E" is required. Considering the rates Eqn.(2.2), we demand that E always dominates the energetic contribution, i.e., $E > \Delta H$ for all jumps along E. Then, our expansion holds in the parameter region where $\beta \Delta H << 1$ at fixed βE, and the case of infinite E (i.e., $E \to \infty$ *before* $\beta \to 0$) is easily included.

To test the reliability of this method in another case, and to obtain additional insights into a novel problem, we apply this simple analytic method to the bilayer system. First, we write the system of equations for the two-point correlation functions. Second, we solve the system and obtain the critical temperature. We describe the phase diagram resulting from this simple approximation, and discuss our conclusions. Finally, we generalize this method and calculate other quantities which are simply related to two-point correlations, such as the particle current and the energy flux for exchanges in the parallel vs transverse directions. For simplicity, we take the

thermodynamic limit within each plane, i.e., $L \to \infty$. The calculations are performed at finite (but large) as well as infinite drive, and using different versions of boundary conditions in z.

2.3.1 The system of equations for the two-point correlation functions

The first step in our study is to derive a system of equations of motion for the two-point correlation functions, starting from the microscopic master equation (1.2):

$$\frac{dP(\sigma,t)}{dt} = \sum_{\sigma'} \{c\left[\sigma' \to \sigma\right] P(\sigma',t) - c\left[\sigma \to \sigma'\right] P(\sigma,t)\} \tag{2.3}$$

In the following, we use spin language for convenience. Before turning to two-point functions, we begin by considering a correlation function of an arbitrary number of spins. Letting $\mathcal{S}$ denote a set of distinct sites, we define the product of the spin variables at these sites:

$$\sigma_{\mathcal{S}} \equiv \prod_{\vec{r}\in\mathcal{S}} \sigma_{\vec{r}} \tag{2.4}$$

Denoting the average of this quantity by $\langle\cdot\rangle$, i.e.,

$$\langle\sigma_{\mathcal{S}}\rangle \equiv \sum_{\{\sigma\}} \sigma_{\mathcal{S}} P(\sigma,t)$$

and invoking the master equation, Eqn.(1.2), we can derive an equation of motion for $\langle\sigma_{\mathcal{S}}\rangle$:

$$\frac{d\left\langle\sigma_{\mathcal{S}}\right\rangle}{dt} = \sum_{NN} \left\langle\sigma_{\mathcal{S}}\left(\sigma_{\vec{r}}\sigma_{\vec{r}\,'} - 1\right) c\left(\vec{r},\vec{r}\,',\sigma\right)\right\rangle \tag{2.5}$$

Here, the sum runs over nearest-neighbor pairs $(\vec{r},\vec{r}\,')$ such that $\vec{r}\in\mathcal{S}$ but $\vec{r}\,'\notin\mathcal{S}$. Stationary correlations are obtained by setting the left hand side to zero.

To proceed, let us write the jump rates in a form which makes their dependence on the spin configuration σ explicit, so that the configurational averages in Eqn.(2.5) can be performed. For *infinite* drive, jumps along the field occur with rate unity, but jumps against the drive are completely suppressed, so that the transition rates *parallel to the field* can be written as:

$$c_{\parallel}^{\infty}\left(\vec{r},\vec{r}+\vec{e}_x,\sigma\right) = \frac{1}{4}(\sigma_{\vec{r}} - \sigma_{\vec{r}+\vec{e}_x} + 2) \tag{2.6}$$

In the case of *finite* drive, our restriction $E > \Delta H$ ensures that the jumps along E still occur with unit rate, while those against E are suppressed by a factor of $\exp(-\beta[\Delta H + E])$. Defining

$$\varepsilon \equiv e^{-\beta E} \tag{2.7}$$

Eqn.(2.6) should be amended to

$$c_{\parallel}(\vec{r}, \vec{r} + \vec{e}_x, \sigma) = \frac{1}{4}(\sigma_{\vec{r}} - \sigma_{\vec{r}+\vec{e}_x} + 2) + \frac{\varepsilon}{4}(\sigma_{\vec{r}+\vec{e}_x} - \sigma_{\vec{r}} + 2)\exp(-\beta\Delta H) \tag{2.8}$$

Transverse to the field we have two jump rates, corresponding to the two transverse directions (y and z). Both of these are regulated by the energy difference due to a jump:

$$\begin{aligned} c_{\perp}(\vec{r}, \vec{r} + \vec{e}_y, \sigma) &= \min(1, \exp(-\beta\Delta H)) \\ c_{\perp}(\vec{r}, \vec{r} + \vec{e}_z, \sigma) &= \min(1, \exp(-\beta\Delta H)) \end{aligned} \tag{2.9}$$

Before turning to any detailed calculations, let us introduce the quantities which will play key roles for the following. The *two-point correlation function* is defined as:

$$G(\vec{r}, \vec{r}\,') = \langle \sigma_{\vec{r}} \sigma_{\vec{r}\,'} \rangle \tag{2.10}$$

which, because of translational invariance, depends only on the *difference* of the two vectors $\vec{r}$ and $\vec{r}\,'$:

$$G(\vec{r}, \vec{r}\,') = G(\vec{r} - \vec{r}\,') \tag{2.11}$$

Thus, the correlation function at the origin is always unity:

$$G(\vec{0}) = \left\langle \sigma_{\vec{r}}^2 \right\rangle = 1 \tag{2.12}$$

We also introduce its Fourier transform, the *structure factor*:

$$S(k, p, q) \equiv \sum_{z=0,1} \sum_{x,y=-\infty}^{\infty} G(x, y, z) e^{-i(kx+py+qz)} \tag{2.13}$$

Since we have taken the thermodynamic limit $L \to \infty$, the wave vectors k and p are continuous, but restricted to the first Brillouin zone $[-\pi, \pi]$, while q is discrete, taking only the two values 0 and π. For completeness, we also give the inverse transform,

$$\begin{aligned} G(x, y, z) &= \frac{1}{2(2\pi)^2} \sum_{q=0,\pi} \int_{-\pi}^{+\pi} dk \int_{-\pi}^{+\pi} dp S(k, p, q) e^{i(kx+py+qz)} \\ &\equiv \int S(k, p, q) e^{i(kx+py+qz)} \end{aligned} \tag{2.14}$$

Here, the second line just defines some simplified notation.

To set up the high temperature expansion, let us first consider the infinite temperature (technically, the non-interacting) limit of this model. Two additional definitions will be convenient, namely,

$$\begin{aligned} K_0 &\equiv \beta J_0 \\ K &\equiv \beta J \end{aligned} \tag{2.15}$$

Clearly, these two quantities are the actual expansion parameters of our theory. For $K = K_0 = 0$, the steady state distribution is exactly known and uniform for all E: $P^* \propto 1$ [40], so that we are expanding about a well-defined zeroth order solution (there are no phase transitions in such systems). The correlation functions and structure factors for this limit are trivial:

$$\begin{aligned} G(0,0,0) &= 1 \\ G(x,y,z) &= 0 \text{ otherwise} \end{aligned} \tag{2.16}$$

whence

$$S(k,p,q) = 1 \equiv \overline{S}(k,p,q) \tag{2.17}$$

Returning to the interacting case, we note that $G(\vec{r})$, for $\vec{r} \neq \vec{0}$, is already of first order in the small parameter. Similarly, we can write the structure factor as a sum of two terms. The first term is just the zeroth order solution, while the second carries the information about the interactions,

$$S(k,p,q) = \overline{S} + \widetilde{S}(k,p,q) \tag{2.18}$$

so that we can recast $G(\vec{r})$, for $\vec{r} \neq \vec{0}$, in the form

$$G(x,y,z) = \int \widetilde{S}(k,p,q) \exp(i(kx+py+qz)) \quad \text{for } x,y,z \neq 0 \tag{2.19}$$

We are now ready to expand the rates in powers of βJ, βJ_0 while keeping βE finite:

$$\begin{aligned} c_{\|} &= \frac{1}{4}(\sigma_{\vec{r}} - \sigma_{\vec{r}+\vec{e}_x} + 2) + \frac{\varepsilon}{4}(\sigma_{\vec{r}+\vec{e}_x} - \sigma_{\vec{r}} + 2)\,(1 + \beta c_2) + O(\beta^2) \\ c_{\perp} &= 1 + \beta c_2 + O(\beta^2) \end{aligned} \tag{2.20}$$

with

$$c_2 = -\frac{1}{2}(\Delta H + |\Delta H|) \tag{2.21}$$

We remark that the infinite E limit is equivalent to letting ε vanish.

Given these simple forms for the rates, we can now derive the equations satisfied by the stationary pair correlations directly from Eqn.(2.5). Keeping only corrections to first order in K, K_0 and neglecting three-point correlations, we obtain a *closed set of linear equations* for $G(x, y, z)$. Since the dynamics contains only nearest-neighbor exchanges, it is not too surprising that, roughly speaking, the equations take the form of an anisotropic lattice Laplacian acting on $G(x, y, z)$. For x, y, z near the origin, the Laplacian may include the origin (e.g., $G(0, 0, 0)$ appears in the equation for $G(1, 0, 0)$) and will thus generate inhomogeneities in the system of equations. The detailed form depends on the chosen boundary conditions, and, of course, on three parameters K, K_0, and ε. In Appendix A, we illustrate this procedure with one example. Below, we show the set of equations for fully periodic boundary conditions. The first three equations result from nearest neighbors of the origin, $\vec{r} = (1, 0, 0)$, $(0, 1, 0)$, and $(0, 0, 1)$:

$$\begin{aligned}
0 &= (1+\varepsilon)[G(2,0,0) - G(1,0,0)] + 4[G(1,1,0) - G(1,0,0)] \\
&\quad +4[G(1,0,1) - G(1,0,0)] + 2\varepsilon K_0 + 8K_0 \\
0 &= 2(1+\varepsilon)[G(1,1,0) - G(0,1,0)] + 2[G(0,2,0) - G(0,1,0)] \\
&\quad +4[G(0,1,1) - G(0,1,0)] + 4\varepsilon K_0 + 6K_0 \\
0 &= 2(1+\varepsilon)[G(1,0,1) - G(0,0,1)] + 4[G(0,1,1) - G(0,0,1)] \\
&\quad +8K + 8\varepsilon K
\end{aligned} \tag{2.22}$$

The next three equations arise from the next-nearest neighbor sites, $\vec{r} = (1, 1, 0)$, $(0, 1, 1)$, and $(1, 0, 1)$:

$$\begin{aligned}
0 &= (1+\varepsilon)[G(2,1,0) + G(0,1,0) - 2G(1,1,0)] + 2[G(1,2,0) + G(1,0,0) \\
&\quad -2G(1,1,0)] + 4[G(1,1,1) - G(1,1,0)] - 2K_0 - 2\varepsilon K_0 \\
0 &= 2(1+\varepsilon)[G(1,1,1) - G(0,1,1)] + 2[G(0,2,1) + G(0,0,1) - 2G(0,1,1)] \\
&\quad +4[G(0,1,0) - G(0,1,1)] - 4[K_0 + K] \\
0 &= (1+\varepsilon)[G(2,0,1) + G(0,0,1) - 2G(1,0,1)] + 4[G(1,1,1) - G(1,0,1)] \\
&\quad +4[G(1,0,0) - G(1,0,1)] - 4\varepsilon K - 4K_0
\end{aligned} \tag{2.23}$$

There are two further next-nearest neighbor sites, $\vec{r} = (2,0,0)$ and $(0,2,0)$:

$$\begin{aligned} 0 &= (1+\varepsilon)[G(3,0,0)+G(1,0,0)-2G(2,0,0)]+4[G(2,1,0)-G(2,0,0)] \\ &\quad +4[G(2,0,1)-G(2,0,0)]-2\varepsilon K_0 \\ 0 &= 2(1+\varepsilon)[G(1,2,0)-G(0,2,0)]+2[G(0,3,0)+G(0,1,0)-2G(0,2,0)] \\ &\quad +4[G(0,2,1)-G(0,2,0)]-2K_0 \end{aligned} \tag{2.24}$$

And finally, all other G's satisfy homogeneous equations:

$$\begin{aligned} 0 &= (1+\varepsilon)[G(i+1,j,k)+G(i-1,j,k)-2G(i,j,k)] \\ &\quad +2[G(i,j+1,k)+G(i,j-1,k)-2G(i,j,k)] \\ &\quad +4[G(i,j,k-1)-G(i,j,k)] \end{aligned} \tag{2.25}$$

We note that the last equation contains the full anisotropic lattice Laplacian, acting on $G(i,j,k)$, without any inhomogeneities being generated.

2.3.2 Solving the system.

To solve this system, we closely follow the method presented in [39]. Returning to Eqn.(2.18), we clearly need to focus only on $\tilde{S}$, since this quantity carries the information about the interactions. Recalling Eqn.(2.19), we first express G through its Fourier transform $\tilde{S}$, exploiting the translation invariance and linearity. Then, we invoke the orthogonality of complex exponentials to project out an equivalent set of (algebraic) equations for $\tilde{S}$.

Keeping the following definitions in mind, namely

$$\delta(k,p,q) = 2(1+\varepsilon)(1-\cos k)+4(1-\cos p)+4(1-\cos q) \tag{2.26}$$

(which is just the anisotropic lattice Laplacian in Fourier space), and

$$\begin{aligned} I_1 &= \int \tilde{S}(1-\cos k) \\ I_2 &= \int \tilde{S}(1-\cos p) \\ I_3 &= \int \tilde{S}(1-\cos q) \end{aligned} \tag{2.27}$$

the system, written in terms of $\widetilde{S}$, is given by:

$$\begin{aligned}
2\varepsilon K_0 + 8K_0 &= \int \widetilde{S}\delta \exp(ik) + (1+\varepsilon)I_1 \\
4\varepsilon K_0 + 6K_0 &= \int \widetilde{S}\delta \exp(ip) + 2I_2 \\
8\varepsilon K + 8K &= \int \widetilde{S}\delta \exp(iq) + 4I_3 \\
-2\varepsilon K_0 - 2K_0 &= \int \widetilde{S}\delta \exp(i(k+p)) \\
-4(K_0 + K) &= \int \widetilde{S}\delta \exp(i(p+q)) \\
-4\varepsilon K - 4K_0 &= \int \widetilde{S}\delta \exp(i(k+q)) \\
-2\varepsilon K_0 &= \int \widetilde{S}\delta \exp(2ik) \\
-2K_0 &= \int \widetilde{S}\delta \exp(2ip)
\end{aligned} \tag{2.28}$$

$$0 = \int \widetilde{S}\delta \exp(i(kx + py + qz)) \text{ for } |x| + |y| + |z| > 2$$

To proceed, we would like to invoke the completeness relation for complex exponentials, namely,

$$\sum_{x,y,z} \exp[i(kx + py + qz)] = 2(2\pi)^2 \delta(k)\delta(p)\delta_{q,0} \tag{2.29}$$

In order to do so, we treat I_1, I_2, I_3 for the time being as pure (ε-dependent) coefficients and move them to the left-hand side. Moreover, we need one additional equation for $x = y = z = 0$, which is easily obtained:

$$\int \widetilde{S}\delta = \int \widetilde{S}[2(1+\varepsilon)(1-\cos k) + 4(1-\cos p) + 4(1-\cos q)] = 2(1+\varepsilon)I_1 + 4I_2 + 4I_3$$

Noting that each right hand side is associated with a lattice site (x, y, z), we multiply each equation by a factor $\exp[-i(k'x + p'y + q'z)]$ and sum over all sites. After exchanging primed and unprimed indices, the right hand side adds to

$$\sum_{x,y,z} \int \widetilde{S}\delta \exp i[(k-k')x + (p-p')y + (q-q')z)] = \widetilde{S}(k,p,q)\delta(k,p,q) \tag{2.30}$$

while the addition of all left hand sides gives us

$$\begin{aligned} L(k,p,q) \;\equiv\; & 2(1+\varepsilon)\,(1-\cos k)\,I_1 + 4\,(1-\cos p)\,I_2 + 4\,(1-\cos q)\,I_3 \\ & + (2\varepsilon K_0 + 8K_0)\,2\cos k + (4\varepsilon K_0 + 6K_0)\,2\cos p \\ & + (8\varepsilon K + 8K)\cos q - (2\varepsilon K_0 + 2K_0)\,4\cos k\cos p \\ & - (4\varepsilon K + 4K_0)\,2\cos k\cos q - 4(K_0+K)2\cos p\cos q \\ & -4\varepsilon K_0\cos 2k - 4K_0\cos 2p \end{aligned} \tag{2.31}$$

so that we finally arrive at

$$\tilde{S}(k,p,q) = \frac{L(k,p,q)}{\delta(k,p,q)} \tag{2.32}$$

However, $\tilde{S}$ is still an implicit function of the three integrals I_1, I_2, and I_3 here, so that we have to find these quantities first in order to obtain an explicit solution. For this purpose, we need three linearly independent equations. One of these equations will come from the value of G at the origin, $1 = G(0,0,0) = \int(\overline{S} + \widetilde{S})$, and the remaining two can be obtained directly from the definitions of I_1 and I_3, once we insert our result for $\tilde{S}$, Eqn. (2.32):

$$\begin{aligned} 0 &= \int \frac{L(k,p,q)}{\delta(k,p,q)} \\ 0 &= -I_1 + \int \frac{L(k,p,q)}{\delta(k,p,q)}(1-\cos k) \\ 0 &= -I_3 + \int \frac{L(k,p,q)}{\delta(k,p,q)}(1-\cos q) \end{aligned} \tag{2.33}$$

This leads to a set of three inhomogeneous, linear equations for the three unknowns I_1, I_2, and I_3, which can be easily solved. Since the details of the associated matrix inversion are somewhat tedious, they are left to Appendix A. We just summarize the following overall features of these quantities:

- All three are functions of K, K_0, and ε;
- As we will see later, all these integrals are related to the nearest-neighbor correlation functions the following way:

$$\begin{aligned} G(1,0,0) &= -I_1 \\ G(0,1,0) &= -I_2 \\ G(0,0,1) &= -I_3 \end{aligned} \tag{2.34}$$

- For the whole range of fields that we studied and for $K_0 = 1$ and $K = \pm 1$ (attractive and repulsive inter-layer interactions), I_1 and I_2 are always negative, while I_3 is positive for $K = -1$ and negative for $K = +1$.

This concludes the calculation of the structure factor. To summarize, we find

$$S(k, p, q) = 1 + \frac{L(k, p, q)}{\delta(k, p, q)} + O(K^2, K_0^2, KK_0) \tag{2.35}$$

Even at this lowest nontrivial order, it carries a significant amount of information about the phase diagram of our system. In particular, we can extract an approximate shape of the critical lines, as we will show in the following.

2.3.3 Locating continuous phase transitions.

The location of a continuous phase transition is marked by the divergence of a suitably chosen structure factor, as a function of the external control parameters. To provide an example, we can locate the order-disorder phase transition of the usual, two-dimensional Ising model by seeking those values of temperature and magnetic field for which the structure factor, $S(\vec{k})$, diverges. We note, first of all, that the only singularity occurs at $\vec{k} = 0$, indicating that the system orders into a spatially homogeneous state. Second, we find that the associated critical temperature takes the Onsager value and the magnetic field must vanish. If the Ising model is interpreted as a lattice gas, so that the total magnetization of the system is conserved, $S(0)$ is fixed by the conservation law, and we need to seek the onset of phase separation, i.e., the emergence of macroscopic spatial inhomogeneities in the system. In this case, singular behavior occurs in $\lim_{\vec{k}\to 0} S(\vec{k})$, provided the system is half-filled and tuned to the Onsager temperature.

For the bilayer system, we need to locate, and distinguish, two types of continuous transitions, namely, from disorder (D) into the strip (S) and the full-empty (FE) phases, respectively. Since the D-S transition is marked by the appearance of phase-separated strips in each layer, aligned with the driving force, it can be located by seeking singularities in $\lim_{p\to 0} S(0, p, 0)$. In contrast, the D-FE transition exhibits homogeneous, but opposite magnetizations in the two planes, so that it can be found by considering $S(0, 0, \pi)$. In fact, these two structure factors were precisely the order parameters chosen in the MC studies [30].

Yet, another subtlety must be considered: in a typical high temperature expansion (such as ours), only a finite number of terms can be computed. Hence, any perturbative result for the structure factor must be finite, and the radius of convergence of the

expansion must be investigated instead. Here, we extract the singularity by looking for *zeroes* of S^{-1}, to first order in K and K_0.

Starting from Eqn.(2.35), we obtain

$$S^{-1}(k,p,q) = 1 - \frac{L(k,p,q)}{\delta(k,p,q)} + O(K^2, K_0^2, KK_0) \tag{2.36}$$

and we need to identify the zeroes of $\lim_{p\to 0} S^{-1}(0,p,0)$ for the D-S transition, and of $S^{-1}(0,0,\pi)$ for the D-FE transition. Of course, we should ensure that these are the first zeroes which we encounter upon lowering the temperature. Thus, we first consider, more generally, the behavior of $S^{-1}(k,p,q)$ as both k,p vanish at fixed q. One finds easily that

$$\begin{aligned} \lim_{k,p\to 0} \delta(k,p,q) &= (1+\varepsilon)k^2 + 2p^2 + 4(1-\cos q) \\ &\quad + O(k^4, p^4, k^2p^2) \end{aligned} \tag{2.37}$$

which vanishes only at the origin since the Laplacian is positive definite. Similarly, we obtain

$$\begin{aligned} \lim_{k,p\to 0} L(k,p,q) &= 16K_0\,(1-\cos q) + 4\,(1-\cos q)\,I_3 \\ &\quad + k^2\,[\,(1+\varepsilon)I_1 + 10\varepsilon K_0 - 4K_0 + (4\varepsilon K + 4K_0)\cos q] \\ &\quad + p^2\,[2I_2 + 6K_0 + (4K_0 + 4K)\cos q] + O(k^4, p^4, k^2p^2) \end{aligned} \tag{2.38}$$

Combining these results, it is apparent that the zeroes of S^{-1} are identical to those of the numerator in Eqn.(2.36), and we may write

$$\begin{aligned} \lim_{k,p\to 0} [\delta(k,p,q) - L(k,p,q)] &\equiv \tau_\parallel(q)k^2 + 2\tau_\perp(q)p^2 + 4\tau_z(1-\cos q) \\ &\quad + O(k^4, p^4, k^2p^2) \end{aligned} \tag{2.39}$$

and read off

$$\begin{aligned} \tau_\parallel(q) &= (1+\varepsilon)\,(1-I_1) - 10\varepsilon K_0 + 4K_0 - (4\varepsilon K + 4K_0)\cos q \\ \tau_\perp(q) &= 1 - I_2 - 3K_0 - (2K_0 + 2K)\cos q \\ \tau_z &= 1 - I_3 - 4K_0 \end{aligned} \tag{2.40}$$

In a field-theoretic context [35], these quantities play the role of diffusion coefficients: $\tau_\parallel$ and $\tau_\perp$ control the in-plane diffusion in the parallel and transverse directions, respectively, while τ_z controls the inter-plane diffusion.

For high temperatures, i.e., small values of $K_0 = \beta J_0$ and $K = \beta J$, all three coefficients are positive. Seeking zeroes of these expressions, as K_0 and K increase, we need to consider the two cases $q = 0$ and $q = \pi$ separately. For $q = 0$, we find that $\tau_\perp(0)$ has a single zero at a critical β_c^S, for given J_0, J and ε. At these parameter values, $\tau_\parallel(0)$ and τ_z remain positive. Similarly, for $q = \pi$, the coefficient τ_z is the one which vanishes first as β increases, reaching zero at a critical β_c^{FE}. Converting into temperatures, we obtain two functions, $T_c^S(J_0, J, \varepsilon)$ and $T_c^{FE}(J_0, J, \varepsilon)$, and we need to identify the larger of the two: If $\max\left[T_c^S(J_0, J, \varepsilon), T_c^{FE}(J_0, J, \varepsilon)\right] = T_c^S(J_0, J, \varepsilon)$, the order-disorder transition is of the D-S type. Otherwise, if $\max\left[T_c^S(J_0, J, \varepsilon), T_c^{FE}(J_0, J, \varepsilon)\right] = T_c^{FE}(J_0, J, \varepsilon)$, the FE phase is selected upon crossing criticality.

While the two critical lines, $T_c^S(J_0, J, \varepsilon)$ and $T_c^{FE}(J_0, J, \varepsilon)$, can in principle be found analytically, the details are not particularly illuminating. Instead, we present a range of numerical results below. For example, for finite E with $\varepsilon = \exp(-\beta E) = 0.5$, we find

$$\begin{aligned} k_B T_c^S(J_0, J, 0.5) &= 4.15 J_0 + 2.03 J \\ k_B T_c^{FE}(J_0, J, 0.5) &= 4.05 J_0 - 1.70 J \end{aligned} \tag{2.41}$$

For $\varepsilon = \exp(-\beta E) = 0.7$, we find

$$\begin{aligned} k_B T_c^S(J_0, J, 0.7) &= 4.08 J_0 + 2.01 J \\ k_B T_c^{FE}(J_0, J, 0.7) &= 4.03 J_0 - 1.83 J \end{aligned} \tag{2.42}$$

and, for infinite E ($\varepsilon = 0$), we obtain

$$\begin{aligned} k_B T_c^S(J_0, J, 0) &= 4.39 J_0 + 2.11 J \\ k_B T_c^{FE}(J_0, J, 0) &= 4.14 J_0 - 1.36 J \end{aligned} \tag{2.43}$$

For comparison, we also quote the equilibrium ($E = 0 \Leftrightarrow \varepsilon = 1$) results (see Appendix A for details):

$$\begin{aligned} k_B T_c^S(J_0, J, 1) &= 4 J_0 + 2 J \\ k_B T_c^{FE}(J_0, J, 1) &= 4 J_0 - 2 J \end{aligned} \tag{2.44}$$

which exhibit the expected $J \to -J$ symmetry.

Recalling that the MC simulations were performed at fixed, positive in-plane coupling J_0, we need to consider only the dependence on the cross-plane coupling J which may take either sign. All of our results show that, for positive J, the D-S transition dominates while, for sufficiently negative J, a D-FE transition is found. However, the

non-equilibrium ($E \neq 0$) results show several novel features which we discuss below in more detail.

We should also caution that our results provide no insight into any first-order transitions since our expansion cannot be extended to describe the ordered phases.

2.4 Results.

2.4.1 The critical line: Comparison with MC simulations

At the end of the last subsection, we already noted that the ordered state is of S-type for positive J, while the FE-phase is found for sufficiently negative J. The two critical lines are shown in Fig. 2.3, for $\varepsilon = 0.5$ and $J_0 = 1$ (in units of $k_B T_{Ons}$) which are perfectly typical values of these parameters.

Since a first order approximation is by definition linear, the phase diagram is also linear. Even though we cannot expect quantitative agreement with the simulation data, the HTE phase diagram shows several of the features found in the simulations: *the existence of two phase transitions* and the *shift of the bicritical point* to higher values of T and negative J. As T is lowered for positive J, the system undergoes a second order phase transition from a disordered state to a strip (S) phase, with strips in both layers. This phase survives also for very small, negative J. For large and negative J, the disordered state orders into the full-empty (FE) phase, characterized by the planes being mainly full or empty.

A magnified view (Fig. 2.4) of the region near the $J = 0$ axis clearly shows the shift of the bicritical point to small negative J. Remarkably, the strip phase survives there, in spite of being energetically unfavorable. This phenomenon can be explained qualitatively by noting that long-range negative correlations transverse to E dominate the ordering process for positive J, and this mechanism continues to be effective for a small region of negative J.

We investigated the critical lines for different cross-plane boundary conditions (periodic, open, and mixed), and the main conclusions of our study, namely, the existence of the two phase transitions and the shift of the bicritical point, hold for all of these variations.

Next, we discuss the dependence of the critical lines (Fig. 2.5), specifically $T_c^S(1, 1, \varepsilon)$ and $T_c^{FE}(1, -1, \varepsilon)$, on the field parameter $\varepsilon = \exp(-\beta E)$. We computed these two

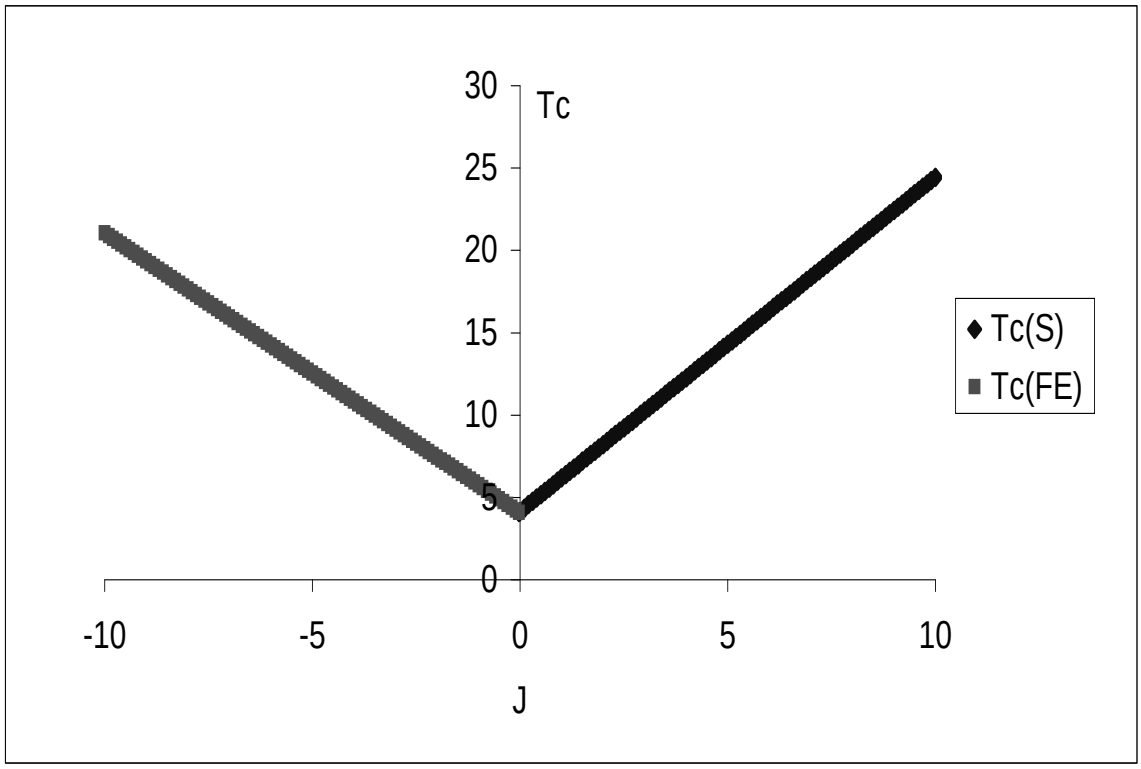

Figure 2.3: The dependence of the critical temperature of the bilayer system on the inter-layer coupling J in the HTE approximation for a finite field $\varepsilon = 0.5, J_0 = 1$ and fully periodic boundary conditions

critical temperatures for a range of ε, keeping the ratio $|J/J_0|$ fixed to unity. In qualitative agreement with the MC data, the critical temperature of the strip phase increases as the field becomes stronger, in contrast with the critical temperature of the FE phase, which decreases with the strength of the drive.

Given an expression for the structure factors, there are several other quantities of physical interest which we can study. Obviously, we can Fourier transform back to obtain the two-point correlation functions; specifically, the nearest-neighbor correlations. These are simply related to the stationary particle and energy currents, as we now proceed to show.

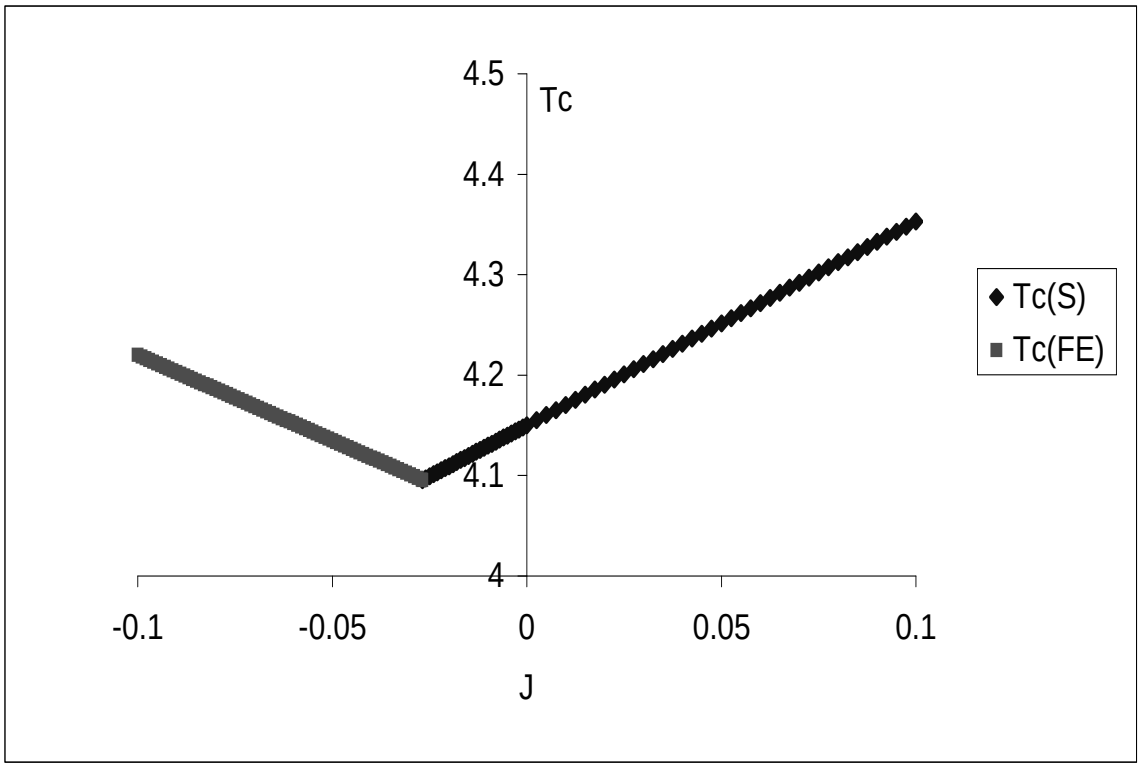

Figure 2.4: Magnified view of the region near the bicritical point showing the presence of the strip phase (S) in the J negative half plane, for the bilayer system with fully periodic boundary conditions, finite field $\varepsilon = 0.5$ and $J_0 = 1$.

2.4.2 Nearest-neighbor correlations.

These are easily found from our solution for the structure factor, Eqn.(2.35). For example, the nearest-neighbor correlations in the field direction are given by :

$$G(1,0,0) = \int \widetilde{S}(k,p,q)\cos k + O(K^2, K_0^2, KK_0) \tag{2.45}$$

Since $\int \widetilde{S} = 0$ by virtue of $G(0,0,0) = 1$, we obtain

$$\begin{aligned} G(1,0,0) &= -\int \widetilde{S}(k,p,q)\,(1-\cos k) + O(K^2, K_0^2, KK_0) \\ &= -I_1 \end{aligned} \tag{2.46}$$

and similarly,

$$\begin{aligned} G(0,1,0) &= -I_2 \\ G(0,0,1) &= -I_3 \end{aligned} \tag{2.47}$$

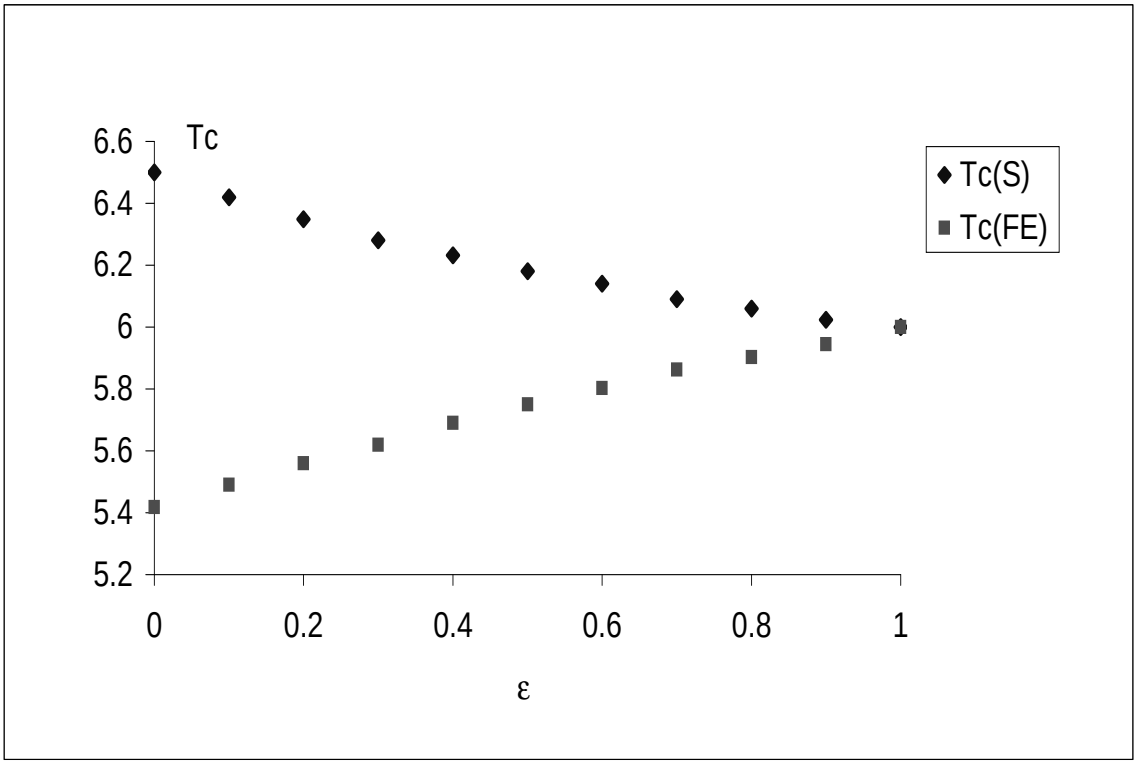

Figure 2.5: The dependence of the critical temperature for the two phases (strip and full-empty)on the strength of the drive for a fixed ratio of the couplings $\left|\frac{J}{J_0}\right| = 1$ and fully periodic boundary conditions

and these three integrals are already known. Specifically, for $\varepsilon = 0.5$ we find

$$\begin{aligned} G(1,0,0) &= 0.949K_0 + 0.030K \\ G(0,1,0) &= 0.849K_0 - 0.034K \\ G(0,0,1) &= -0.055K_0 + 1.702K \end{aligned} \tag{2.48}$$

For reference, we also quote the first order results for the equilibrium ($\varepsilon = 1$) correlations (see Appendix A):

$$\begin{aligned} G^{eq}(1,0,0) &= G^{eq}(0,1,0) = K_0 \\ G^{eq}(0,0,1) &= 2K \end{aligned} \tag{2.49}$$

The factor of 2 in $G(0,0,1)$ is due to the fully periodic boundary conditions across the two planes.

In the following graphs, we show the drive dependence of the three nearest-neighbor correlation functions, at $K_0 = 1$ and $K = \pm 1$, to illustrate their behavior in two

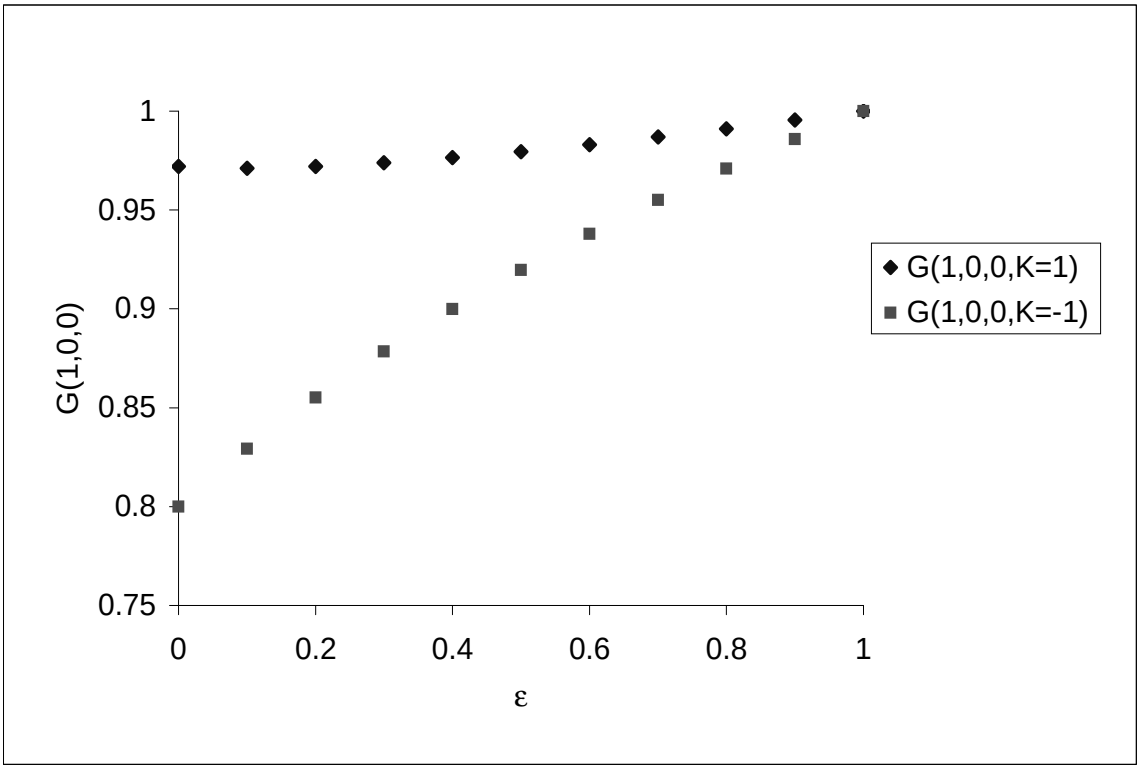

Figure 2.6: The drive dependence of the nearest-neighbor correlation function along the field at $K_0 = 1$ and $K = \pm 1$ for the fully periodic bilayer system

typical domains (attractive and repulsive cross-layer coupling). Consistent with our interpretation of the drive as an "additional noise", all correlations are reduced compared to their equilibrium value ($\varepsilon = 1$). Also, as the field is switched on, the $J \to -J$ symmetry of the equilibrium system is broken, and the correlations for repulsive and attractive cross-layer coupling differ from one another. The details of how they differ provides some insight into the ordered phases which will eventually emerge.

The first plot (Fig. 2.6) shows the correlation function for a nearest-neighbor bond within a given plane, and aligned with the drive direction. It is interesting to note that the correlations for repulsive cross-layer coupling are more strongly suppressed than their counterparts for attractive J. This feature becomes more transparent when we consider nearest-neighbor correlations transverse to the drive, but still within the same plane (Fig. 2.7). For attractive cross-layer coupling, we note that $G(1, 0, 0)$ is considerably enhanced over $G(0, 1, 0)$, while the two correlations are roughly equal in the repulsive case. This indicates a tendency to form droplets of correlated spins which are elongated in the field direction for $J = +1$ while remaining approximately

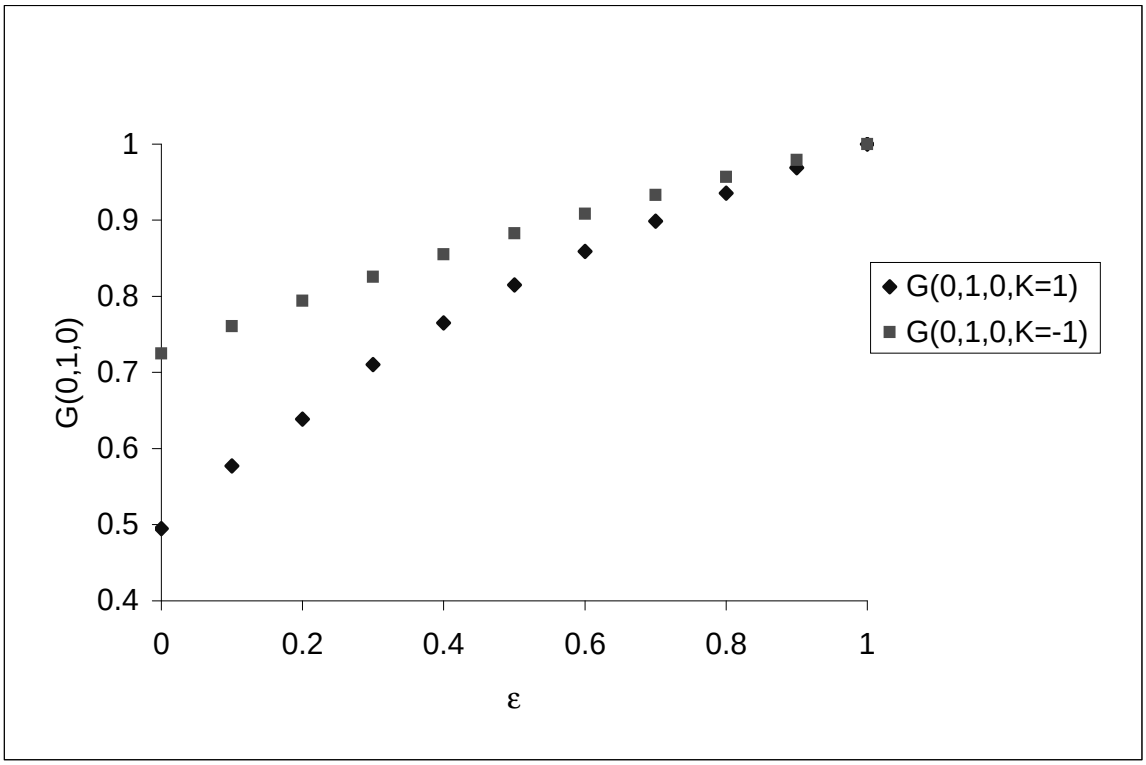

Figure 2.7: The drive dependence of the nearest-neighbor correlation function transverse to the field (in the same layer)at $K_0 = 1$ and $K = \pm 1$ for the fully periodic bilayer system

isotropic for $J = -1$, hinting at the nature of the associated ordered phases (strip-like vs uniform within each layer).

This picture is completed when we consider the cross-plane correlations $G(0, 0, 1)$ (Fig. 2.8): These are positive in the attractive, and negative in the repulsive case, demonstrating the tendency towards equal vs opposite local magnetizations on the two layers.

Given that we have performed only a first order calculation, the results really carry a remarkable amount of information about the system. Encouraged by these observations, we now consider two other quantities, namely, the particle and energy currents.

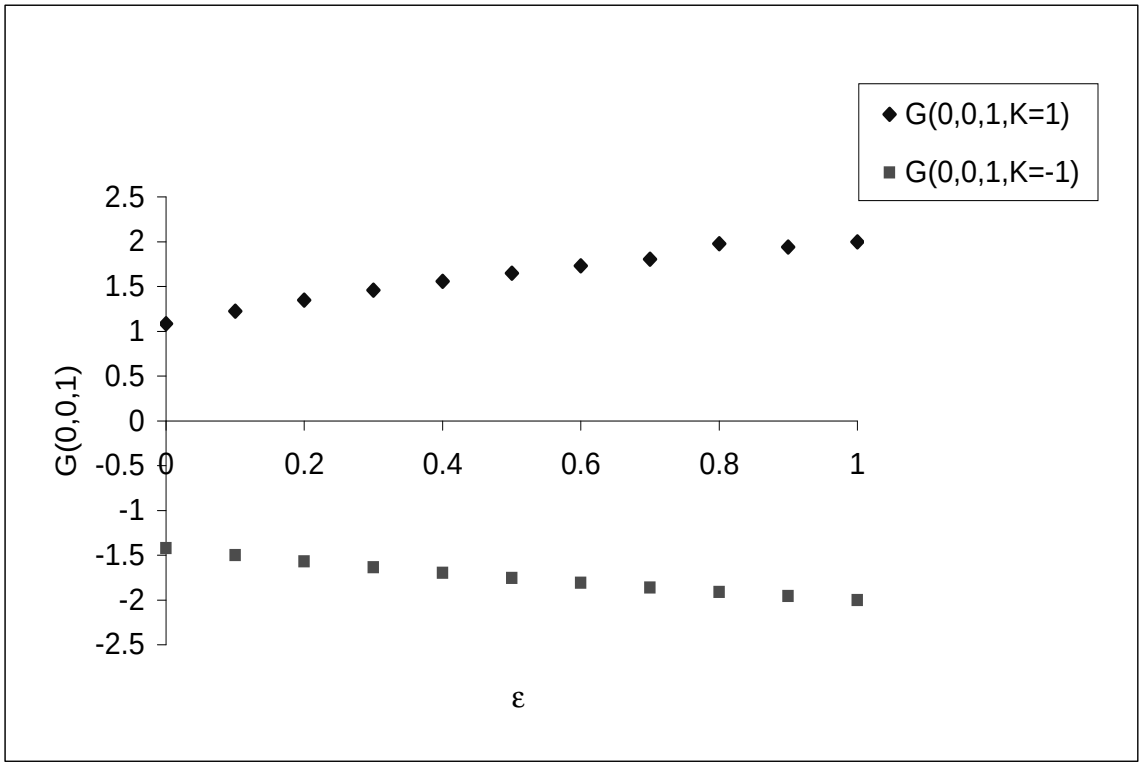

Figure 2.8: The drive dependence of the nearest-neighbor correlation function transverse to the field (different layers) at $K_0 = 1$ and $K = \pm 1$ for the fully periodic bilayer system

2.4.3 The particle current.

Due to the bias in conjunction with periodic boundary conditions, the bilayer system carries a net particle current, $\langle j \rangle$. Since only nearest-neighbor exchanges are possible, this current is proportional to the density (number per site) of available particle-hole pairs in the field direction. A factor $c_{\|}$ then counts the fraction of these pairs which will actually exchange per unit time. Specifically, in configuration σ, the particle current consists of two terms. The first accounts for all particles which have a neighboring hole in the field direction and will give a positive contribution to the current, with rate $c_{\|}$, while the second keeps track of exchanges in the opposite direction:

$$j(\sigma) = \frac{1}{L^2}\left\{\sum_{\vec{r}} \frac{(1+\sigma_{\vec{r}})}{2}\frac{(1-\sigma_{\vec{r}+\vec{e}_x})}{2} c_{\|}(\vec{r},\vec{r}+\vec{e}_x) - \sum_{\vec{r}} \frac{(1-\sigma_{\vec{r}})}{2}\frac{(1+\sigma_{\vec{r}+\vec{e}_x})}{2} c_{\|}(\vec{r},\vec{r}+\vec{e}_x)\right\} \tag{2.50}$$

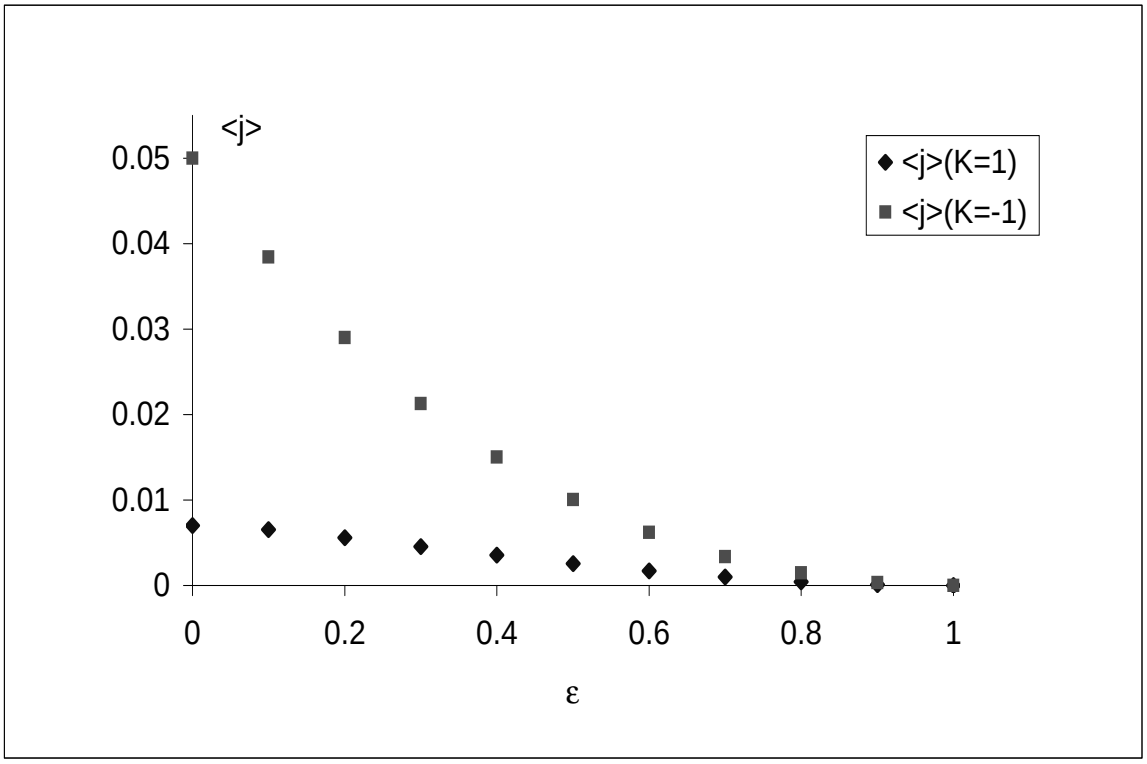

Figure 2.9: The drive dependence of the average particle current at $K_0 = 1$ and $K = \pm 1$ for the fully periodic bilayer system

For infinite E only the first term remains, since particles are prohibited from jumping against the field.
After a few straightforward algebraic manipulations (see Appendix A), the average current has the following form:

$$\langle j \rangle = \frac{1}{4}(1-\varepsilon)[1 - G(1,0,0)] \tag{2.51}$$

which shows that the current is non-zero only if $E \neq 0$, takes its maximum value at infinite temperature and is reduced by (attractive) nearest-neighbor interactions. The graph (Fig. 2.9) shows the field-dependence of this current, for $K_0 = 1$ and $K = \pm 1$.

Since nearest-neighbor correlations along the field are much larger for positive J, the current is proportionately smaller, compared to the repulsive case.

2.4.4 Energy currents.

Another very interesting phenomenon associated with driven dynamics is the change in configurational energy during one Monte Carlo step. In the steady state, by definition, the net average change must vanish. However, particle-hole exchanges parallel to the field direction tend to increase the energy, while exchanges transverse to E tend to decrease it [41]:

$$\left\langle \frac{dH}{dt} \right\rangle_{\parallel} = - \left\langle \frac{dH}{dt} \right\rangle_{\perp} > 0 \tag{2.52}$$

Even if a particle current were absent, the presence of energy currents would signal the *non-equilibrium* steady state [9].
Since the configurational energy involves only nearest neighbor bonds, it is apparent that only the time evolution of nearest-neighbor correlations plays a role in these two fluxes. Specifically, we have

$$\left\langle \frac{dH}{dt} \right\rangle_{\parallel} = - J_0 \left(\frac{d}{dt} \right)_{\parallel} [G(1,0,0) + G(0,1,0)] - 2J \left(\frac{d}{dt} \right)_{\parallel} G(0,0,1) \tag{2.53}$$

where the subscript on the time derivative reminds us to select only those processes which are due to parallel exchanges alone. Of course, there is an analogous equation for $\langle dH/dt \rangle_{\perp}$. Thus, we find

$$\begin{aligned} \left\langle \frac{dH}{dt} \right\rangle_{\parallel} &= -J_0 \{(1+\varepsilon)[G(2,0,0) - G(1,0,0)] + 2(1+\varepsilon)[G(1,1,0) - G(0,1,0)] \\ &\quad +6\varepsilon K_0\} - 2J\{2(1+\varepsilon)[G(1,0,1) - G(0,0,1)] + 8\varepsilon K\} \qquad (2.54) \\ \left\langle \frac{dH}{dt} \right\rangle_{\perp} &= -J_0 \{4[G(1,1,0) - G(1,0,0)] + 4[G(1,0,1) - G(1,0,0)] \\ &\quad +2[G(0,2,0) - G(0,1,0)] + 4[G(0,1,1) - G(0,1,0)] + 14K_0\} \qquad (2.55) \\ &\quad -2J\{4[G(0,1,1) - G(0,0,1)] + 8K\} \end{aligned}$$

The next-next-nearest neighbor correlation functions which appear here can again be computed (see Appendix A). The result, for $\langle dH/dt \rangle_{\parallel}$ at $K_0 = 1$ and $K = \pm 1$, is shown in Fig. 2.10 as a function of ε. As expected, this flux is always non-negative and monotonically increasing as a function of E.

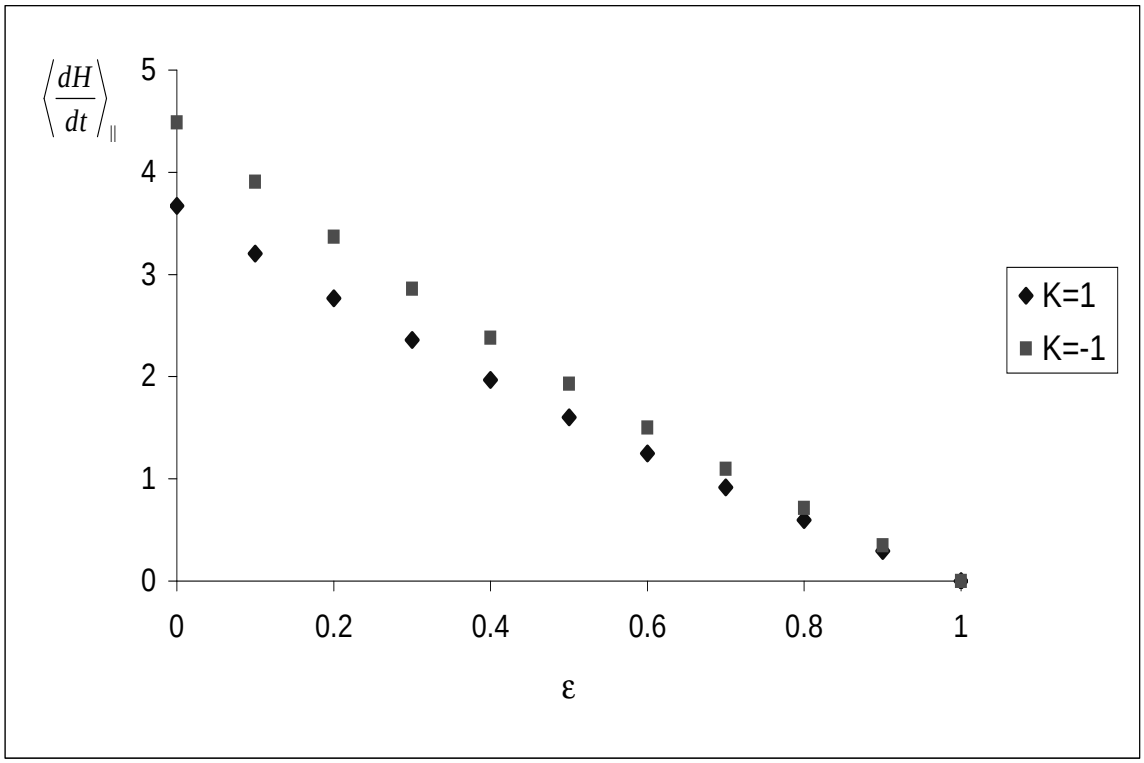

Figure 2.10: The drive dependence of the average energy current parallel to the field at $K_0 = 1$ and $K = \pm 1$ for the fully periodic bilayer system

2.5 Concluding remarks

The high temperature series provides us with a simple analytic tool which is based directly on the microscopic dynamics. Given the coarseness of a first order approximation, it is remarkable how many features of the MC simulations for the driven bilayer lattice gas are at least qualitatively reproduced. We derived, and solved, a set of equations for the stationary correlation functions, which are just as easily expressed as their Fourier transforms, the structure factors. By matching the series expansion of the latter with the expected critical singularity, we found two critical lines, separating the disordered phase from the strip phase (S) and the full-empty phase (FE), respectively. We also recovered the shift of the bicritical point, in very good qualitative agreement with the simulations.

Next, we calculated other quantities such as the correlations along and transverse to the field, the change in energy during one Monte Carlo step along the drive and transverse to it, and the particle current, j, for both infinite and finite fields. In

agreement with the theory, we found the variation of the energy along the field to be positive and equal in magnitude (but opposite in sign) with the one transverse to the field. As for the current, our value agreed with the one reported by Zhang [19], for infinite drive.

The high temperature expansion method proves to be a very simple analytic complement to the MC simulations. It can help predict qualitative phase diagrams and it gives us direct microscopic information about the driven diffusive systems.

Chapter 3

Driven diffusive lattice gas with anisotropic jump rates:Monte Carlo and high-temperature series studies

In this chapter, we turn to a second variant of the standard model. Returning to a purely two-dimensional case, we now investigate the effect of having anisotropic exchange rates: particle-hole exchanges along one axis will be attempted more often than along the other axis. One might imagine particles being driven through a square grid of channels, with channels in one direction being easier to traverse than in the other. We focus especially on the critical dynamics. Introducing anisotropic rates of this type amounts to a modification of the local dynamics, leaving the configurational energetics unchanged. For a system in equilibrium (i.e., if detailed balance still holds), such modifications do not affect any steady state properties. In a far-from-equilibrium model, however, any changes of the dynamical rules will usually modify the steady state, and even universal properties may be affected. The fundamental question of interest here is the following: How does the anisotropy in the jump rates affect the steady state properties of the system and its universal behavior?

We will study our model using both Monte Carlo simulation techniques and a high temperature expansion. We seek to find its phase diagram and identify its universality class. In the first part of this chapter we present the model and simulation results. Next, we discuss the finite size scaling technique and its application to this particular model. Furthermore, we present succinctly the high temperature approximation and

the phase diagram obtained using this simple analytical method and compare results from the two methods. We discover that the phase diagram shows some interesting features while universal properties remain in the universality class of the standard model.

3.1 The model

Anisotropic exchange rates were first introduced by van Beijeren and Schulman [25], in an attempt to arrive at an exactly soluble far-from-equilibrium model. Their modified version of the driven lattice gas has two key components. First, two different microscopic time scales are introduced, so that particle-hole exchanges in the field direction are attempted at a much greater rate than exchanges perpendicular to the drive. Second, the drive is set at infinity, so that particles can never hop backwards and forward jumps are completely independent of the local energetics. In this "fast rate limit", the dynamics within a given lattice column, aligned with the field, decouples from its neighbors. Thus, the particle distribution in each column can equilibrate, independently of the configuration of all other columns. As a consequence, the effective spatial dimension of the model is reduced by one, simplifying an analytic study of this model [42]. To be more specific, we label the two inverse time scales $\Gamma_{\parallel}$ and $\Gamma_{\perp}$, controlling the jumps in the parallel and transverse directions respectively. Of course, only their *ratio*, $\Gamma \equiv \Gamma_{\parallel}/\Gamma_{\perp}$, is relevant. The fast rate limit then corresponds to $\Gamma \to \infty$. A detailed and systematic study of this limit was performed by Krug *et al* [42]. They employed both Monte Carlo simulation techniques and mean field theory in their work, and considered several choices of rate functions (Metropolis, heat bath, etc.). Their main result was that, in this limit, the critical exponents of the transition are classical, except for anomalous energy fluctuations.

We extend this study by allowing for a whole range of anisotropic jump rates, including values of Γ smaller than unity. Our major goal is to map out the phase diagram, as a function of Γ. More specifically, we address the following questions:

i) How does the critical temperature depend on the anisotropic jump rates, i.e., Γ?

ii) How does the phase diagram obtained using the high temperature expansion approximation compare with the Monte Carlo simulations?

iii) Is this model in the same universality class as the standard model?

We begin with a detailed description of our model. It is defined on a square lattice

of size $L_x \times L_y$. Each site $i = (x, y)$ can be full or empty, and in order to describe a particular configuration, we define a set of occupation numbers n_i, n being 0 for an empty site and 1 for an occupied site. We also use spin notation $\sigma_i = 2n_i - 1$, with $\sigma_i = 1$ for a full cell and $\sigma_i = -1$ for an empty cell. To access the Ising critical point, we restrict our study to half-filled lattices.

Next we endow the spins with nearest-neighbor interactions, as in the standard model:

$$H = -J_0 \sum_{\langle i,j \rangle} n_i n_j \tag{3.1}$$

This Hamiltonian describes the usual two-dimensional Ising model with coupling J_0. Our study is restricted to positive J_0. Similar to the standard model, we couple the system to a heat bath at temperature T and apply an external drive to force the system out of equilibrium. Thus, particles jump to nearest-neighbor empty sites, subject to the local energetics and biased by the drive. Particle-hole exchanges parallel (transverse) to E are attempted with a frequency $\Gamma_\parallel$ ($\Gamma_\perp$). To summarize, the implemented rates have the form

$$c(\vec{r}, \vec{r} + \vec{e}, \sigma) = \begin{cases} \Gamma_\parallel \min\left(1, \exp\left(-\beta\left[\Delta H - bE\right]\right)\right) & \text{for parallel exchanges} \\ \Gamma_\perp \min\left(1, \exp\left(-\beta \Delta H\right)\right) & \text{for transverse exchanges} \end{cases} \tag{3.2}$$

with $b = +1$ (-1) for particle moves along (against) the field. In the following, we choose E to be infinite, so that exchanges along the field always take place and exchanges against E are completely forbidden.

Clearly, only the ratio

$$\Gamma \equiv \frac{\Gamma_\parallel}{\Gamma_\perp} \tag{3.3}$$

enters the simulations as a control parameter. For example, for $\Gamma = 2$ we want to ensure that two parallel bonds are selected for each transverse one. Similarly, $\Gamma = 1/2$ corresponds to selecting two transverse bonds for each parallel one. The standard model corresponds to $\Gamma = 1$.

To build a better understanding of the behavior of this system, we turn to Monte Carlo simulation methods. In particular, we wish to probe how the order-disorder phase transition of the standard model is affected by having Γ differ from unity. Specifically, we determine the phase diagram for an extensive range of Γ's; and we perform a state-of-the-art finite size scaling study for selected values of Γ in order to compute the associated critical exponents. Earlier Monte Carlo results [37] were restricted to $\Gamma \geq 1$ and isotropic lattices as well as limited in terms of computational power. They

do, however, show that the model has a continuous order-disorder transition at a critical temperature T_c which depends on Γ. The ordered phase consists of a single particle-rich strip aligned with the field, as in the standard model.

3.2 Monte Carlo simulations

3.2.1 Technical parameters of the simulations

Simulations prove to be very useful in studying non-equilibrium systems. Originally, they were designed for equilibrium statistical mechanics, where the idea is to replace, when calculating averages, the sum over all configurations $\{\sigma_l\}$ with a sum over a characteristic subset of space points. These points are chosen at random, using a random number generator. This method is also called "simple sampling". Later on, Metropolis [13] suggested not to choose the successive states $\{\sigma_l\}$ independently of each other, but to build a Markov process, where each state σ_{l+1} is constructed from a previous state σ_l via a suitable transition probability $c(\sigma_l \to \sigma_{l+1})$. This is also known as the "importance sampling" method. The transition rates are then chosen in such a way that, after a very long time ($l \to \infty$), we will recover the equilibrium Boltzmann distribution:

$$P(\sigma_l) \to P_{eq}(\sigma_l) = \frac{1}{Z} \exp(-\beta H(\sigma_l)) \tag{3.4}$$

provided the rates are chosen so that they obey detailed balance (cf. Chapter 1):

$$\frac{c\left[\sigma^{'} \to \sigma\right]}{c\left[\sigma \to \sigma^{'}\right]} = \frac{P_{eq}(\sigma)}{P_{eq}(\sigma^{'})} = \exp(\beta \Delta H) \tag{3.5}$$

For a system far from equilibrium, the rates generically violate this condition, but importance sampling can still be used to investigate non-equilibrium steady states. Starting from an appropriately chosen initial condition, the rates given in Eqn.(3.2) generate a Markov process on the space of configurations which will eventually converge to the (unique) steady state.

We begin with some technical details of our simulations. The field points along the positive y-axis. To select parallel and transverse bonds with the appropriate frequency ratio Γ, we define

$$\tilde{\Gamma} = \frac{\max(\Gamma_{\parallel}, \Gamma_{\perp})}{\min(\Gamma_{\parallel}, \Gamma_{\perp})} \geq 1 \tag{3.6}$$

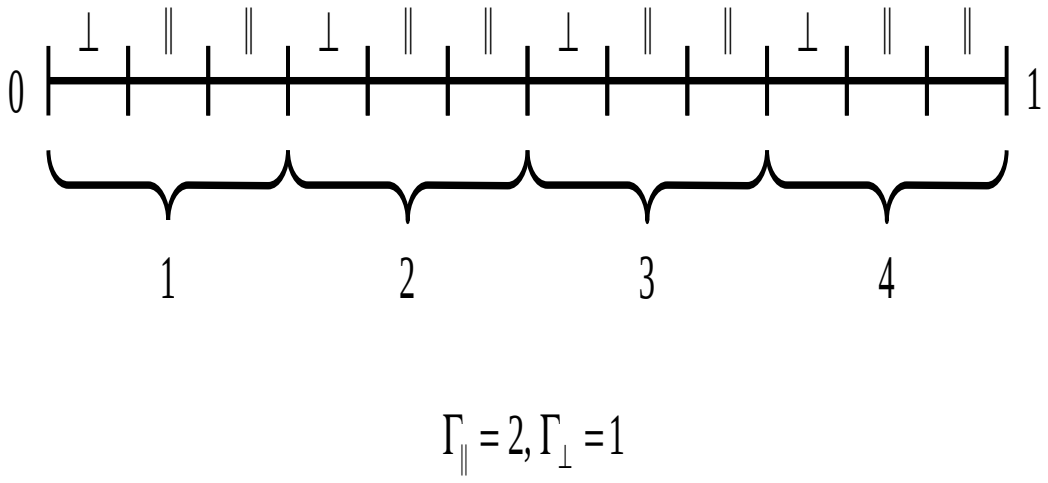

Figure 3.1: Illustration of the Monte Carlo simulation technique for a set of 4 spins

Clearly, $\tilde{\Gamma} = \Gamma$ if $\Gamma_{\parallel} \geq \Gamma_{\perp}$ and $\tilde{\Gamma} = 1/\Gamma$ otherwise. We describe the procedure for integer values of $\tilde{\Gamma}$ but it can easily be generalized to simple fractions (3/2, 5/4, 5/3, etc). We now use a single random number r, with $0 < r < 1$, to select a site and a direction (always along the positive x- or y-axis). While the details of the Fortran code are slightly different, involving manipulations with integers and careful tracking of interval boundaries, the basic idea is the following (see Fig. 3.1): Divide the interval $(0, 1)$ into $\left(1 + \tilde{\Gamma}\right) L_x L_y$ segments of equal length. Number the lattice sites $1, 2, ..., L_x L_y$ and identify the first $\left(1 + \tilde{\Gamma}\right)$ segments with site 1, the next $\left(1 + \tilde{\Gamma}\right)$ segments with site 2, etc. Now, consider the $\left(1 + \tilde{\Gamma}\right)$ segments associated with a given site, e.g., k, and assign the first of these segments to the slow direction and the remaining $\tilde{\Gamma}$ to the fast one. Now, we simply have to find the segment which contains the random number r, and we have selected a bond with the correct statistical weight. We then check the two spins on the bond, and attempt an exchange if they are different. We repeat this process $L_x L_y$ times to complete one Monte Carlo step per site (MCS).

Unless otherwise indicated, all runs start from random initial configurations. To ensure that the system has reached steady state, we monitor the time evolution of the order parameter, and discard the first M MCS. To minimize correlations between subsequent measurements, data are taken at intervals of P MCS. The table below provides numerical values for M and P, for a range of system sizes, $L_x \times L_y$, and temperatures, T. T is measured in units of the Onsager temperature and ranges between 0.8 and 1.8.

$L_x \times L_y$	MCS	M (initial)	P (data)
20×20	1.2×10^6	1.5×10^5	200
24×34	1.2×10^6	1.5×10^5	200
26×44	1.5×10^6	1.5×10^5	200
30×66	1.5×10^6	2.0×10^5	200
32×82	1.8×10^6	4.0×10^5	200
34×98	2.0×10^6	6.0×10^5	200

(3.7)

3.2.2 The phase diagram.

To probe the behavior of our system, we need to introduce several suitable observables. Due to the conservation law on the particle number (total magnetization), the system phase separates into a particle-rich strip aligned with the field. A quantity which is sensitive to any spatial structures is the structure factor which is the Fourier transform of the two-point correlation function. To be specific, we start with the Fourier transform of the local spin variable:

$$s(k_x, k_y) = \sum_{x,y} s(x, y) \exp\left[2\pi i \left(\frac{k_x x}{L_x} + \frac{k_y y}{L_y}\right)\right] \tag{3.8}$$

where $k_x = 0, 1, ...L_x$, $k_y = 0, 1, ..., L_y$ are integer wave numbers. Since strips can form anywhere in the lattice, we first eliminate the phase of this complex number. One possible definition of an order parameter would involve averages of $|s(k_x, k_y)|$; another would involve averages of $|s(k_x, k_y)|^2$. Both have their advantages: the former appears to produce slightly better data collapse in a finite-size scaling analysis (see next section) while the latter is more accessible analytically. We use the second definition here to determine the phase diagram.

When we average $|s(k_x, k_y)|^2$, we arrive at the structure factor, $S(k_x, k_y)$. Including a suitable normalization factor (see below), we define:

$$S(k_x, k_y) = \frac{1}{L_x L_y} \left\langle |s(k_x, k_y)|^2 \right\rangle \tag{3.9}$$

Strips parallel to the drive are signalled by a large value of $S(1,0)$. Thus, this quantity is a good indicator for the onset of order, and can be used as an order parameter. The normalization here is chosen such that all S approach unity in the fully disordered phase ($T \to \infty$). For the fully ordered phase (a single strip parallel to E with perfectly flat interfaces), one finds easily that all $s(k_x, k_y)$ with $k_y \neq 0$ vanish and

$$|s(k_x, 0)| = 2L_y \frac{\sin^2(\pi k_x/2)}{\sin(\pi k_x/L_x)} \tag{3.10}$$

so that

$$S(k_x, 0) = 4\frac{L_y}{L_x} \frac{\sin^4(\pi k_x/2)}{\sin^2(\pi k_x/L_x)} \tag{3.11}$$

Specifically,

$$S(1,0) = \frac{L_y}{L_x} \frac{4}{\sin^2(\pi/L_x)} \simeq \frac{4}{\pi^2} L_x L_y \tag{3.12}$$

where the far right hand side is the result of expanding the sin function for small argument. Fig. 3.2 illustrates the behavior of $S(1,0)$ as a function of temperature for a 30×66 system at $\Gamma = 1$. The transition occurs near $T \simeq 1.4$ where S begins to rise steeply as T is lowered.

Even though S will rise more steeply for larger system sizes, it will remain a smooth function for any finite system, so that it is not possible to extract a reliable estimate for the critical temperature T_c from such data. However, taking our queue from the behavior of a susceptibility in an equilibrium system, we monitor the variance of $S(1,0)$:

$$\Delta S \equiv \left\langle |s(1,0)|^4 \right\rangle - S^2(1,0) \tag{3.13}$$

For finite systems, ΔS exhibits a peak near T_c. In the thermodynamic limit, it diverges at T_c. Fig. 3.3 shows ΔS for a 30×30 system, with $\Gamma = 1$. For the purposes of obtaining a phase diagram, we approximate the true critical temperature by the temperature where the fluctuations reach their peak.

Restricting ourselves to 30×30 systems, we measure the structure factor and its fluctuations. For a given value of Γ, we take data over a range of temperatures in steps of 0.025. For the purposes of obtaining a qualitative phase diagram, we approximate the true critical temperature by the temperature – labelled as $T_c(\Gamma)$ – where the fluctuations reach their peak. To have the standard model appear at the center of each graph, we choose $\ln \Gamma$ (as opposed to Γ) for the horizontal axis. Our results are shown in Fig. 3.4 and can be summarized as follows:

i) For the whole range of investigated Γ's, $0.04 < \Gamma < 30$, the system undergoes a phase transition. As the temperature is lowered, the system goes from a disordered phase into an ordered phase, with particles arranged in a strip parallel to the drive.

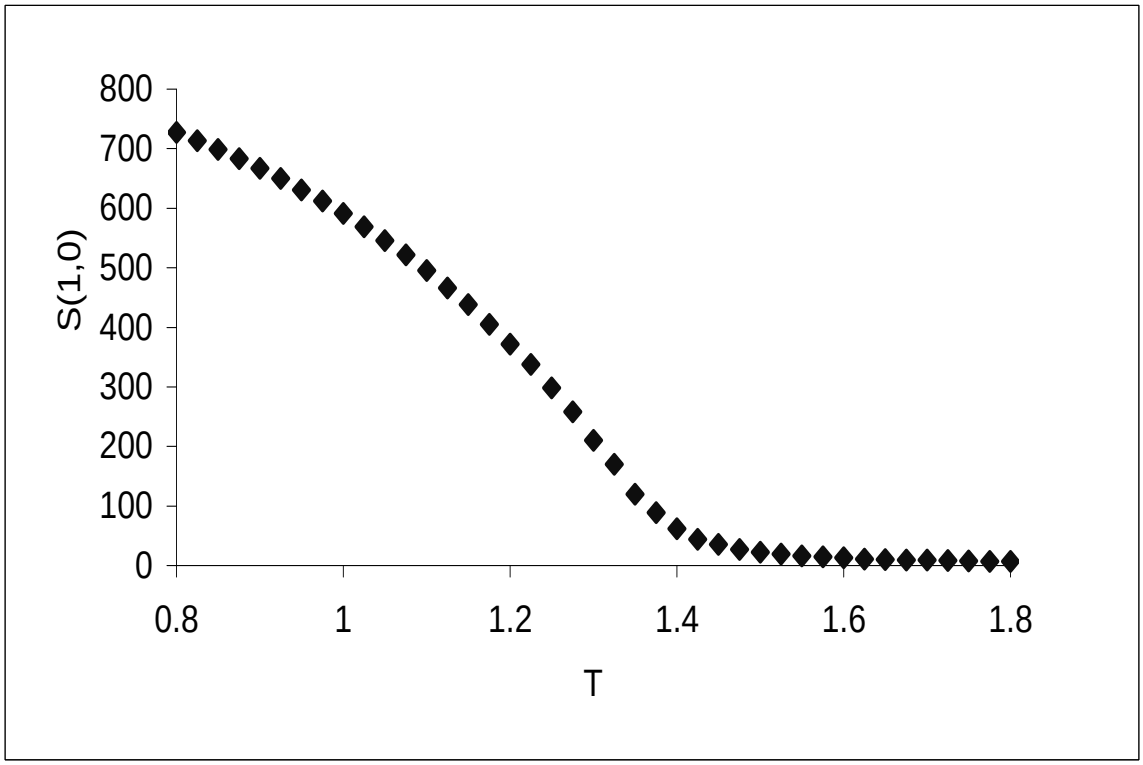

Figure 3.2: The behavior of the structure factor $S(1,0)$ as a function of temperature for a 30×66 system at $\Gamma = 1$

ii) The critical temperature depends on the ratio Γ, which is a measure of the anisotropy in the jump rates.

iii) The critical temperature reaches a maximum near $\Gamma \simeq 1/2$ and then decreases on both sides, but with different slopes. For $\Gamma > 1$, $T_c(\Gamma)$ decreases faster than for $\Gamma < 1/3$. We attempted to determine the location of the maximum more precisely, by performing longer runs at $\Gamma = 1$, $1/2$, and $1/3$, and by interpolating additional values of Γ, but $T_c(\Gamma)$ is so flat in this region that we could not reach a more reliable estimate using just ΔS.

3.2.3 A finite size scaling study

Having established a qualitative phase diagram, we turn to the question of critical behavior. The universal properties of the standard model have been explored extensively, using both Monte Carlo simulations [7] and analytic methods [17, 18]. Here,

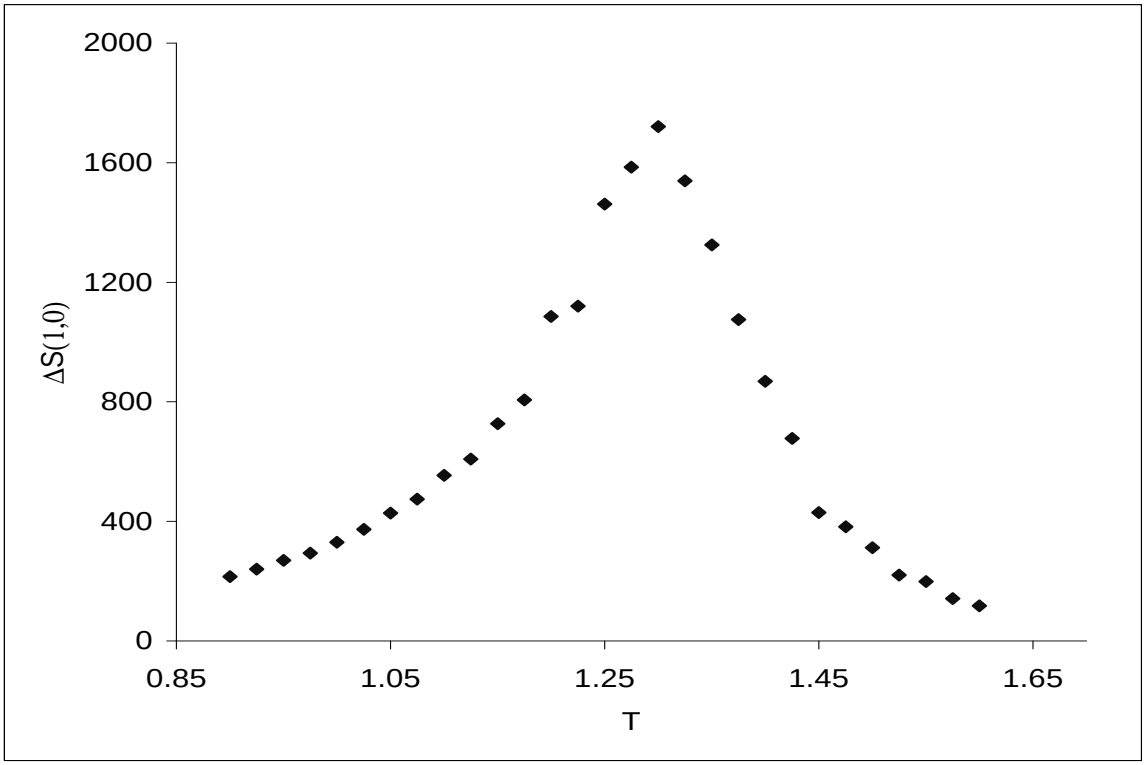

Figure 3.3: The variance of of the structure factor $S(1,0)$ as a function of temperature for a 30×30 system, with $\Gamma = 1$

we will focus on the vicinity of the critical point for two values of Γ, namely $\Gamma = 2$ and $\Gamma = 1/2$, to test whether the critical properties of these systems are in the same universality class as those of the standard model ($\Gamma = 1$). Data for the latter are presented for comparison. We will assume that the critical properties remain unaffected by having anisotropic rates, and hence, we will use the well known critical exponents of the standard model when analyzing data for $\Gamma \neq 1$. If the scaling collapse is as good or better, our assumption will be vindicated. Otherwise, poor data collapse should signal novel universal behavior.

It is well known that the singularities in the thermodynamic functions associated with the critical point occur only in the thermodynamic limit, when all the dimensions of the system go to ∞. If some of them remain finite, the thermodynamic behavior is modified. A central task in the interpretation of Monte Carlo data, when studying phase transitions, is to extrapolate to the thermodynamic limit from results for relatively small systems. The most widely used method of extrapolation to larger sizes is based on phenomenological finite size scaling.

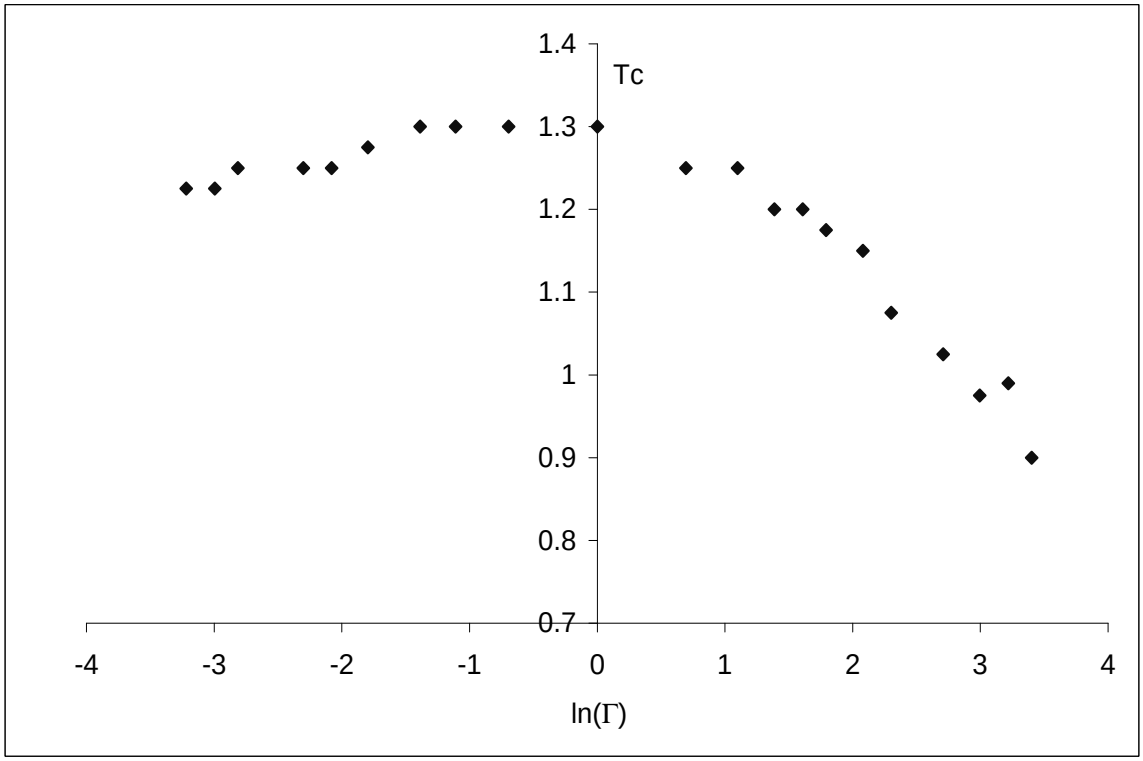

Figure 3.4: Phase diagram for a 30×30 lattice gas with anisotropic jump rates, showing the dependence of the critical temperature on the rate anisotropy, $\ln(\Gamma)$

The earliest studies [7, 43, 37] involved isotropic finite size scaling, performed on lattices with square dimensions $L_x = L_y$, following the standard routines in analyzing equilibrium systems. These studies led to critical exponents quite different from those which were predicted by field theoretic methods [17, 18]**.** Moreover, the field theory studies[17, 18] indicate that the driven lattice gas is characterized by *strong anisotropy*, i.e., wave vectors transverse and parallel to the drive should scale with different powers: $k_{\|} \sim k_{\perp}^{1+\Delta}$. Here, Δ is a new "anisotropy" exponent, with $\Delta = 2$ in two dimensions, according to the field theoretic prediction. Thus, Monte Carlo simulations should naturally be performed on lattices whose dimensions $L_y \equiv L_{\|}$ (parallel to E) and $L_x \equiv L_{\perp}$ (transverse to E) obey the field theoretic length scaling. Specifically, it was pointed out in [21] that the shape factor,

$$\mathcal{S} \equiv \frac{L_{\|}}{L_{\perp}^{1+\Delta}} \tag{3.14}$$

should remain constant as part of a careful anisotropic finite size scaling analysis. Under these conditions, most observables (with only one notable exception which we

will discuss below) produce good data collapse, consistent with the field theoretic predictions for the critical exponents, namely

$$\beta = \frac{1}{2},\ \gamma = 1,\ \nu_{\parallel} = \frac{3}{2},\ \nu_{\perp} = \frac{1}{2},\ \Delta = 2 \tag{3.15}$$

The interpretation of these exponents is the same as in equilibrium second-order phase transitions: β is the exponent with which the order parameter vanishes when the system approaches criticality, γ gives us the critical behavior of the susceptibility, and ν is related to the correlation length. Since our system is highly anisotropic, we have two correlation lengths, parallel and transverse to the field, and therefore two critical exponents, $\nu_{\parallel}$ and $\nu_{\perp}$.

The finite size scaling study was conducted for a shape factor

$$\mathcal{S} = \frac{L_{\parallel}}{L_{\perp}^{1+\Delta}} = 0.135 \tag{3.16}$$

In the following, we use the order parameter of Binder and Wang [45] and Leung [21] which involves a suitably normalized average of $|s(1,0)|$. Demanding that this order parameter should equal unity for a perfectly ordered strip parallel to E (cf. Eqn.(3.10)) we define

$$\tilde{s}(1,0) = \frac{\sin(\pi/L_x)}{2L_y}\ |s(1,0)| \tag{3.17}$$

so that the order parameter is just $\langle \tilde{s}(1,0) \rangle$. In the following, we will usually suppress the arguments.

A quantity that has proven very useful in determining the critical temperature is the Binder (fourth-order) cumulant, defined as:

$$g = 2 - \frac{\langle \tilde{s}^4 \rangle}{\langle \tilde{s}^2 \rangle^2} \tag{3.18}$$

The fourth-order cumulant goes from 0 to 1 as the temperature goes from ∞ to 0. A typical plot is shown in Fig. 3.5.

We collected data for $\langle \tilde{s} \rangle$ and g for three values of Γ (2, 1, and 1/2) and a range of system sizes consistent with fixed shape factor: 20×20, 24×34, 26×44, 30×66, 32×82, and 34×98. Larger system sizes would have been highly desirable but were outside our computational resources.

Before measuring any critical exponents, we first need a reliable estimate for the critical temperature. For the standard model, the best estimate is due to Wang [46]:

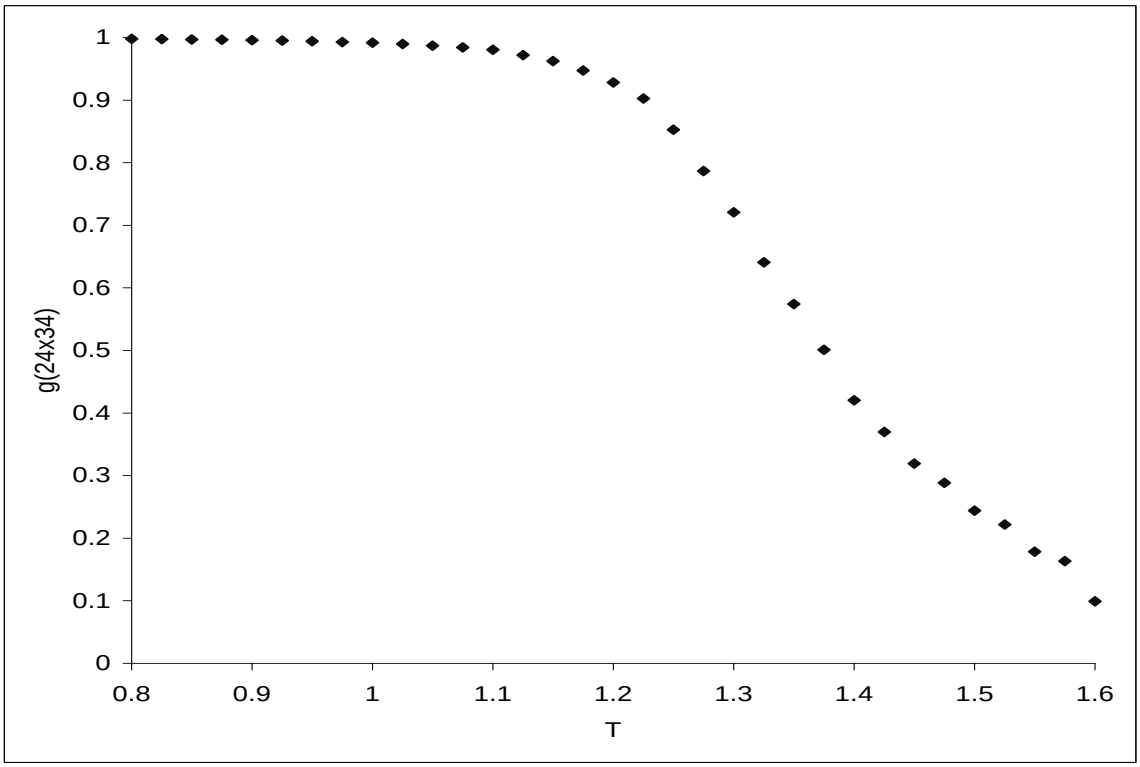

Figure 3.5: A typical plot for the Binder cumulant as a function of temperature for a 24×34 system with $\Gamma = 2$

$T_c = 1.408 \pm 0.004$. This value is the result of high precision measurements, and we will use it as a benchmark for our data. Earlier estimates ranged from 1.3 ± 0.01 by Achahbar and Marro [10] and 1.355 ± 0.003 by Valles and Marro [37] to Leung's result [21] 1.418 ± 0.005. Of course, we could monitor the "susceptibility", i.e., the fluctuations of the order parameter, and identify the peak location with T_c. This method is relatively fast and was therefore exploited in our search for a qualitative phase diagram. However, it is not accurate enough for our purposes here. A much more reliable method exploits the known fact [28] that, if scaling is obeyed, different fourth-order cumulant curves for different system sizes should intersect at exactly the same temperature, namely, T_c. Fig. 3.6 and Fig.3.8 show the Binder cumulants for $\Gamma = 2$ and $\Gamma = 1/\dot{2}$. Our data for $\Gamma = 1$ (see Fig. 3.7) are provided as a benchmark.

These data in conjection with the scaling plots to be presented below, lead to the

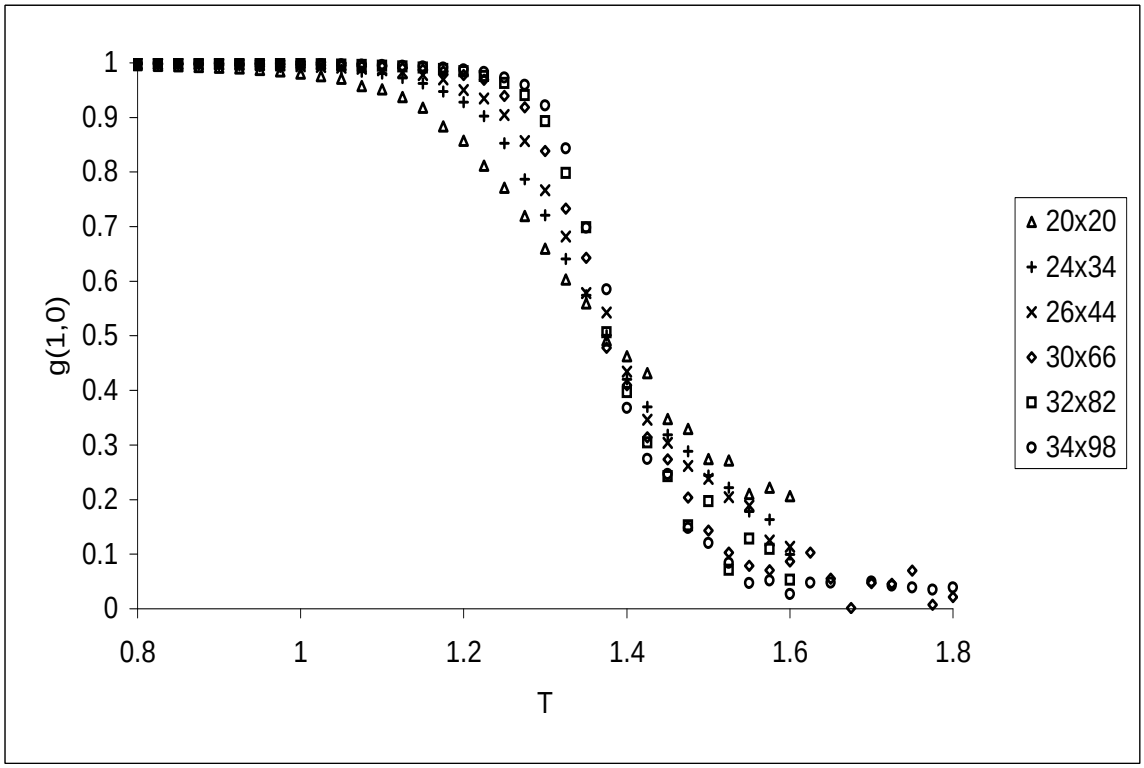

Figure 3.6: Finding the critical temperature as the intersection point of the Binder cumulants for a shape factor S=0.135 and $\Gamma = 2$

following estimates for $T_c(\Gamma)$:

$$\begin{aligned} T_c(2) &= 1.395 \pm 0.005 \\ T_c(1) &= 1.418 \pm 0.005 \\ T_c(1/2) &= 1.390 \pm 0.005 \end{aligned} \tag{3.19}$$

We note that our value for $T_c(1)$ is 1.418 ± 0.005 compared to Wang's estimate of 1.408 ± 0.004. We have a very good agreement with the result reported by Leung [21]. We recall our values from the phase diagram obtained for the 30×30 system:

$$\begin{aligned} T_c(2) &\simeq 1.25 \\ T_c(1) &\simeq 1.30 \\ T_c(1/2) &\simeq 1.30 \end{aligned} \tag{3.20}$$

First, we notice that the values for the 30×30 system are lower, an expected feature since our estimates using the finite-size scaling are made for the infinite system.

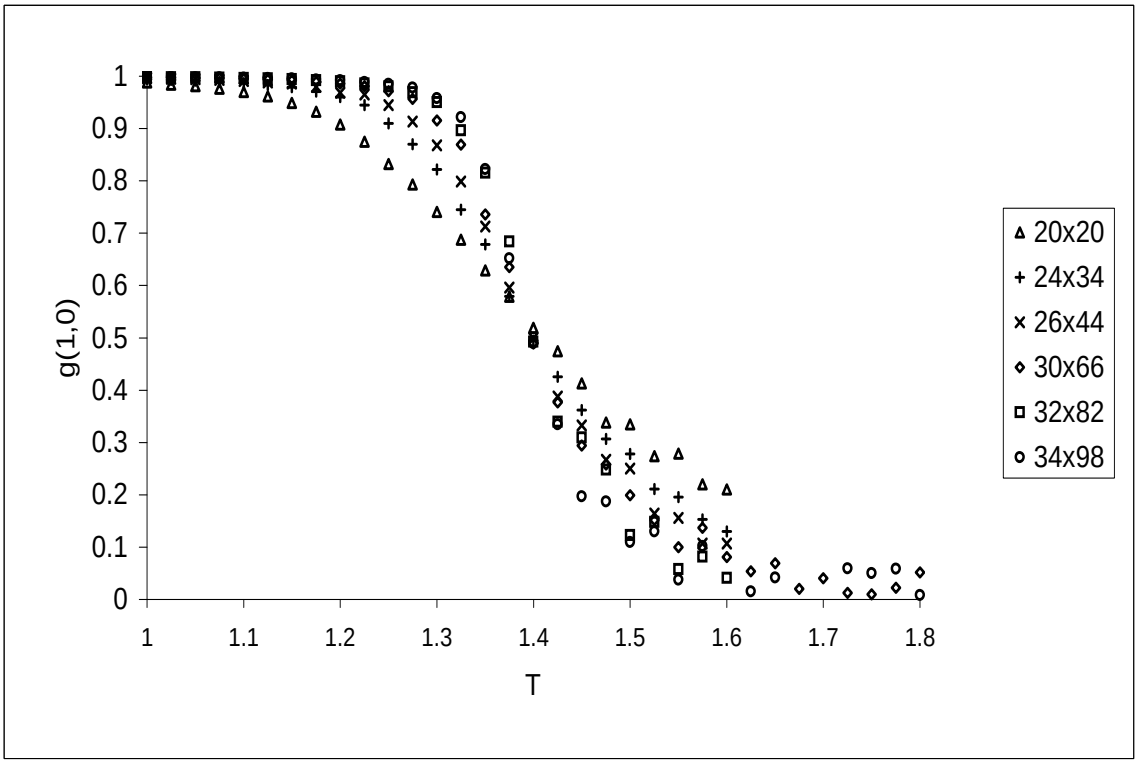

Figure 3.7: Finding the critical temperature as the intersection point of the Binder cumulants for a shape factor S=0.135 and $\Gamma = 1$

Second, we can see that the critical temperature estimated in the thermodynamic limit decreases with a different slope than the one for the 30×30 lattice.Third, we should mention that the finite-size scaling technique is a lot more accurate in estimating the critical temperature than our study of the 30×30 system.

These values (Eqn.(3.19)) will enter the finite size scaling forms which we will need below.

To test whether the model with anisotropic exchange rates is still in the same universality class as the standard model, we plot the fourth order cumulant and the order parameter in scaled form, using the critical exponents of the standard model, Eqn.(3.15). We introduce the scaled temperature

$$T_s(\Gamma) = L_{\|}^{1/\nu_{\|}}(T - T_c(\Gamma))/T_c(\Gamma) \tag{3.21}$$

Assuming that the usual finite size scaling forms are obeyed, the Binder cumulant

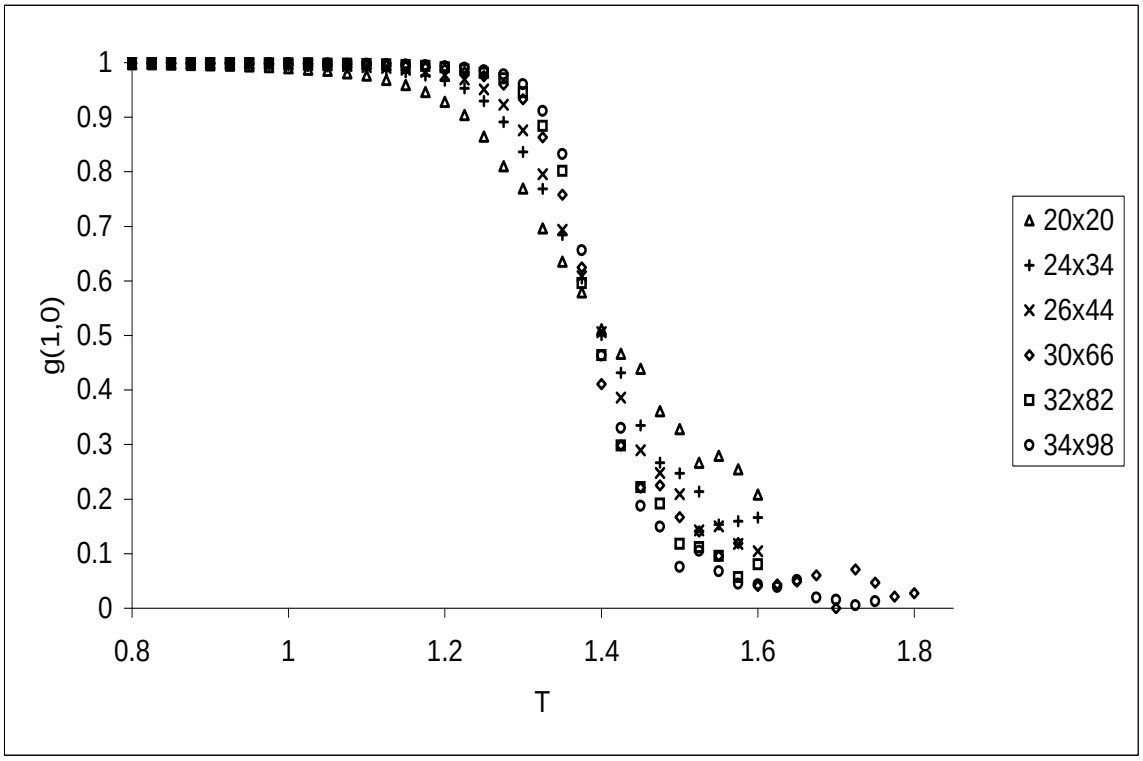

Figure 3.8: Finding the critical temperature as the intersection point of the Binder cumulants for a shape factor S=0.135 and $\Gamma = 0.5$

should depend only on the scaled temperature T_s and the shape factor $\mathcal{S}$:

$$g(T, L_\parallel, L_\perp) = \widetilde{g}(T_s, \mathcal{S}) \tag{3.22}$$

As a result, data for g, taken at fixed $\mathcal{S}$, should all fall on the same universal curve (denoted by $\widetilde{g}$) when plotted against the scaled temperature. To minimize deviations from scaling, we must ensure that our data carry only small statistical errors and are taken in a sufficiently narrow window around T_c, the critical region. In addition, there are always unknown corrections to scaling.

In Figs. 3.9, 3.10, and 3.11 we show $\widetilde{g}(T_s, S)$ vs T_s, for three values of Γ. The quality of data collapse for $\Gamma \neq 1$ is comparable to that for $\Gamma = 1$, supporting our conjecture that Γ does not affect universal properties.

This conclusion is further borne out by our data for the order parameter. Here, again, we anticipate scaling, of the following form:

$$\langle \tilde{s} \rangle (T, L_\parallel, L_\perp) = L_\parallel^{\beta/\nu_\parallel} \Phi_\pm(T_s, \mathcal{S}) \tag{3.23}$$

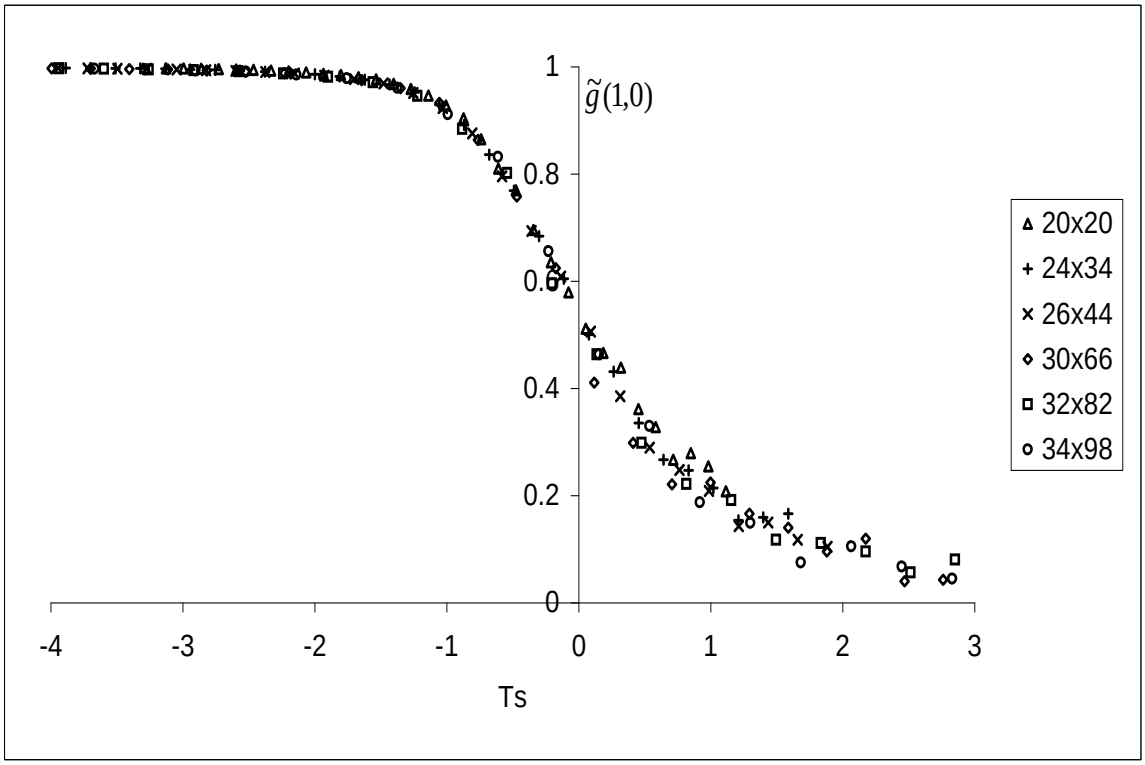

Figure 3.9: Binder cumulants as a function of the scaled temperature for a shape factor S=0.135, $\Gamma = 0.5$ and a critical temperature $T_c = 1.390$

Thus, we should plot our data for $L_{\|}^{-\beta/\nu_{\|}} \langle \tilde{s} \rangle$, taken at fixed $\mathcal{S}$, vs the scaled temperature, T_s. Here, data points taken below the critical temperature should fall onto a scaling curve Φ_-, while data taken above T_c follow a different curve, Φ_+. Our results for three values of Γ are presented in Figs. 3.12, 3.13, and 3.14. The upper (lower) branch corresponds to data from $T < T_c$ ($T > T_c$). Clearly, the data collapse is quite good on the high-temperature branch, but not nearly as satisfactory on the low-temperature branch. The latter feature, however, is not limited to data at $\Gamma \neq 1$, as Fig. 3.12 demonstrates. In fact, all good quality data for the standard model show these characteristic deviations from scaling which plague only the order parameter, and only data taken below T_c. At present, their origin is not well understood. In any case, their appearance for $\Gamma \neq 1$ does not invalidate our conjecture regarding universal behavior.

In conclusion, the Monte Carlo simulations helped us arrive at the following results:

i) Choosing an appropriate structure factor and monitoring its fluctuations, we found

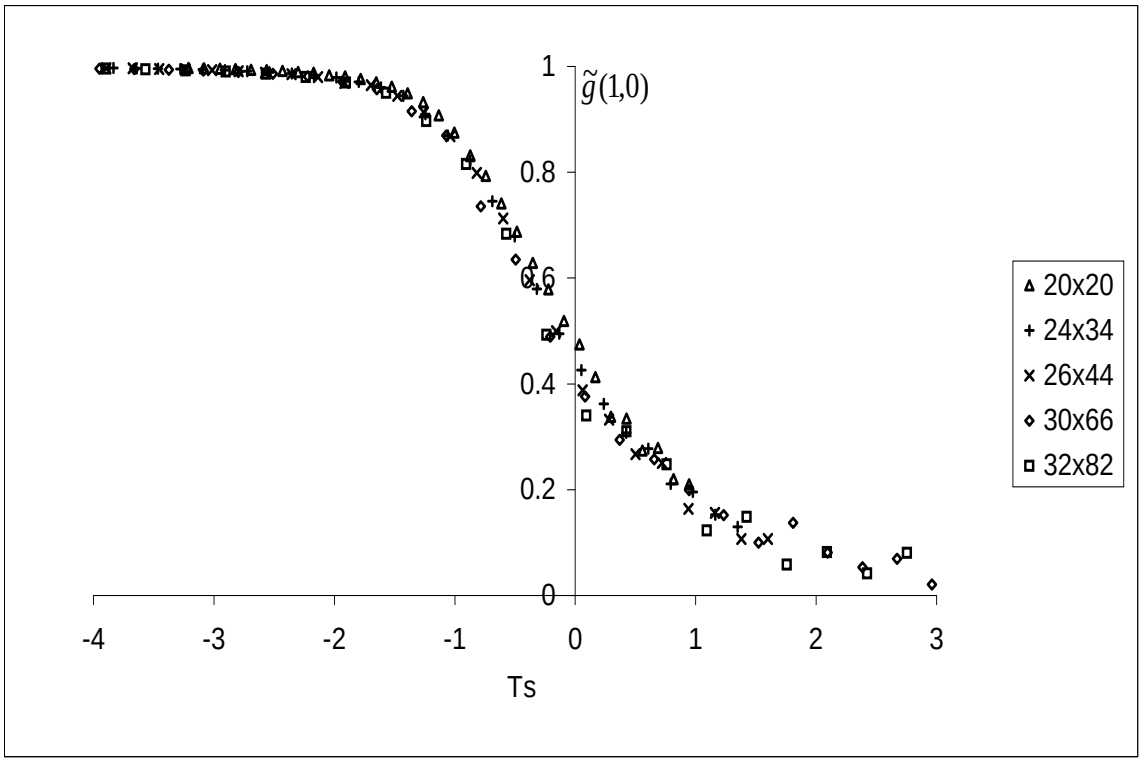

Figure 3.10: Binder cumulants as a function of the scaled temperature for a shape factor S=0.135, $\Gamma = 1$ and a critical temperature $T_c = 1.418$

that, for a large range of Γ's, the system undergoes a second order phase transition from a disordered phase to an ordered phase, with particles arranged in a strip parallel to the drive.

ii) To obtain a qualitative phase diagram, the critical temperature was identified with the temperature where the fluctuations of the structure factor reach their peak. As a function of Γ, the critical temperature of the system has a maximum near $\Gamma = 1$, and slowly decreases for both $\Gamma > 1$ and $\Gamma < 1$. Our data indicate quite clearly that the slope of the decrease is different for the two regions.

iii) An anisotropic finite-size scaling study was performed for three values of Γ, namely 1/2, 1, and 2, in an effort to explore the universal properties of our model. We monitored the fourth-order cumulant and a suitably defined order parameter. Our conclusion is that all three system fall into the same universality class, namely, that of the standard model: the critical exponents agree and the scaling assumptions [21, 46] are obeyed.

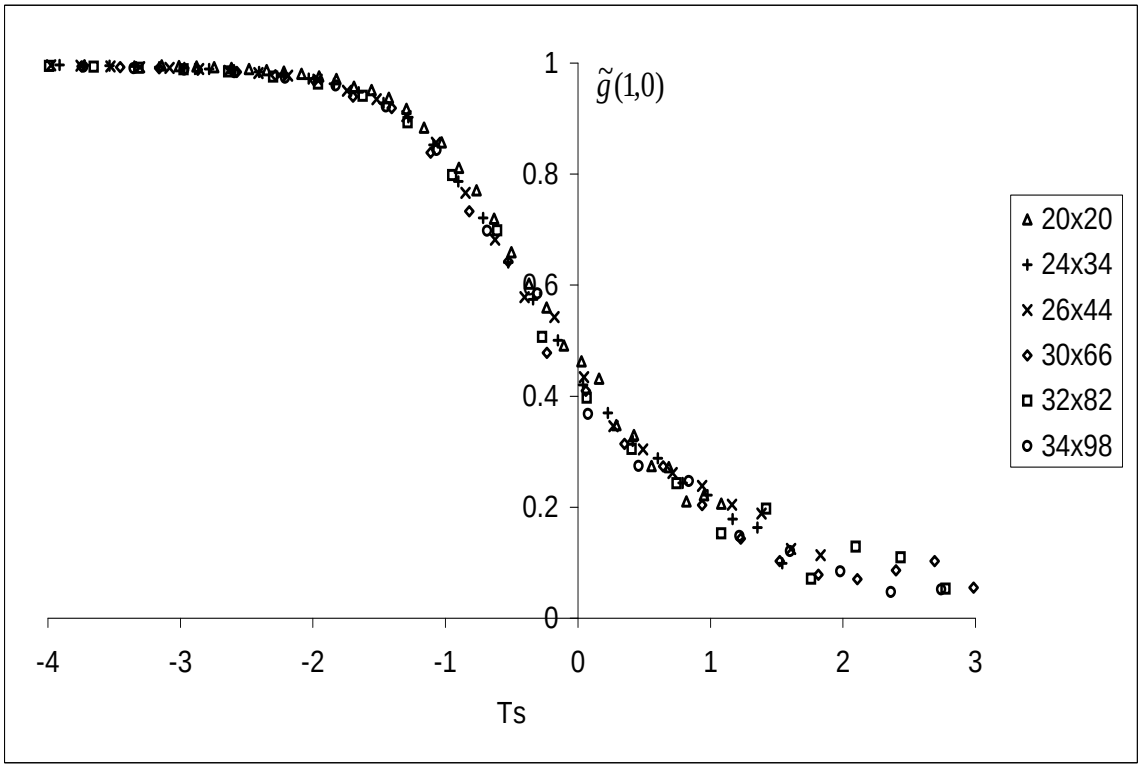

Figure 3.11: Binder cumulants as a function of the scaled temperature for a shape factor S=0.135, $\Gamma = 2$ and a critical temperature $T_c = 1.395$

In the next section, we perform a high temperature expansion for this model in order to provide an additional point of view.

3.3 The phase diagram(high temperature expansion approach)

Since this method was already described in our studies of the bilayer system in the previous chapter, we need not provide all the details here. Again, we begin with the master equation, and write down the equation of motion for the two-point correlation functions $G(\vec{r}-\vec{r}\,') = \langle \sigma_{\vec{r}} \sigma_{\vec{r}\,'} \rangle$. Here, we restrict ourselves to infinite E, for simplicity. After expanding terms $\exp(-\beta \Delta H)$ for small nearest neighbor coupling constant βJ_0, we arrive at a set of equations describing the steady state. The resulting equations

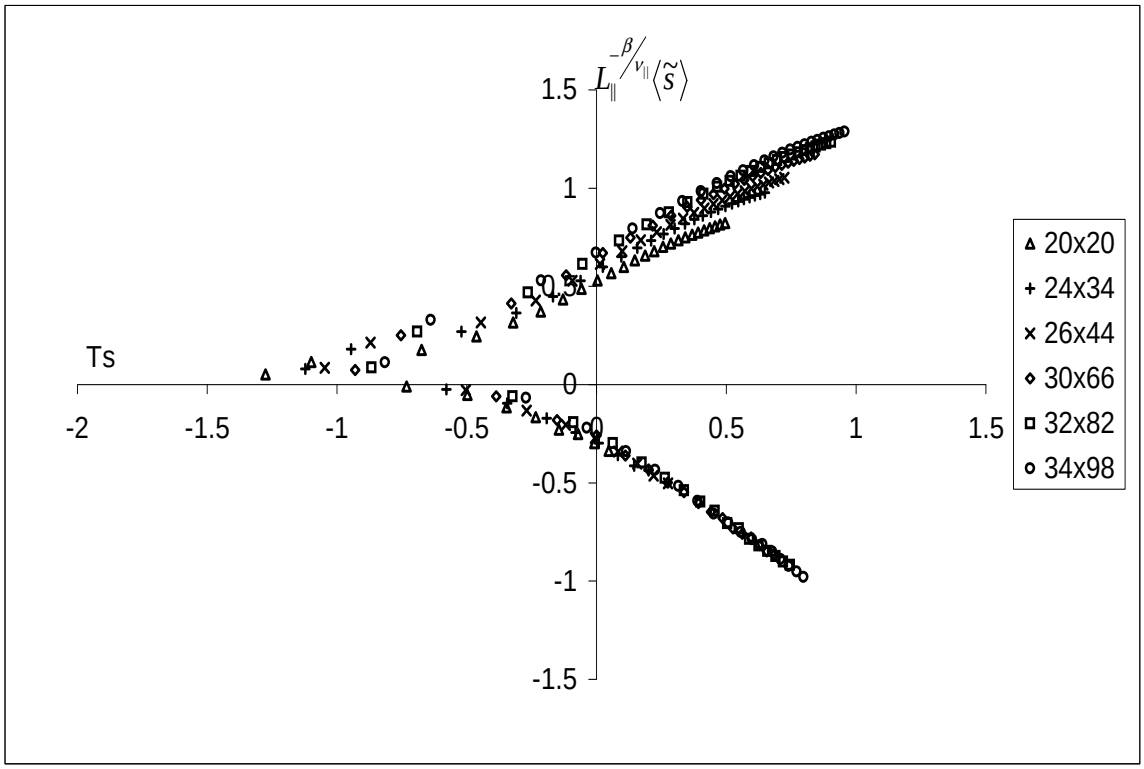

Figure 3.12: The dependence of the scaled order parameter on the scaled temperature for a shape factor S=0.135, $\Gamma = 0.5$ and a critical temperature $T_c = 1.390$

depend on two parameters:

$$\begin{aligned} \Gamma &= \frac{\Gamma_{\parallel}}{\Gamma_{\perp}} \\ K_0 &= \beta J_0 \end{aligned} \tag{3.24}$$

and take the form:

$$\begin{aligned} 0 &= \Gamma[G(2,0) - G(1,0)] + 4[G(1,1) - G(1,0)] + 4K_0 \\ 0 &= 2\Gamma[G(1,1) - G(0,1)] + 2[G(0,2) - G(0,1)] + 2K_0 \\ 0 &= \Gamma[G(2,1) + G(0,1) - 2G(1,1)] + 2[G(1,2) + G(1,0) - 2G(1,1)] - 2K_0 \\ 0 &= \Gamma[G(3,0) + G(1,0) - 2G(2,0)] + 4[G(2,1) - G(2,0)] \end{aligned} \tag{3.25}$$

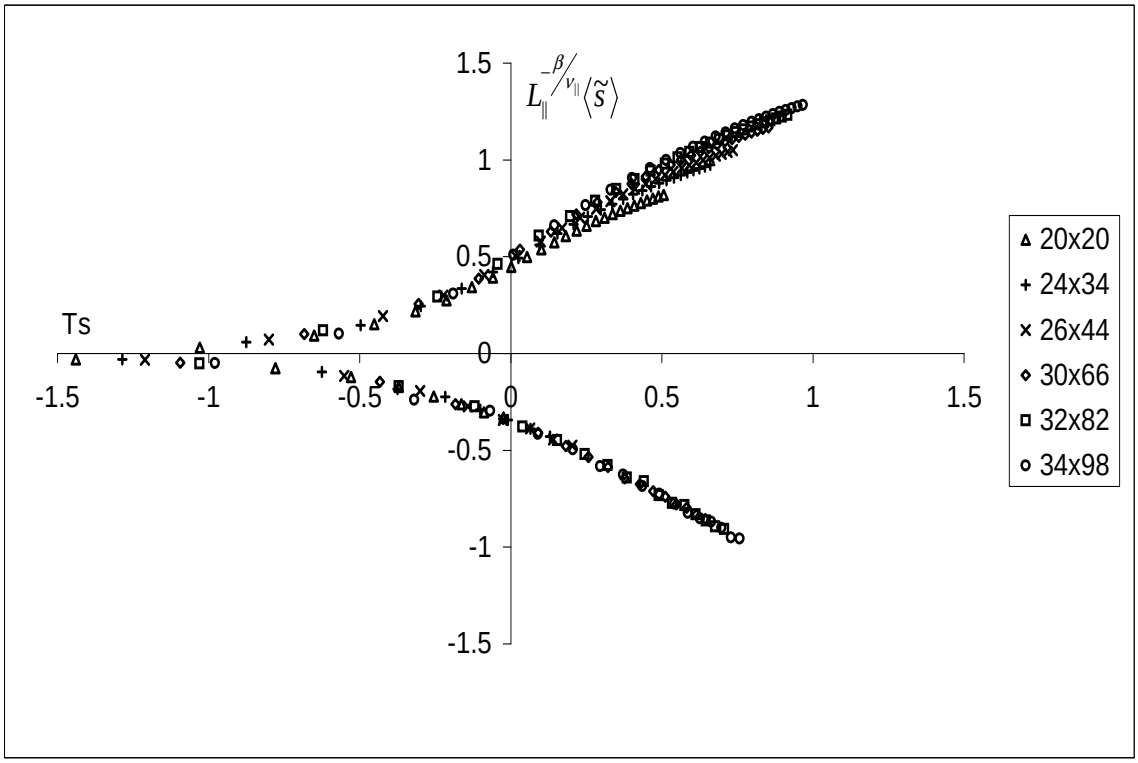

Figure 3.13: The dependence of the scaled order parameter on the scaled temperature for a shape factor S=0.135, $\Gamma = 1$ and a critical temperature $T_c = 1.418$

$$0 = 2\Gamma[G(1,2) - G(0,2)] + 2[G(0,3) + G(0,1) - 2G(0,2)] - 2K_0$$

$$0 = \Gamma[G(i+1,j) + G(i-1,j) - 2G(i,j)] + 2[G(i,j+1) + G(i,j-1) - 2G(i,j)]$$

In solving the system we follow closely the method presented in [39] which was outlined in the previous chapter.

We introduce the *structure factor* as the Fourier transform of the correlation function:

$$S(k,p) \equiv \sum_{x,y=-\infty}^{\infty} G(x,y)e^{-i(kx+py)} \tag{3.26}$$

Writing the structure factor as

$$S(k,p) = \overline{S} + \widetilde{S}(k,p) \tag{3.27}$$

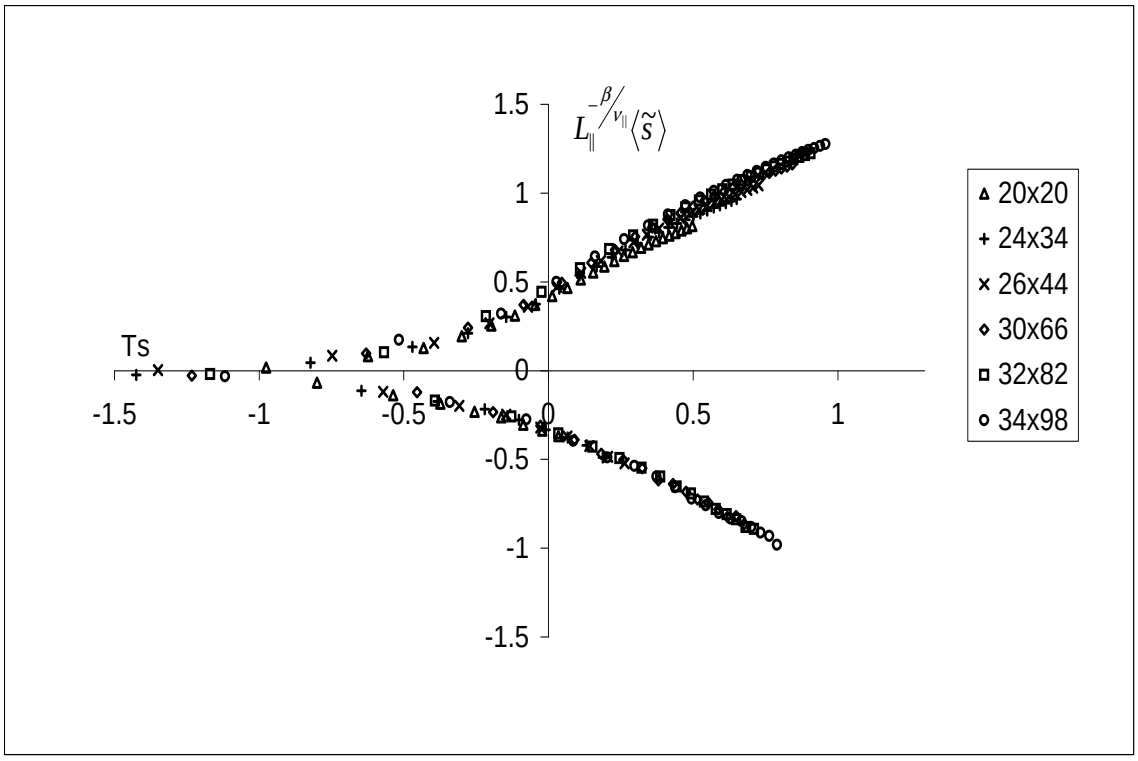

Figure 3.14: The dependence of the scaled order parameter on the scaled temperature for a shape factor S=0.135, $\Gamma = 2$ and a critical temperature $T_c = 1.395$

with $\overline{S} = 1$ being the zeroth order solution, we focus on $\tilde{S}(k, p, q)$, because this is the quantity which carries information about the interactions. The inverse transform has the following form:

$$G(x, y) = \int S(k, p) e^{i(kx+py)} \tag{3.28}$$

where the unlabelled integral sign stands for:

$$\int \equiv \frac{1}{(2\pi)^2} \int_{-\pi}^{\pi} dk \int_{-\pi}^{\pi} dp \tag{3.29}$$

With the following notations in mind:

$$\begin{aligned} \delta &= 2\Gamma(1 - \cos k) + 4(1 - \cos p) \\ I_1 &= \int \tilde{S}(1 - \cos(k)) \\ I_2 &= \int \tilde{S}(1 - \cos(p)) \end{aligned} \tag{3.30}$$

The system can be rewritten as:

$$\begin{aligned} 2\Gamma I_1 + 4I_2 &= \int S\delta \\ 4K_0 - \Gamma I_1 &= \int S\delta \exp(ik) \\ 2K_0 - 2I_2 &= \int S\delta \exp(ip) \\ -2K_0 &= \int S\delta \exp(i(k+p)) \\ 0 &= \int S\delta \exp(2ik) \\ -2K_0 &= \int S\delta \exp(2ip) \\ 0 &= \int S\delta \exp(i(kx+py)) \end{aligned} \tag{3.31}$$

We briefly mention here the steps we followed in finding the structure factor and the critical temperature (see [39] for more details):

i) We invoke the completeness relation (Appendix, [39]) in order to find $\tilde{S}$ as an implicit function of I_1 and I_2 :

$$\tilde{S} = \frac{L(k,p)}{\delta(k,p)} \tag{3.32}$$

ii) We determine I_1 and I_2. For this purpose, we need two linearly independent equations. One of the equations will come from the fact that $G(0,0) = 1$ and the remaining one is just the definition of I_1:

$$\begin{aligned} 0 &= \int \frac{L}{\delta} \\ 0 &= -I_1 + \int \tilde{S}(1-\cos(k)) \end{aligned} \tag{3.33}$$

These equations can be solved.

iii) We estimate the critical temperature. Using the same argument as in [39], we match our expansion for the structure factor with the form known from field-theoretic

considerations. Specifically, we seek zeroes of S^{-1}. The latter should take the form [39]:

$$S^{-1}(k,p) = \frac{\tau_{\|}k^2 + \tau_{\perp}p^2 + O(k^4, p^4, k^2p^2)}{n_{\|}k^2 + n_{\perp}p^2} \tag{3.34}$$

where $n_{\|} > 0$ and $n_{\perp} > 0$ are measures of thermal noise in the longitudinal and transverse directions, and $\tau_{\|}$ and $\tau_{\perp}$ are the anisotropic diffusion coefficients. We identify the critical temperature by the vanishing of the anisotropic diffusion coefficient $\tau_{\perp}$ (see [39]):

$$\tau_{\perp} = (1 - I_2 - 5K_0) \tag{3.35}$$

Using this method, we find the critical temperature for a large range of Γ's, both larger and less than 1. Below, we present the phase diagram (Fig. 3.15) obtained using this approximation. Here, the match between the simulations and the high temperature study is not very good. For $\Gamma < 1$, the two phase diagrams agree qualitatively, but for $\Gamma > 1$, the expansion predicts a rise of the critical temperature with Γ, in contrast to the simulation study. The origin of this discrepancy remains to be explored.

3.4 Conclusions

We studied a variation of the standard model, namely the two-dimensional driven diffusive lattice with anisotropic exchange rates employing two different methods. The first one was an extensive Monte Carlo study which also included a finite-size scaling approach. We found the phase diagram for a large range of Γ's, and tested different scaling assumptions. The conclusion is that the new model belongs to the same universality class as the standard model, and its critical temperature $T_c(\Gamma)$ has a maximum at $\Gamma \simeq 1$. The second method was an analytical study using the high temperature expansion approximation. The match between the two methods is not very satisfactory. Further studies should elucidate the origin of the mismatch, in order to obtain better insights into the reliability of the high temperature expansion.

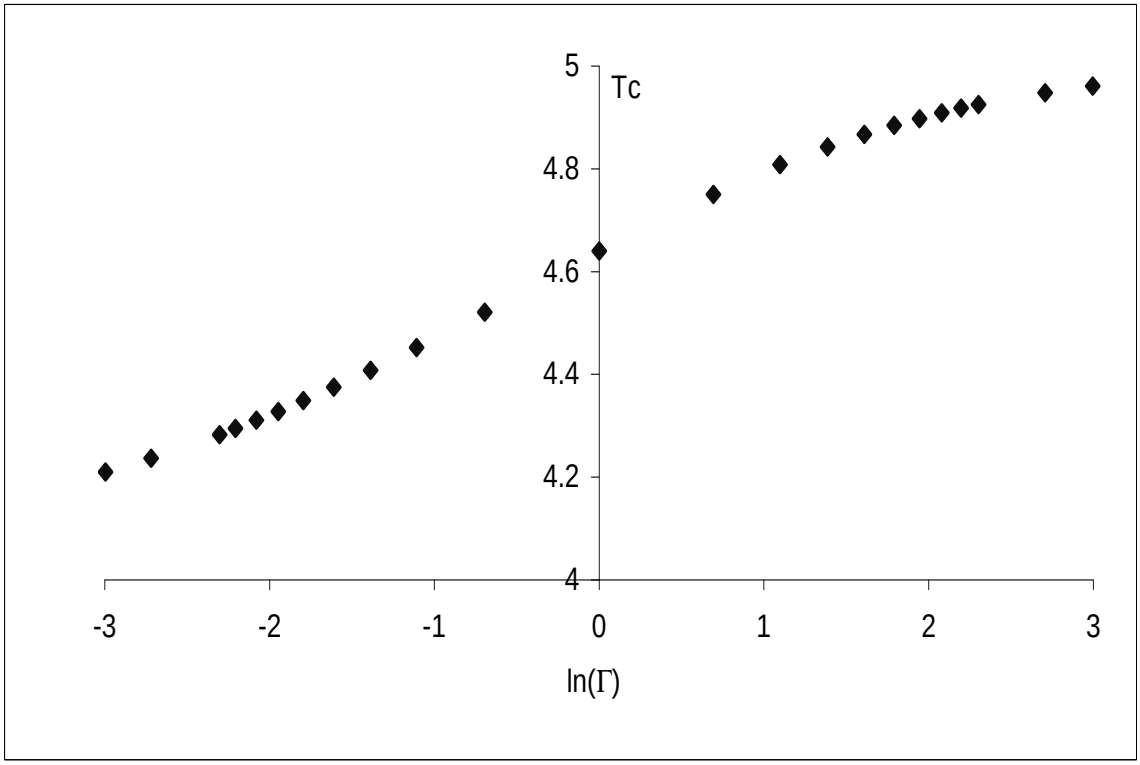

Figure 3.15: Phase diagram in the high temperature series expansion for a two dimensional lattice gas with anisotropic jump rates

Chapter 4

Exact solutions for small systems

In this chapter, we will present briefly some *exact solutions* for the steady state probability distribution in a related non-equilibrium system, namely, the two-temperature kinetic Ising model. The main difference to the models considered in the previous chapters is the absence of the conservation law: spins can flip individually, as opposed to only exchanging places with a neighbor. Due to the complexity of many-body systems, exact results can only be obtained in exceptional cases, such as systems containing only a few degrees of freedom. Nevertheless, such a calculation provides a glance at the microscopic level dynamics of small systems and, hopefully, some pointers regarding the non-equilibrium steady state behavior of larger systems. Solving the master equation is a very difficult task, virtually impossible as the system size increases. In the following section we are presenting some sample calculations and results for a 1×6 lattice. It is fascinating to discover the completely different probability spectrum when we switch from equilibrium to non-equilibrium systems by turning on a non-equilibrium perturbation. We start by defining the model and then present some of the exact results.

4.1 The model

Our model is a one dimensional version of the two-temperature kinetic Ising model. Examples of "multi-temperature systems" are all around us, for example a water tank with an immersion heater. Imagine a set of sites arranged on a circle. Each site i can be full or empty, and in order to describe a particular configuration we define a set of occupation numbers n_i, n_i being 0 for an empty site and 1 for an occupied

site. We can also use the spin language notation $\sigma_i = 2n_i - 1$, with $\sigma_i = 1$ for a full cell and $\sigma_i = -1$ for an empty cell. We consider an even number of sites and impose periodic boundary conditions in such a way that $\sigma_{N+1} = \sigma_1$. The spins are in contact with *two* heat baths at *different* temperatures T_e and T_o, in such a way that spins on even lattice sites experience T_e and those on odd sites, T_o. Imposing $T_e \neq T_o$ drives the system out of equilibrium: each heat bath tries to drive the system towards equilibrium with the same Hamiltonian but at its own temperature [1]. As a result, energy flows from one sublattice to the other and the steady state is a nonequilibrium one.

We endow the spins with nearest-neighbor interactions, according to the usual Ising Hamiltonian:

$$H = -J \sum_i \sigma_i \sigma_{i+1} \tag{4.1}$$

The dynamics is modelled by a generalization of the familiar Glauber rates [47]. The n-th spin is flipped with a rate, on a time scale τ, of

$$w_n(\{\sigma\}) = \frac{1}{2\tau}\left(1 - \frac{\gamma_n}{2}\sigma_n\left(\sigma_{n+1} + \sigma_{n-1}\right)\right) \tag{4.2}$$

where $0 \leq \gamma_n \leq 1$ is related to the local temperature according to

$$\gamma_n = \begin{cases} \tanh(\dfrac{2J}{k_B T_e}) & n \text{ even} \\ \text{for} & \\ \tanh(\dfrac{2J}{k_B T_o}) & n \text{ odd} \end{cases} \tag{4.3}$$

We should mention here that, unlike all the other models discussed in the previous chapters, this model is a non-conserved one, since it is governed by a spin-flip (as opposed to exchange) dynamics.

These rates are invariant under a global spin flip $\{\sigma\} \to \{-\sigma\}$ and under translations by an even number of sites $\sigma_n \to \sigma_{n+2j}$ for all n, $j = 1, 2, ..N$ (translational invariance modulo 2). Therefore, we expect the same symmetries to hold for the steady state distribution $P^*(\{\sigma\})$, namely, $P^*(\{\sigma\}) = P^*(\{-\sigma\})$ and $P^*(\{\sigma_n\}) = P^*(\{\sigma_{n+2j}\})$

When the two heat baths have the same temperature, $T_e = T_o = T$, the above Hamiltonian and rates define the exactly solvable Glauber model [47] which relaxes to the equilibrium state of the Ising model.

The non-equilibrium version of this one-dimensional kinetic model was well studied [27, 48] . The two-spin steady-state correlations were obtained exactly and related

to the average energy and the energy flux between the two sublattices. Here, we attempt to find an exact expression for the *full* probability distribution, but at the price of restricting ourselves to very small systems. However, the comparison with the equilibrium distribution is still quite interesting.

Below we show the principal steps of the calculations and the most significant results.

4.2 Equivalence classes

As usual, we start with the master equation which tells us how a particular configuration evolves in time:

$$\frac{\partial P\left(\{\sigma\},t\right)}{\partial t}=\sum_{n=1}^{N}\left[w_n(\{\sigma^{[n]}\})P\left(\{\sigma^{[n]}\},t\right)-w_n(\{\sigma\})P\left(\{\sigma\},t\right)\right] \tag{4.4}$$

where the state $\{\sigma^{[n]}\}$ differs from $\{\sigma\}$ by a flipping of the n-th spin and the rates are given by Eqn. (4.2). We seek the steady state solution:

$$P^{*}\left(\{\sigma\}\right)\equiv\lim_{t\to\infty}P\left(\{\sigma\},t\right) \tag{4.5}$$

Since Eqn. (4.4) is linear and discrete, it can be written in matrix form: Labelling the configurations $\{\sigma\}_1$, $\{\sigma\}_2$,...,$\{\sigma\}_{2^N}$, the steady state equation for $P^{*}\left(\{\sigma\}_i\right)$, $i=1,2,...,2^N$, takes the form

$$0=\sum_{j}W_{ij}P^{*}\left(\{\sigma\}_j\right)$$

where the matrix W_{ij} is easily constructed from the transition rates between configurations $\{\sigma\}_i$ and $\{\sigma\}_j$. To simplify further, we note that configurations which are related by symmetries of the dynamics will obviously occur with the same probability. For example, the configurations $+-++$ and $+++-$ will have the same probability in a 1×4 system, since they result from each other by a translation modulo 2. Similarly, $+-++$ and $-+--$ are related by a global spin flip. We can therefore define "equivalence classes", each class consisting of those configurations related to one another by a symmetry transformation. So, the total number of configurations, 2^N, is reduced greatly, and we need to solve only the reduced system of equations.

Below, we pursue this program for a 1×6 system. The exact stationary probabilities will be determined and studied as a function of a single parameter,

$$m \equiv \frac{\gamma_e}{\gamma_o} \tag{4.6}$$

for some fixed, suitably chosen value of γ_o. Clearly, the equilibrium limit is represented by $m = 1$.

4.3 Steady state equations and solution

For a 1×6 system, there are 10 equivalence classes, numbered (in some arbitrary order) $i = 0, 1, ..., 9$. The degeneracy d_i of each class is defined as the number of configurations in this class. P_i denotes the stationary probability associated with class i. The table below shows one representative for each class.

Class	Configuration	Degeneracy	Probability
0	$++++++$	2	P_0
1	$+++++-$	6	P_1
2	$++++-+$	6	P_2
3	$+++-+-$	6	P_3
4	$++-+-+$	6	P_4
5	$++++--$	12	P_5
6	$-++-++$	6	P_6
7	$---++$	6	P_7
8	$+-+-+-$	2	P_8
9	$-+--++$	12	P_9

(4.7)

To write the steady state equation for P_0, we need to identify the "neighbors" of class 0 in configuration space, i.e., those configurations which can be reached from P_0 via a single spin flip, and vice versa: these configurations obviously belong to classes 1 or 2. Similarly, class 1 is related to classes 0, 3, 5, and 6 via a single spin flip. Using the rates for each transition, we arrive at a set of 10 equations:

$$2\tau\partial_t P_0 = 3(1+\gamma_e)P_1 + 3\,(1+\gamma_o)\,P_2 - 3P_0\,[(1-\gamma_e)+(1-\gamma_o)] \tag{4.8}$$

$$2\tau\partial_t P_1 = (1-\gamma_e)P_0 + 2\,(1+\gamma_e)\,P_3 + 2P_5 + (1+\gamma_o)\,P_6 - P_1\,[6-\gamma_e-\gamma_o]$$

$$2\tau\partial_t P_2 = (1-\gamma_o)P_0 + 2\,(1+\gamma_o)\,P_4 + 2P_5 + (1+\gamma_e)\,P_6 - P_2\,[6-\gamma_e-\gamma_o]$$

$$2\tau\partial_t P_3 = 2(1-\gamma_e)P_1 + (1-\gamma_o)\,P_7 + 2P_9 + (1+\gamma_e)\,P_8 - P_3\,[6+\gamma_e+\gamma_o]$$

$$
\begin{aligned}
2\tau\partial_t P_4 &= 2(1-\gamma_o)P_2 + (1-\gamma_e)\,P_7 + 2P_9 + (1+\gamma_o)\,P_8 - P_4\,[6+\gamma_e+\gamma_o] \\
2\tau\partial_t P_5 &= P_1 + P_2 + 2P_7 + (2+\gamma_o+\gamma_e)\,P_9 - P_5\,[6-\gamma_e-\gamma_o] \\
2\tau\partial_t P_6 &= (1-\gamma_o)P_1 + (1-\gamma_e)P_2 + 2P_7 + 4P_9 - P_6\,[6+\gamma_e+\gamma_o] \\
2\tau\partial_t P_7 &= (1+\gamma_o)P_3 + (1+\gamma_e)P_4 + 4P_5 - P_7\,[6-\gamma_e-\gamma_o] \\
2\tau\partial_t P_8 &= 3(1-\gamma_e)P_3 + 3(1-\gamma_o)P_4 - 3P_8\,[2+\gamma_e+\gamma_o] \\
2\tau\partial_t P_9 &= (2-\gamma_o-\gamma_e)P_5 + 2P_6 + P_3 - P_9\,[6+\gamma_e+\gamma_o]
\end{aligned}
$$

Since our probabilities are normalized, we have one additional equation, namely,

$$1 = \sum_{i=0}^{9} d_i P_i \tag{4.9}$$

Thus, we first determine all probabilities in terms of P_0 and normalize them at the end. We should caution, however, that our graphs below show *non-normalized* results: all P_i, for $i \geq 1$, are given in terms of P_0 which is set to unity: $P_0 = 1$.

The probabilities for the equilibrium case $\gamma_o = \gamma_e \equiv \gamma$ are given by the Boltzmann factor, $\exp(-\beta H)$. Thus, probabilities are grouped not only by symmetry, but also by their configurational energy. With a little algebra, one can convert the exponentials into functions of γ to arrive at:

$$
\begin{aligned}
P_1 = P_2 = P_5 = P_7 &= P_0\frac{(1-\gamma)}{(1+\gamma)} \\
P_3 = P_4 = P_6 = P_9 &= P_0\frac{(1-\gamma)^2}{(1+\gamma)^2} \\
P_8 &= P_0\frac{(1-\gamma)^3}{(1+\gamma)^3}
\end{aligned}
\tag{4.10}
$$

As we can see, at equilibrium only four different probabilities remain, reflecting the four possible values of configurational energy: (i) no broken (i.e., $+-$) bonds – class 0; (ii) two broken bonds – classes 1, 2, 5, 7 (iii) four broken bonds – classes 3, 4, 6, 9,

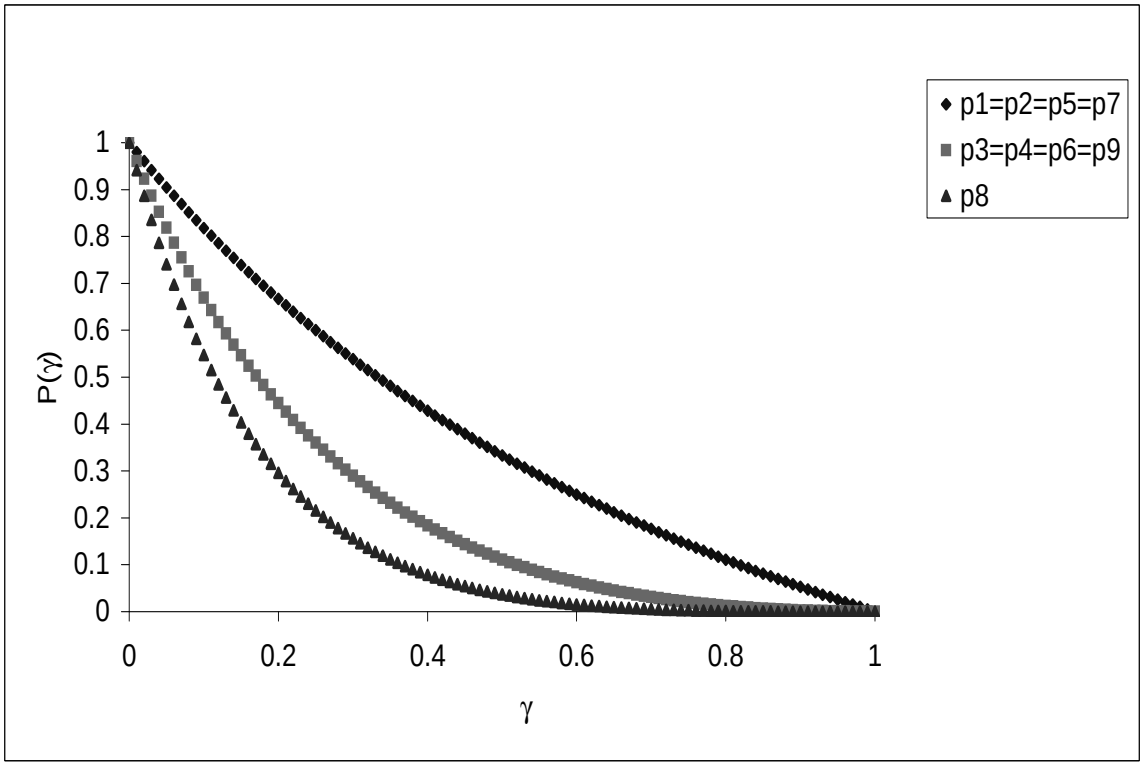

Figure 4.1: The probability distribution of the 1x6 system as a function of $\gamma = \tanh(\frac{2J}{k_B T})$ in the equilibrium case, when the even and odd sites are in contact with heat baths at the same temperature $T_e = T_0 = T$

and (iv) six broken bonds – class 8. In Fig. 4.1 we show their dependence on γ. All probabilities become equal for $\gamma \to 0$ which corresponds to the infinite temperature limit, and all – except $P_0 = 1$ – vanish for $\gamma \to 1$, i.e., $T \to 0$.

This picture changes drastically when we are in the non-equilibrium steady state, i.e., $\gamma_o \neq \gamma_e$.(see Fig. 4.2). Again, all P_i, for $i \geq 1$, are given in terms of $P_0 = 1$, and we are plotting P_1, P_2,...,P_9 vs m, for $\gamma_o = 0.5$. So, m ranges between 0 and 2. First of all, we observe that all P's are generically different: the plot shows eight distinct curves, as opposed to three for the equilibrium case. Of course, some crossings must occur for $m = 1$, where only three distinct values can persist. We also note that P_0 remains the most probable configuration (since $P_i < 1$, for $i \geq 1$). Finally, we observe a grouping of curves: The probabilities of configurations which share equal configurational energy track each other quite closely, and those associated with *different* configurational energy *never cross*. One might be tempted to conjecture that this is a generic feature

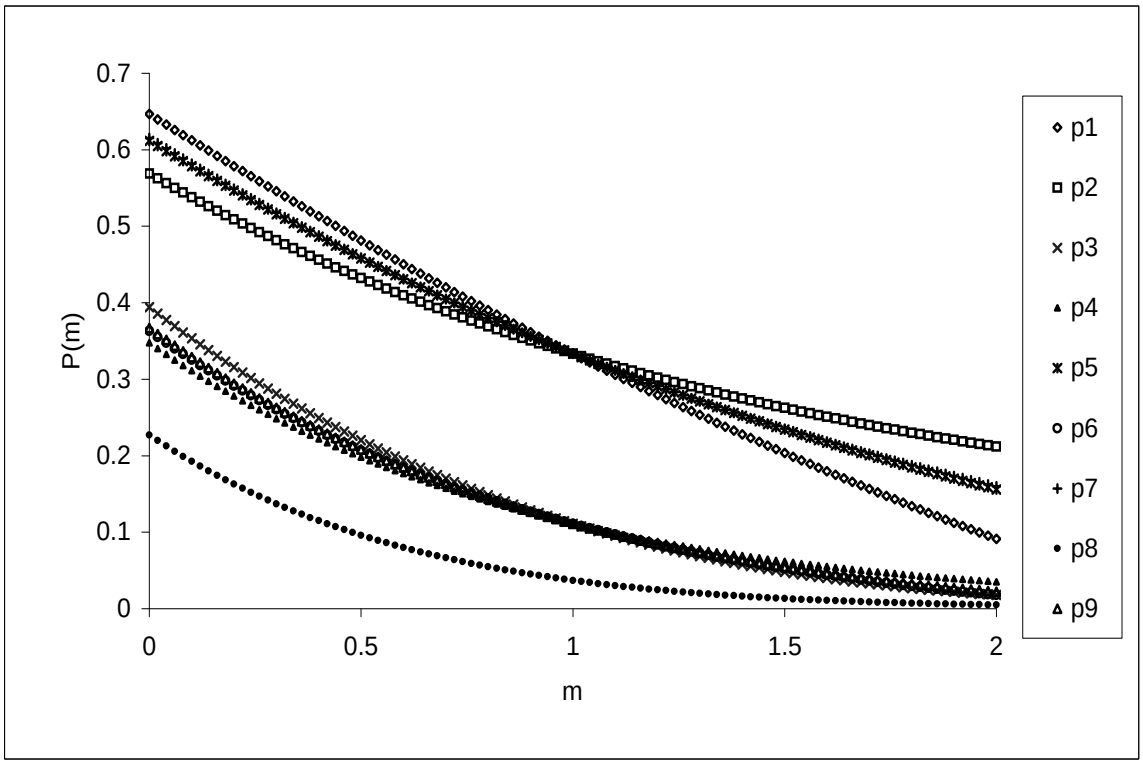

Figure 4.2: The probability distribution of the 1x6 system as a function of $m = \frac{\gamma_e}{\gamma_o}$ in the driven case, with $\gamma_o = 0.5$.

of this simple non-equilibrium system. Unfortunately, going to larger system sizes (2×4) to check this hypothesis, we discovered a counter example. Another purpose of this study was to seek configurations, *unrelated* by symmetry, which would nevertheless occur with the same probability. In equilibrium, such configurations would all have the same energy, i.e., degeneracies (beyond symmetry) are controlled by energy. Far from equilibrium, it is not known which quantity controls such degeneracies. By identifying degenerate configurations we were hoping to home in on this unknown function. Remarkably, we *never* found *any* degeneracies beyond those obviously due to symmetries. Whether this is a generic feature of this simple non-equilibrium steady state remains to be explored.

The difference between equilibrium and non-equilibrium probabilities is quite dramatic, and any connections between the two are far from obvious. To summarize, by studying the system coupled to two different baths at unequal temperatures we obtain a completely new distribution that requires new tools to be studied.

Chapter 5

Summary and Outlook

In this Dissertation, we studied the steady state properties of some driven diffusive systems. We focused on some simple models, variations of the standard model, and employed both Monte Carlo simulation techniques and analytical approaches in order to find their critical behavior and obtain the phase diagram. We also worked out the exact steady state for a small Ising-like system coupled to two temperatures.

Our first system studied was the bilayer model, a stack of two driven Ising lattice gases allowed to interact. We studied this model under various boundary conditions, focusing specifically on fully periodic boundary conditions which are closest to the three-dimensional case. We used a very simple analytic approximation, the high temperature expansion. Building on existing simulation data and field theory results, our goal was to test how faithfully the series expansion could reproduce the Monte Carlo phase diagram. We found that the agreement between our calculations and the already reported simulation results was remarkably good. The main characteristics of the model were seen: the presence of the three phases, namely, the disordered, the strip and the full-empty phase, and the shift of the bicritical point into the negative region of J. We also calculated the correlation functions, the particle current and the energy flux for the longitudinal and transverse directions, and studied their dependence on large, but finite driving field.

The next model was a two-dimensional driven lattice gas with anisotropic jump rates: jumps along the longitudinal and transverse lattice directions were attempted with different frequencies, $\Gamma_{\parallel}$ and $\Gamma_{\perp}$. We performed Monte Carlo simulations of the system, considering a range of different values for the ratio $\Gamma = \Gamma_{\parallel}/\Gamma_{\perp}$. The phase diagram shows us that the critical temperature decreases on both sides ($\Gamma > 1$ and $\Gamma < 1$) of the standard model which corresponds to $\Gamma = 1$. Next we continued

with a finite-size scaling study, in order to determine the universality class of this variant of the standard model. We chose $\Gamma = 2$ and $\Gamma = 1/2$, and concluded that the parameter Γ does not enter into universal critical properties: the modified model is in the same universality class as the standard model. Finally, we used the high temperature approximation again and obtained the phase diagram analytically. In this case, the agreement between theory and simulation is not very satisfactory.

The third model in our study was a two temperature kinetic model with Glauber dynamics. We solved the master equation exactly for small system sizes, and found the particle probability distribution.

Possible extensions of this research include the following projects:

(i) An extension of the finite-size scaling study for other Γ's and different system sizes, in an effort to improve the date collapse and to make a more accurate prediction of the critical temperature in the thermodynamic limit.

(ii) Exact solutions for other small systems, including two dimensional ones, in order to gain better insight into the fundamental differences between equilibrium and non-equilibrium distributions.

To summarize, we studied some simple driven models and we explored generic non-equilibrium features as well as novel behavior. We employed in our work both simulation techniques and analytical tools, and we believe that our findings will constitute one extra step in the collective effort directed at a better understanding of far from equilibrium systems.

Appendix A

Sample calculations using the high temperature series for the bilayer system

A.1 Sample calculation for finding the equations for the two-point correlations:

Here, we give a few details of our calculations. In particular, we show how we can obtain the equation for the two-point correlation G(1,1,0):

We start with the equation of motion for our set of sites:

$$\frac{d\left\langle \sigma_S \right\rangle}{dt} = \sum_{NN} \left\langle \sigma_{\mathcal{S}} \left(\sigma_{\vec{r}} \sigma_{\vec{r}\,'} \ - 1 \right) c\left(\vec{r}, \vec{r}\,', \sigma \right) \right\rangle \tag{A.1}$$

Here, the sum runs over nearest-neighbor pairs $(\vec{r}, \vec{r}\,')$ such that $\vec{r} \in \mathcal{S}$ but $\vec{r}\,' \notin \mathcal{S}$.

We define the neighboring sites:

For the first layer (labelled with 0) we choose a pair of sites (a_0, b_0) and label their

nearest neighbors as follows:

$$\begin{array}{ccc} & m_0 & \\ e_0 & \mathbf{b_0} & n_0 \\ c_0 \quad \mathbf{a_0} & d_0 & \\ f_0 & & \end{array} \tag{A.2}$$

We are doing the same thing for the second layer (labelled with 1):

$$\begin{array}{ccc} & m_1 & \\ e_1 & \mathbf{b_1} & n_1 \\ c_1 \quad \mathbf{a_1} & d_1 & \\ f_1 & & \end{array} \tag{A.3}$$

The field is along the x direction, defined in this picture as going downward.

The next step is to write the jump rates parallel and transverse to the field. For convenience, we rewrite Eqn.(2.20) as a sum of two terms:

$$c_{\parallel}\left(\vec{r},\vec{r}+\vec{e}_x,\sigma\right)=c_{\parallel}^{\infty}\left(\vec{r},\vec{r}+\vec{e}_x,\sigma\right)+c_{\parallel}^{\varepsilon}\left(\vec{r},\vec{r}+\vec{e}_x,\sigma\right) \tag{A.4}$$

with

$$\begin{aligned} c_{\parallel}^{\infty}\left(\vec{r},\vec{r}+\vec{e}_x,\sigma\right) &= \frac{1}{4}(\sigma_{\vec{r}}-\sigma_{\vec{r}+\vec{e}_x}+2) \\ c_{\parallel}^{\varepsilon}\left(\vec{r},\vec{r}+\vec{e}_x,\sigma\right) &= \frac{\varepsilon}{4}(\sigma_{\vec{r}+\vec{e}_x}-\sigma_{\vec{r}}+2)\left(1+\beta c_2\right) \\ c_2 &= -\frac{1}{2}(\Delta H+|\Delta H|) \end{aligned} \tag{A.5}$$

$c_{\parallel}^{\infty}\left(\vec{r},\vec{r}+\vec{e}_x,\sigma\right)$ is the jump rate in the case of an infinite field, and its expression is telling us that all jumps parallel to the field happen with rate 1, and the ones against the drive are forbidden.

$c_{\parallel}^{\varepsilon}\left(\vec{r},\vec{r}+\vec{e}_x,\sigma\right)$ is the correction introduced by the presence of a large, but finite field, and c_2 is a function of σ and it depends on the change of the internal energy of the system when a jump is attempted.

Transverse to the field we have:

$$c_{\perp}=1+\beta c_2+O(\beta^2) \tag{A.6}$$

The *two-point correlation function* is defined as:

$$G(\vec{r},\vec{r}\,')=\langle\sigma_{\vec{r}}\sigma_{\vec{r}\,'}\rangle \tag{A.7}$$

With these notations in mind, we proceed with our specific example, when we consider a set of two sites marked as a_0 and b_0 and write the equation of motion for the steady state:

$$\begin{aligned} 0 &= \frac{d\left\langle \sigma_{a_o b_0}\right\rangle}{dt} = A_{\parallel} + A_{\perp} = A_{\parallel}^{\infty} + A_{\parallel}^{\varepsilon} + A_{\perp} \\ &= \sum_{NN} \left\langle \sigma_{a_o b_0} \left(\sigma_{\vec{r}}\sigma_{\vec{r}\,'} - 1\right) \left(c_{\parallel}^{\infty}\left(\vec{r}, \vec{r} + \vec{e}_x, \sigma\right) + c_{\parallel}^{\varepsilon}\left(\vec{r}, \vec{r} + \vec{e}_x, \sigma\right)\right)\right\rangle + \\ &\quad \sum_{NN} \left\langle \sigma_{a_o b_0} \left(\sigma_{\vec{r}}\sigma_{\vec{r}\,'} - 1\right) \left(c_{\perp}\left(\vec{r}, \vec{r} + \vec{e}_{\perp}, \sigma\right)\right\rangle \end{aligned} \tag{A.8}$$

We are separating again the jumps parallel to the field from the jumps perpendicular to it, and write the equation as a sum of two terms. The first term describes the jumps parallel to the field, and it is split into two: $A_{\parallel}^{\infty}$ is considering the jumps along the field with the ones against it prohibited (which is the case for an infinite drive) and $A_{\parallel}^{\varepsilon}$ shows the corrections introduced by the presence of a finite field. The second term, $A_{\perp}$ takes care of the jumps transverse to the field.

We find $A_{\parallel}^{\infty}$ first:

$$\begin{aligned} A_{\parallel}^{\infty} &= \left\langle \sigma_{a_o}\sigma_{b_o}(\sigma_{a_o}\sigma_{f_o} - 1)\frac{1}{4}(\sigma_{a_0} - \sigma_{f_0} + 2)\right\rangle + \\ &\quad \left\langle \sigma_{a_o}\sigma_{b_o}(\sigma_{a_o}\sigma_{e_o} - 1)\frac{1}{4}(\sigma_{e_0} - \sigma_{a_0} + 2)\right\rangle + \\ &\quad \left\langle \sigma_{a_o}\sigma_{b_o}(\sigma_{b_o}\sigma_{d_o} - 1)\frac{1}{4}(\sigma_{b_0} - \sigma_{d_0} + 2)\right\rangle + \\ &\quad \left\langle \sigma_{a_o}\sigma_{b_o}(\sigma_{b_o}\sigma_{m_o} - 1)\frac{1}{4}(\sigma_{m_0} - \sigma_{b_0} + 2)\right\rangle \\ &= \frac{1}{4}\left\{\langle\sigma_{b_o}(\sigma_{f_o} - \sigma_{a_0})(\sigma_{a_0} - \sigma_{f_0} + 2)\rangle + \right. \\ &\quad \langle\sigma_{b_o}(\sigma_{e_o} - \sigma_{a_0})(\sigma_{e_0} - \sigma_{a_0} + 2)\rangle + \\ &\quad \langle\sigma_{a_o}(\sigma_{f_o} - \sigma_{b_o})(\sigma_{a_0} - \sigma_{f_0} + 2)\rangle + \\ &\quad \left.\langle\sigma_{a_o}(\sigma_{e_o} - \sigma_{b_o})(\sigma_{e_0} - \sigma_{a_0} + 2)\rangle\right\} \end{aligned} \tag{A.9}$$

We keep in mind that $\langle\sigma_{\vec{r}}\rangle = 0$ ($\sigma_{\vec{r}}$ can take only two discrete values, +1 and -1) and that we neglect the three-point correlation functions, and we get the following expression for $A_{\parallel}^{\infty}$:

$$\begin{aligned} A_{\parallel}^{\infty} &= \frac{1}{4}\left\{2\left\langle\sigma_{b_o}\sigma_{f_o}\right\rangle + 2\left\langle\sigma_{b_o}\sigma_{e_o}\right\rangle + 2\left\langle\sigma_{a_o}\sigma_{m_o}\right\rangle + \right. \\ &\quad \left. 2\left\langle\sigma_{a_o}\sigma_{d_o}\right\rangle - 8\left\langle\sigma_{b_0}\sigma_{a_0}\right\rangle\right\} \end{aligned} \tag{A.10}$$

Identifying the pairs of spins with the appropriate correlation functions, we can write $A_{\|}^{\infty}$ as:

$$A_{\|}^{\infty} = G(2,1,0) + G(0,1,0) - 2G(1,1,0) \tag{A.11}$$

Following the same procedure, we continue with $A_{\|}^{\varepsilon}$:

$$\begin{aligned} A_{\|}^{\varepsilon} &= \left\langle \sigma_{a_o}\sigma_{b_o}(\sigma_{a_o}\sigma_{f_o}-1)\frac{\varepsilon}{4}(\sigma_{f_0}-\sigma_{a_0}+2)\,(1+\beta c_2(a_0,f_0))\right\rangle + \\ &\quad \left\langle \sigma_{a_o}\sigma_{b_o}(\sigma_{a_o}\sigma_{e_o}-1)\frac{\varepsilon}{4}(\sigma_{a_o}-\sigma_{e_o}+2)\,(1+\beta c_2(a_0,e_0))\right\rangle + \\ &\quad \left\langle \sigma_{a_o}\sigma_{b_o}(\sigma_{b_o}\sigma_{d_o}-1)\frac{\varepsilon}{4}(\sigma_{d_o}-\sigma_{b_o}+2)\,(1+\beta c_2(b_0,d_0))\right\rangle + \\ &\quad \left\langle \sigma_{a_o}\sigma_{b_o}(\sigma_{b_o}\sigma_{m_o}-1)\frac{\varepsilon}{4}(\sigma_{b_o}-\sigma_{m_o}+2)\,(1+\beta c_2(b_0,m_0))\right\rangle \\ &= \frac{\varepsilon}{4}\{\langle\sigma_{b_o}(\sigma_{f_o}-\sigma_{a_0})(\sigma_{f_0}-\sigma_{a_0}+2)\,(1+\beta c_2(a_0,f_0))\rangle + \\ &\quad \langle\sigma_{b_o}(\sigma_{e_o}-\sigma_{a_0})(\sigma_{a_0}-\sigma_{e_o}+2)\,(1+\beta c_2(a_0,e_0))\rangle + \\ &\quad \langle\sigma_{a_o}(\sigma_{f_o}-\sigma_{b_o})(\sigma_{d_o}-\sigma_{b_o}+2)\,(1+\beta c_2(b_0,d_0))\rangle + \\ &\quad \langle\sigma_{a_o}(\sigma_{e_o}-\sigma_{b_o})(\sigma_{b_o}-\sigma_{m_o}+2)\,(1+\beta c_2(b_0,m_0))\rangle\} \end{aligned} \tag{A.12}$$

Here we separate the terms that contain β from the free terms:

$$\begin{aligned} A_{\|}^{\varepsilon} &= \frac{\varepsilon}{4}\{\langle\sigma_{b_o}(\sigma_{f_o}-\sigma_{a_0})(\sigma_{f_0}-\sigma_{a_0}+2)\rangle + \\ &\quad \langle\sigma_{b_o}(\sigma_{e_o}-\sigma_{a_0})(\sigma_{a_o}-\sigma_{e_o}+2)\rangle + \\ &\quad \langle\sigma_{a_o}(\sigma_{f_o}-\sigma_{b_o})(\sigma_{d_o}-\sigma_{b_o}+2)\rangle + \\ &\quad \langle\sigma_{a_o}(\sigma_{e_o}-\sigma_{b_o})(\sigma_{b_o}-\sigma_{m_o}+2)\rangle +\} \\ &\quad \frac{\varepsilon}{4}\beta\{\langle\sigma_{b_o}(\sigma_{f_o}-\sigma_{a_0})(\sigma_{f_0}-\sigma_{a_0}+2)c_2(a_0,f_0)\rangle + \\ &\quad \langle\sigma_{b_o}(\sigma_{e_o}-\sigma_{a_0})(\sigma_{a_o}-\sigma_{e_o}+2)c_2(a_0,e_0)\rangle + \\ &\quad \langle\sigma_{a_o}(\sigma_{f_o}-\sigma_{b_o})(\sigma_{d_o}-\sigma_{b_o}+2)c_2(b_0,d_0)\rangle + \\ &\quad \langle\sigma_{a_o}(\sigma_{e_o}-\sigma_{b_o})(\sigma_{b_o}-\sigma_{m_o}+2)c_2(b_0,m_0)\rangle\} \end{aligned} \tag{A.13}$$

As we recall, $c_2 = -\frac{1}{2}(\Delta H + |\Delta H|)$.

Looking at our configuration of spins, we can see that the only non-zero c_2's are the ones for the following pairs: $c_2(a_0,e_0)$ and $c_2(b_0,d_0)$ and their combined contribution is $-8J_0$.

Summarizing our calculations so far, we have for $A_{\|}$ the following expression:

$$A_{\|} = (1+\varepsilon)(G(2,1,0) + G(0,1,0) - 2G(1,1,0)) - 2\varepsilon K_0 \tag{A.14}$$

Moving on to the transverse jumps, we can see that we have two directions perpendicular to the field, namely, one in the same plane as the drive, and one between the two layers:

$$\begin{aligned}
A_\perp &= \langle\sigma_{a_o}\sigma_{b_o}(\sigma_{a_o}\sigma_{c_o}-1)c_\perp(a_0,c_0)\rangle + \langle\sigma_{a_o}\sigma_{b_o}(\sigma_{a_o}\sigma_{d_o}-1)c_\perp(a_0,d_0)\rangle \\
&\quad +2\langle\sigma_{a_o}\sigma_{b_0}(\sigma_{b_o}\sigma_{a_0}-1)c_\perp(a_0,a_1)\rangle + \langle\sigma_{a_o}\sigma_{b_o}(\sigma_{b_o}\sigma_{e_o}-1)c_\perp(b_0,e_0)\rangle \\
&\quad + \langle\sigma_{a_o}\sigma_{b_o}(\sigma_{b_o}\sigma_{n_o}-1)c_\perp(b_0,n_0)\rangle + 2\langle\sigma_{a_o}\sigma_{b_0}(\sigma_{b_o}\sigma_{b_1}-1)c_\perp(b_0,b_1)\rangle \\
&= \langle\sigma_{a_o}\sigma_{b_o}(\sigma_{a_o}\sigma_{c_o}-1)(1+\beta c_2(a_0,c_0))\rangle + \\
&\quad \langle\sigma_{a_o}\sigma_{b_o}(\sigma_{a_o}\sigma_{d_o}-1)(1+\beta c_2(a_0,d_0))\rangle + \\
&\quad 2\langle\sigma_{a_o}\sigma_{b_0}(\sigma_{b_o}\sigma_{a_0}-1)(1+\beta c_2(a_0,a_1))\rangle + \\
&\quad \langle\sigma_{a_o}\sigma_{b_o}(\sigma_{b_o}\sigma_{e_o}-1)(1+\beta c_2(b_0,e_0))\rangle + \\
&\quad \langle\sigma_{a_o}\sigma_{b_o}(\sigma_{b_o}\sigma_{n_o}-1)(1+\beta c_2(b_0,n_0))\rangle + \\
&\quad 2\langle\sigma_{a_o}\sigma_{b_0}(\sigma_{b_o}\sigma_{b_1}-1)(1+\beta c_2(b_0,b_1))\rangle \\
&= \langle\sigma_{b_o}(\sigma_{c_o}-\sigma_{a_o})\rangle + \langle\sigma_{b_o}(\sigma_{d_o}-\sigma_{a_o})\rangle + 2\langle\sigma_{b_0}(\sigma_{a_1}-\sigma_{a_0})\rangle + \langle\sigma_{a_o}(\sigma_{e_o}-\sigma_{b_o})\rangle + \\
&\quad \langle\sigma_{a_o}(\sigma_{n_o}-\sigma_{b_o})\rangle + 2\langle\sigma_{a_o}(\sigma_{b_1}-\sigma_{b_o})\rangle + \\
&\quad \beta\{\langle\sigma_{b_o}(\sigma_{c_o}-\sigma_{a_o})c_2(a_0,c_0))\rangle + \langle\sigma_{b_o}(\sigma_{d_o}-\sigma_{a_o})c_2(a_0,d_0))\rangle + \\
&\quad 2\langle\sigma_{b_0}(\sigma_{a_1}-\sigma_{a_0})c_2(a_0,a_1))\rangle + \\
&\quad \langle\sigma_{a_o}(\sigma_{e_o}-\sigma_{b_o})c_2(b_0,e_0))\rangle + \langle\sigma_{a_o}(\sigma_{n_o}-\sigma_{b_o})c_2(b_0,n_0))\rangle + \\
&\quad 2\langle\sigma_{a_o}(\sigma_{b_1}-\sigma_{b_o})c_2(b_0,b_1))\rangle\}
\end{aligned} \tag{A.15}$$

Again, the only non-zero contributions out of the change in the internal energy (c_2's) are the ones for the following pairs: $c_2(a_0,d_0)$ and $c_2(b_0,e_0)$ and their combined contribution is $-2J_0$.

Finally, we get

$$\begin{aligned}
A_\perp &= 2[G(1,2,0)+G(1,0,0)-2G(1,1,0)]+4[G(1,1,1)-G(1,1,0)] \\
&\quad -2K_0
\end{aligned} \tag{A.16}$$

and the equation for the two point correlation function is:

$$\begin{aligned}
0 &= (1+\varepsilon)[G(2,1,0)+G(0,1,0)-2G(1,1,0)]+2[G(1,2,0)+G(1,0,0) \\
&\quad -2G(1,1,0)]+4[G(1,1,1)-G(1,1,0)]-2K_0-2\varepsilon K_0
\end{aligned} \tag{A.17}$$

A.2 Sample calculation for finding the structure factor

As mentioned in chapter 2, the structure factor has the following form:

$$\tilde{S}(k,p,q) = \frac{L(k,p,q)}{\delta(k,p,q)} \tag{A.18}$$

where $L(k,p,q)$ is:

$$\begin{aligned} L(k,p,q) \equiv\ & 2(1+\varepsilon)\,(1-\cos k)\,I_1 + 4\,(1-\cos p)\,I_2 + 4\,(1-\cos q)\,I_3 + \\ & (2\varepsilon K_0 + 8K_0)\,2\cos k + (4\varepsilon K_0 + 6K_0)\,2\cos p + \\ & (8\varepsilon K + 8K)\cos q - (2\varepsilon K_0 + 2K_0)\,4\cos k\cos p - \\ & (4\varepsilon K + 4K_0)\,2\cos k\cos q - 4(K_0+K)2\cos p\cos q - \\ & 4\varepsilon K_0\cos 2k - 4K_0\cos 2p \end{aligned} \tag{A.19}$$

The I_1, I_2, and I_3 integrals are defined as:

$$\begin{aligned} I_1 &= \int \tilde{S}(1-\cos k) \\ I_2 &= \int \tilde{S}(1-\cos p) \\ I_3 &= \int \tilde{S}(1-\cos q) \end{aligned} \tag{A.20}$$

and $\delta(k,p,q)$(which is just the anisotropic lattice Laplacian in Fourier space) has the following expression:

$$\delta(k,p,q) = 2(1+\varepsilon)(1-\cos k) + 4(1-\cos p) + 4(1-\cos q) \tag{A.21}$$

Since $\tilde{S}$ is still an implicit function of the three integrals I_1, I_2, and I_3 here, we will give a few details about how to find the explicit solution. For this purpose, we need three linearly independent equations in order to find the three integrals. As mentioned before in chapter two , one of these equations will come from the value of G at the origin, $1 = G(0,0,0) = \int(\overline{S} + \widetilde{S})$, and the remaining two can be obtained

directly from the definitions of I_1 and I_3, once we insert our result for $\tilde{S}$:

$$\begin{aligned} 0 &= \int \frac{L(k,p,q)}{\delta(k,p,q)} \\ 0 &= -I_1 + \int \frac{L(k,p,q)}{\delta(k,p,q)}(1-\cos k) \\ 0 &= -I_3 + \int \frac{L(k,p,q)}{\delta(k,p,q)}(1-\cos q) \end{aligned} \tag{A.22}$$

Taking advantage of the following identities:

$$\begin{array}{l} \cos k(1-\cos p) = (1-\cos p) - (1-\cos k)(1-\cos p) \\ \cos k(1-\cos q) = (1-\cos q) - (1-\cos k)(1-\cos q) \\ \cos p(1-\cos q) = (1-\cos q) - (1-\cos q)(1-\cos p) \\ \cos q(1-\cos p) = (1-\cos p) - (1-\cos q)(1-\cos p) \\ \cos p - \cos(2p) = 3(1-\cos p) - 2(1-\cos p)^2 \end{array} \tag{A.23}$$

we write the structure factor in a slightly different form:

$$\begin{aligned} L(k,p,q) \equiv\ & 2(1+\varepsilon)I_1 + 4\varepsilon(5K_0+2K)\,(1-\cos k) + \\ & 4(I_2+5K_0+2K)\,(1-\cos p) + 4\,(I_3+4K_0)\,(1-\cos q) - \\ & 8K_0(1+\varepsilon)\,(1-\cos k)\,(1-\cos p) - \\ & 8\,(K+K_0)\,(1-\cos p)\,(1-\cos q) - \\ & 8\,(\varepsilon K+K_0)\,(1-\cos k)\,(1-\cos q) - \\ & 8\varepsilon K_0\,(1-\cos k)^2 - 8K_0\,(1-\cos p)^2 \end{aligned} \tag{A.24}$$

and we substitute the structure factor into the system of equations (A.22)

The following integrals come into play:

$$Q_{lmn} = \int \frac{(1-\cos(k))^l(1-\cos(p))^m(1-\cos(q))^n}{\delta} \tag{A.25}$$

Where the integral sign stands for:

$$\int = \frac{1}{2}\frac{1}{(2\pi)^2}\int_{-\pi}^{\pi} dk \int_{-\pi}^{\pi} dp \sum_{q=0,\pi} \tag{A.26}$$

With these notations, the system of equations becomes:

$$\begin{array}{l} 2(1+\varepsilon)I_1 + 4\varepsilon(5K_0+2K)Q_{100} + 4(I_2+5K_0+2K)Q_{010} \\ +4\left(I_3+4K_0\right)Q_{001} - 8K_0(1+\varepsilon)Q_{110} - 8\left(K+K_0\right)Q_{011} \\ -8\left(\varepsilon K+K_0\right)Q_{101} - 8\varepsilon K_0 Q_{200} - 8K_0 Q_{020} = 0 \end{array}$$

$$\begin{array}{l} -I_1 + 2(1+\varepsilon)I_1 + 4\varepsilon(5K_0+2K)Q_{200} + 4(I_2+5K_0+2K)Q_{110} \\ +4\left(I_3+4K_0\right)Q_{101} - 8K_0(1+\varepsilon)Q_{210} - 8\left(K+K_0\right)Q_{111} \\ -8\left(\varepsilon K+K_0\right)Q_{201} - 8\varepsilon K_0 Q_{300} - 8K_0 Q_{120} = 0 \end{array} \qquad \text{(A.27)}$$

$$\begin{array}{l} -I_3 + 2(1+\varepsilon)I_1 + 4\varepsilon(5K_0+2K)Q_{101} + 4(I_2+5K_0+2K)Q_{011} \\ +4\left(I_3+4K_0\right)Q_{002} - 8K_0(1+\varepsilon)Q_{111} - 8\left(K+K_0\right)Q_{012} \\ -8\left(\varepsilon K+K_0\right)Q_{102} - 8\varepsilon K_0 Q_{201} - 8K_0 Q_{021} = 0 \end{array}$$

The calculations (made in Maple) are simplified by a series of identities, namely:

$$\begin{aligned} \int \frac{\delta}{\delta} &= 1 = 2(1+\varepsilon)Q_{100} + 4Q_{010} + 4Q_{001} \\ \int (1-\cos(k))\frac{\delta}{\delta} &= 1 = 2(1+\varepsilon)Q_{200} + 4Q_{110} + 4Q_{101} \\ \int (1-\cos(p))\frac{\delta}{\delta} &= 1 = 2(1+\varepsilon)Q_{110} + 4Q_{020} + 4Q_{011} \\ \int (1-\cos(k))^2\frac{\delta}{\delta} &= \frac{3}{2} = 2(1+\varepsilon)Q_{300} + 4Q_{210} + 4Q_{201} \\ \int (1-\cos(p))^2\frac{\delta}{\delta} &= \frac{3}{2} = 2(1+\varepsilon)Q_{120} + 4Q_{030} + 4Q_{021} \\ \int (1-\cos(k))(1-\cos(p))\frac{\delta}{\delta} &= 1 = 2(1+\varepsilon)Q_{210} + 4Q_{120} + 4Q111 \qquad \text{(A.28)} \\ \int (1-\cos(q))\frac{\delta}{\delta} &= 1 = 2(1+\varepsilon)Q_{101} + 4Q_{011} + 4Q_{002} \end{aligned}$$

After we calculated the Q integrals, we substituted all the coefficients into (A.27) and solved for I_1, I_2 and I_3, thus finding the structure factor.

Below we present the equilibrium solution for the structure factor:

A.3 Equilibrium solution

A word of caution is in order here. Since our expansion presumed $E > \Delta H$, we may not simply set $\varepsilon = 1$ in our equations of motion for the two-point correlations. Instead, one needs to rederive the whole set carefully, noting the absence of the driving field. Of course, since we know the equilibrium (Boltzmann) distribution, it is trivial to obtain the two-point correlations and hence the structure factors, to first order in the couplings, directly from there.

To this order, only nearest-neighbor correlations can be non-zero, so that the only non-vanishing G's are

$$\begin{aligned} G^{eq}(0,0,0) &= 1 \\ G^{eq}(\pm 1,0,0) &= G^{eq}(0,\pm 1,0) = K_0 \\ G^{eq}(0,0,\pm 1) &= K \end{aligned} \tag{A.29}$$

Performing the Fourier transform to structure factors, we find immediately that

$$\begin{aligned} S(k,p,q) &= \sum_{z=0,1} \sum_{x,y=-\infty}^{\infty} G(x,y,z) e^{-i(kx+py+qz)} \\ &= 1 + 2K_0 (\cos k + \cos p) + 2K \cos q \end{aligned} \tag{A.30}$$

resulting in

$$\begin{aligned} \lim_{k,p\to 0} S^{-1}(k,p,q) &= 1 - 2K_0 \left(2 - \frac{1}{2}k^2 - \frac{1}{2}p^2\right) - 2K\cos q + O(k^4, p^4) \\ &\equiv \tau(q) + O(k^2, p^2) \end{aligned} \tag{A.31}$$

with

$$\tau(q) = 1 - 4K_0 - 2K\cos q \tag{A.32}$$

For $q = 0$, this vanishes at

$$k_B T_c^S = 4J_0 + 2J \tag{A.33}$$

and for $q = \pi$, the zero shifts to

$$k_B T_c^{FE} = 4J_0 - 2J \tag{A.34}$$

A.4 Energy currents

We give a few extra steps followed in calculating the change in energy along the two directions (parallel and transverse to the drive):

$$\left\langle \frac{dH}{dt} \right\rangle_{\parallel} = -\ J_0 \left(\frac{d}{dt} \right)_{\parallel} [G(1,0,0) + G(0,1,0)] - 2J \left(\frac{d}{dt} \right)_{\parallel} G(0,0,1) \tag{A.35}$$

where the subscript on the time derivative reminds us to select only those processes which are due to parallel exchanges alone. Of course, there is an analogous equation for $\langle dH/dt \rangle_{\perp}$:

$$\left\langle \frac{dH}{dt} \right\rangle_{\perp} = -\ J_0 \left(\frac{d}{dt} \right)_{\perp} [G(1,0,0) + G(0,1,0)] - 2J \left(\frac{d}{dt} \right)_{\perp} G(0,0,1) \tag{A.36}$$

We start with the equations for the G(1,0,0),G(0,1,0),G(0,0,1) correlation functions :

$$\begin{aligned}
0 &= (1+\varepsilon)[G(2,0,0) - G(1,0,0)] + 4[G(1,1,0) - G(1,0,0)] \\
&\quad +4[G(1,0,1) - G(1,0,0)] + 2\varepsilon K_0 + 8K_0 \\
0 &= 2(1+\varepsilon)[G(1,1,0) - G(0,1,0)] + 2[G(0,2,0) - G(0,1,0)] \\
&\quad +4[G(0,1,1) - G(0,1,0)] + 4\varepsilon K_0 + 6K_0 \\
0 &= 2(1+\varepsilon)[G(1,0,1) - G(0,0,1)] + 4[G(0,1,1) - G(0,0,1)] \\
&\quad +8K + 8\varepsilon K
\end{aligned} \tag{A.37}$$

In the steady state

$$\begin{aligned}
\frac{dG(1,0,0)}{dt} &= 0 \\
\frac{dG(0,1,0)}{dt} &= 0 \\
\frac{dG(0,0,1)}{dt} &= 0
\end{aligned} \tag{A.38}$$

In these equations there is a contribution due to the parallel jumps and another one due to the perpendicular jumps in the same plane and across the planes.

We can write the following:

$$\begin{aligned}
\frac{dG(1,0,0)}{dt} &= B_{\parallel}^{1} + B_{\perp}^{1} \\
\frac{dG(0,1,0)}{dt} &= B_{\parallel}^{2} + B_{\perp}^{2} \\
\frac{dG(0,0,1)}{dt} &= B_{\parallel}^{3} + B_{\perp}^{3}
\end{aligned} \tag{A.39}$$

We identify these terms as:

$$\begin{aligned}
B_{\parallel}^{1} &= (1+\varepsilon)[G(2,0,0) - G(1,0,0)] + 2\varepsilon K_0 \\
B_{\parallel}^{2} &= 2(1+\varepsilon)[G(1,1,0) - G(0,1,0)] + 4\varepsilon K_0 \\
B_{\parallel}^{3} &= 2(1+\varepsilon)[G(1,0,1) - G(0,0,1)] + 8\varepsilon K \\
B_{\perp}^{1} &= 4[G(1,1,0) - G(1,0,0)] + 4[G(1,0,1) - G(1,0,0)] + 8K_0 \\
B_{\perp}^{2} &= 2[G(0,2,0) - G(0,1,0)] + 4[G(0,1,1) - G(0,1,0)] + 6K_0 \\
B_{\perp}^{3} &= 4[G(0,1,1) - G(0,0,1)] + 8K
\end{aligned} \tag{A.40}$$

Thus, we find

$$\begin{aligned}
\left\langle \frac{dH}{dt} \right\rangle_{\parallel} &= -J_0 \left\{ B_{\parallel}^{1} + B_{\parallel}^{2} \right\} - 2J B_{\parallel}^{3} \\
&= -J_0 \{(1+\varepsilon)[G(2,0,0) - G(1,0,0)] + 2\varepsilon K_0 \\
&\quad +2(1+\varepsilon)[G(1,1,0) - G(0,1,0)] + 4\varepsilon K_0\} \\
&\quad -2J \{2(1+\varepsilon)\,[G(1,0,1) - G(0,0,1)] + 8\varepsilon K\}
\end{aligned} \tag{A.41}$$

$$\begin{aligned}
\left\langle \frac{dH}{dt} \right\rangle_{\perp} &= -J_0 \left\{ B_{\perp}^{1} + \ B_{\perp}^{2} \right\} - 2J \ B_{\perp}^{3} \\
&= -J_0 \{4[G(1,1,0) - G(1,0,0)] + 4[G(1,0,1) - G(1,0,0)] \\
&\quad +2[G(0,2,0) - G(0,1,0)] + 4[G(0,1,1) - G(0,1,0)] + 14K_0\} \\
&\quad -2J \{4\,[G(0,1,1) - G(0,0,1)] + 8K\}
\end{aligned}$$

So we have to calculate the following correlation functions:

$G(1,1,0), G(2,0,0), G(0,2,0), G(1,0,1)$ and $G(0,1,1)$. We want to write these correlation functions in terms of the already calculated integrals I_1, I_2, I_3 and also in terms of the set of Q integrals defined earlier.

We start with the definition for G(2,0,0) and substitute the expression for the structure factor:

$$\begin{aligned} G(2,0,0) &= \int S\exp 2ik = \int S\cos 2k = \int S(2\cos^2 k - 1) \\ &= 2(\int S(1-\cos k)^2 - 2\int S(1-\cos k)) \\ &= 2(\int S(1-\cos k)^2 - 2I_1) \\ &= 2\{2(1+\varepsilon)I_1Q_{200} + 4\varepsilon(5K_0+2K)Q_{300} + \\ &\quad 4(I_2+5K_0+2K)Q_{210} + 4\left(I_3+4K_0\right)Q_{201} - \\ &\quad 8K_0(1+\varepsilon)Q_{310} - 8\left(K+K_0\right)Q_{211} - \\ &\quad 8\left(\varepsilon K+K_0\right)Q_{301} - 8\varepsilon K_0Q_{400} - 8K_0Q_{220} - 2I_1\} \end{aligned} \tag{A.42}$$

Due to symmetry we can write directly G(0,2,0):

$$\begin{aligned} G(0,2,0) &= 2(\int S(1-\cos p)^2 - 2I_2) \\ &= 2\{2(1+\varepsilon)I_1Q_{020} + 4\varepsilon(5K_0+2K)Q_{120} + \\ &\quad 4(I_2+5K_0+2K)Q_{030} + 4\left(I_3+4K_0\right)Q_{021} - \\ &\quad 8K_0(1+\varepsilon)Q_{130} - 8\left(K+K_0\right)Q_{031} - \\ &\quad 8\left(\varepsilon K+K_0\right)Q_{121} - 8\varepsilon K_0Q_{220} - 8K_0Q_{040} - 2I_2\} \end{aligned} \tag{A.43}$$

We continue with G(1,1,0),G(0,1,1),G(1,0,1) following the same method:

$$\begin{aligned} G(1,1,0) &= \int S\exp ik\exp ip = \int S\cos k\cos p \\ &= \int S(1-\cos k)(1-\cos p) - I_1 - I_2 \\ &= \{2(1+\varepsilon)I_1Q_{110} + 4\varepsilon(5K_0+2K)Q_{210} + \\ &\quad 4(I_2+5K_0+2K)Q_{120} + 4\left(I_3+4K_0\right)Q_{111} - \\ &\quad 8K_0(1+\varepsilon)Q_{220} - 8\left(K+K_0\right)Q_{121} - \\ &\quad 8\left(\varepsilon K+K_0\right)Q_{211} - 8\varepsilon K_0Q_{310} - 8K_0Q_{130} - I_1 - I_2\} \end{aligned} \tag{A.44}$$

$$\begin{aligned} G(1,0,1) &= \int S \exp ik \exp iq = \int S \cos k \cos q \\ &= \int S(1-\cos(k))(1-\cos(q)) - I_1 - I_3 \\ &= \{2(1+\varepsilon)I_1 Q_{101} + 4\varepsilon(5K_0+2K)Q_{201} + \\ &\quad 4(I_2+5K_0+2K)Q_{111} + 4\left(I_3+4K_0\right)Q_{102} - \\ &\quad 8K_0(1+\varepsilon)Q_{211} - 8\left(K+K_0\right)Q_{112} - \\ &\quad 8\left(\varepsilon K+K_0\right)Q_{202} - 8\varepsilon K_0 Q_{301} - \\ &\quad 8K_0 Q_{121} - I_1 - I_3\} \end{aligned} \tag{A.45}$$

$$\begin{aligned} G(0,1,1) &= \int S \exp ip \exp iq = \int S \cos p \cos q \\ &= \int S(1-\cos p)(1-\cos q) - I_2 - I_3 \\ &= \{2(1+\varepsilon)I_1 Q_{011} + 4\varepsilon(5K_0+2K)Q_{111} + \\ &\quad 4(I_2+5K_0+2K)Q_{021} + 4\left(I_3+4K_0\right)Q_{012} - \\ &\quad 8K_0(1+\varepsilon)Q_{121} - 8\left(K+K_0\right)Q_{022} - \\ &\quad 8\left(\varepsilon K+K_0\right)Q_{112} - 8\varepsilon K_0 Q_{211} - \\ &\quad 8K_0 Q_{031} - I_2 - I_3\} \end{aligned} \tag{A.46}$$

In conclusion, by knowing the I_1, I_2, I_3 and Q integrals, we can calculate the other correlation functions and solve for the energy currents.

A.5 Particle current

As mentioned in chapter two, we define the particle current as:

$$\begin{aligned} j(\sigma) &= \frac{1}{L^2}\left\{\sum_{\vec{r}} \frac{(1+\sigma_{\vec{r}})}{2}\frac{(1-\sigma_{\vec{r}+\vec{e}_x})}{2} c_{\parallel}(\vec{r},\vec{r}+\vec{e}_x) - \right. \\ &\quad \left. \sum_{\vec{r}} \frac{(1-\sigma_{\vec{r}})}{2}\frac{(1+\sigma_{\vec{r}+\vec{e}_x})}{2} c_{\parallel}(\vec{r},\vec{r}+\vec{e}_x)\right\} \end{aligned} \tag{A.47}$$

with

$$c_{\parallel}\left(\vec{r},\vec{r}+\vec{e}_x,\sigma\right) = \frac{1}{4}(\sigma_{\vec{r}} - \sigma_{\vec{r}+\vec{e}_x} + 2) + \frac{\varepsilon}{4}(\sigma_{\vec{r}+\vec{e}_x} - \sigma_{\vec{r}} + 2)\exp(-\beta\Delta H) \tag{A.48}$$

The first term is the contribution of the jumps along the field, the second one of the jumps against the field.
For *infinite* E only the first term remains, since the jumps against the field are prohibited and the exchange rates are:

$$c_{\parallel}^{\infty}(\vec{r},\vec{r}+\vec{e}_x,\sigma)=\frac{1}{4}(\sigma_{\vec{r}}-\sigma_{\vec{r}+\vec{e}_x}+2) \tag{A.49}$$

In this case, we have the following expression for the current:

$$\begin{aligned} j(\sigma) &= \frac{1}{L^2}\sum_{\vec{r}}\frac{(1+\sigma_{\vec{r}})}{2}\frac{(1-\sigma_{\vec{r}+\vec{e}_x})}{2}c_{\parallel}^{\infty}(\vec{r},\vec{r}+\vec{e}_x) \\ &= \frac{1}{L^2}\sum_{\vec{r}}\frac{(1+\sigma_{\vec{r}})}{2}\frac{(1-\sigma_{\vec{r}+\vec{e}_x})}{2}\frac{1}{4}(\sigma_{\vec{r}}-\sigma_{\vec{r}+\vec{e}_x}+2) \\ &= \frac{1}{16}\frac{1}{L^2}\sum_{\vec{r}}(1+\sigma_{\vec{r}})(1-\sigma_{\vec{r}+\vec{e}_x})(\sigma_{\vec{r}}-\sigma_{\vec{r}+\vec{e}_x}+2) \end{aligned} \tag{A.50}$$

Knowing that $\sigma_r^2=1$ we obtain for the current of a certain configuration :

$$j(\sigma)=\frac{1}{16}\frac{1}{L^2}\sum_{\vec{r}}(4-4\sigma_{\vec{r}}\sigma_{\vec{r}+\vec{e}_x}+4\sigma_{\vec{r}}-4\sigma_{\vec{r}+\vec{e}_x}) \tag{A.51}$$

After we take the average of this expression we are left with:

$$< j >= \frac{1}{4}[1-G(1,0,0)] \tag{A.52}$$

because

$$\begin{aligned} &< \sigma_{\vec{r}} >= 0 \\ &< \sigma_{\vec{r}+\vec{e}_x} >= 0 \end{aligned} \tag{A.53}$$

For *finite* E we consider also the jumps against the field, and we provide below a few

intermediary steps followed in finding the particle current:

$$\begin{aligned} j(\sigma) &= \frac{1}{L^2}\left\{\sum_{\vec{r}} \frac{(1+\sigma_{\vec{r}})}{2}\frac{(1-\sigma_{\vec{r}+\vec{e}_x})}{2} c_{\|}(\vec{r},\vec{r}+\vec{e}_x) - \right. \\ &\quad \left. \sum_{\vec{r}} \frac{(1-\sigma_{\vec{r}})}{2}\frac{(1+\sigma_{\vec{r}+\vec{e}_x})}{2} c_{\|}(\vec{r},\vec{r}+\vec{e}_x)\right\} \\ &= \frac{1}{L^2}\left\{\sum_{\vec{r}} \frac{(1+\sigma_{\vec{r}})}{2}\frac{(1-\sigma_{\vec{r}+\vec{e}_x})}{2}\left[\frac{1}{4}(\sigma_{\vec{r}} - \sigma_{\vec{r}+\vec{e}_x} + 2)\right]\right. \\ &\quad \left. - \sum_{\vec{r}} \frac{(1-\sigma_{\vec{r}})}{2}\frac{(1+\sigma_{\vec{r}+\vec{e}_x})}{2}\frac{\varepsilon}{4}(\sigma_{\vec{r}+\vec{e}_x} - \sigma_{\vec{r}} + 2)\exp(-\beta\Delta H)\right\} \\ &= \frac{1}{L^2}\left\{\sum_{\vec{r}} \frac{(1+\sigma_{\vec{r}})}{2}\frac{(1-\sigma_{\vec{r}+\vec{e}_x})}{2}\left[\frac{1}{4}(\sigma_{\vec{r}} - \sigma_{\vec{r}+\vec{e}_x} + 2)\right]\right. \\ &\quad \left. - \sum_{\vec{r}} \frac{(1-\sigma_{\vec{r}})}{2}\frac{(1+\sigma_{\vec{r}+\vec{e}_x})}{2}\frac{\varepsilon}{4}(\sigma_{\vec{r}+\vec{e}_x} - \sigma_{\vec{r}} + 2)(1+\beta c_2)\right\} \\ &= \frac{1}{L^2}\left\{\sum_{\vec{r}} \frac{(1+\sigma_{\vec{r}})}{2}\frac{(1-\sigma_{\vec{r}+\vec{e}_x})}{2}\left[\frac{1}{4}(\sigma_{\vec{r}} - \sigma_{\vec{r}+\vec{e}_x} + 2)\right]\right. \\ &\quad \left. - \sum_{\vec{r}} \frac{(1-\sigma_{\vec{r}})}{2}\frac{(1+\sigma_{\vec{r}+\vec{e}_x})}{2}\frac{\varepsilon}{4}(\sigma_{\vec{r}+\vec{e}_x} - \sigma_{\vec{r}} + 2)\right\} \\ &= \frac{1}{16}\frac{1}{L^2}(1-\varepsilon)\sum_{\vec{r}}(4 - 4\sigma_{\vec{r}}\sigma_{\vec{r}+\vec{e}_x} + 4\sigma_{\vec{r}} - 4\sigma_{\vec{r}+\vec{e}_x}) \end{aligned} \tag{A.54}$$

From the same considerations as for the infinite case, we get for the average current the following expression:

$$< j >= \frac{1}{4}(1-\varepsilon)\left[1 - G(1,0,0)\right] \tag{A.55}$$

Since $G(1,0,0) = -I_1$ the average current can be easily calculated.

$$\langle j \rangle = \frac{1}{4}(1-\varepsilon)[1 + I_1] \tag{A.56}$$

Appendix B

Sample Fortran code used in Monte Carlo simulations

```
cDRIVEN DIFFUSIVE SYSTEM WITH ANISOTROPIC JUMP RATES
implicit integer (i-n), real (a-h,o-z)
integer ns(20,20),lx,ly
real T,EE,st
real S(0:6,0:6),S1(0:6,0:6),RE(0:6,0:6),
& rep(0:39),SR(0:6,0:6),SR1(0:6,0:6),IMAG(0:6,0:6),
& imp(0:39),FLC(0:6,0:6),g(0:6,0:6),rep2(0:39),imp2(0:39)
COMMON/params/ iseed
COMMON/temp/T
COMMON/el/E
COMMON/NN/nr(20,20),nl(20,20),nu(20,20),nd(20,20)
open(23,file='SR20x20_gamma2_b.d')
open(25,file='g20x20_gamma2_b.d')
do T=0.8,1.6,0.025
```

```
lx=20
ly=20
iseed = -1657894
E=50
B=1./T
EE=1./2.269
nfr=200
NPL=200
A=lx*ly
kxmax=6
kymax=6
call RANL(ns,lx,ly)
do 20 ix=1,lx
do 10 iy=1,ly
ixp=ix+1
if (ix.eq.lx) ixp=1
ixm=ix-1
if (ix.eq.1) ixm=lx
iyp=iy+1
if (iy.eq.ly) iyp=1
iym=iy-1
if (iy.eq.1) iym=ly
nr(ix,iy)=ixp
nl(ix,iy)=ixm
```

```
nu(ix,iy)=iyp
nd(ix,iy)=iym
10 continue
20 continue
do kx=0,kxmax
do ky=0,kymax
SR(kx,ky)=0
SR1(kx,ky)=0
g(kx,ky)=0
FLC(kx,ky)=0
enddo
enddo
j=1
do i=1,1200000
if ((i.gt.150000).and.(MOD(i,nfr).eq.0)) then
call MEASURE(ns,lx,ly,S,S1)
do kx=0,kxmax
do ky=0,kymax
SR(kx,ky)=((S(kx,ky))+((j-1)*(SR(kx,ky))))/j
SR1(kx,ky)=((S1(kx,ky))+((j-1)*(SR1(kx,ky))))/j
FLC(kx,ky)=SR1(kx,ky)-((SR(kx,ky))**2)
g(kx,ky)=2-(SR1(kx,ky)/(SR(kx,ky)**2))
enddo
enddo
```

```
iv=j
j=j+1
else
call SIMUL(ns,lx,ly)
endif
enddo
write(23,*) T, SR(1,0)
write(25,*) T, g(1,0)
enddo
close(23)
close(25)
end
cSIMULATION SUBROUTINE
SUBROUTINE SIMUL(ns,lx,ly)
implicit integer (i-n), real (a-h,o-z)
integer ns(20,20), nx,ny,iex
real EE,p,q
COMMON/params/ iseed
COMMON/temp/T
COMMON/el/E
COMMON/NN/nr(20,20),nl(20,20),nu(20,20),nd(20,20)
lx=20
ly=20
A=lx*ly
```

```
B=1./T
EE=1./2.269
do 30 l=1,2*A
Jen=0
r1=ran2(iseed)
m=INT(r1*3*A)
m1=(m+3-MOD(m,3))/3
iy=int((m1-1)/lx)+1
ix=MOD(m1,lx)
if (MOD(m1,lx).eq.0) ix=lx
nx=ix
ny=iy
if (MOD(m,3).eq.0) then
nx=nr(ix,iy)
else
ny=nu(ix,iy)
endif
cccCheck the occupation
if(ns(ix,iy).eq.ns(nx,ny)) goto 30
if (MOD(m,3).eq.0) then
ixl=nl(ix,iy)
iyu=nu(ix,iy)
iyd=nd(ix,iy)
nxr=nr(nx,ny)
```

```
if (ns(ix,iy).eq.ns(ixl,iy)) then
Jen=Jen+1
else
Jen=Jen-1
endif
if (ns(ix,iy).eq.ns(ix,iyu)) then
Jen=Jen+1
else
Jen=Jen-1
endif
if (ns(ix,iy).eq.ns(ix,iyd)) then
Jen=Jen+1
else
Jen=Jen-1
endif
if (ns(nx,ny).eq.ns(nx,iyu)) then
Jen=Jen+1
else
Jen=Jen-1
endif
if (ns(nx,ny).eq.ns(nx,iyd)) then
Jen=Jen+1
else
Jen=Jen-1
```

```
endif
if (ns(nx,ny).eq.ns(nxr,ny)) then
Jen=Jen+1
else
Jen=Jen-1
endif
Dh1=(2*EE*Jen)
if (Dh1.gt.0) then
pr1=exp(-B*Dh1)
r2=ran2(iseed)
If (r2.lt.pr1) then
iex=ns(ix,iy)
ns(ix,iy)=ns(nx,ny)
ns(nx,ny)=iex
endif
else
iex=ns(ix,iy)
ns(ix,iy)=ns(nx,ny)
ns(nx,ny)=iex
endif
else
ixl=nl(ix,iy)
ixr=nr(ix,iy)
nyu=nu(nx,ny)
```

```
iyd=nd(ix,iy)
cccCalculate the bond energies
if (ns(ix,iy).eq.ns(ix,iyd)) then
Jen=Jen+1
else
Jen=Jen-1
endif
if (ns(ix,iy).eq.ns(ixl,iy)) then
Jen=Jen+1
else
Jen=Jen-1
endif
if (ns(ix,iy).eq.ns(ixr,iy)) then
Jen=Jen+1
else
Jen=Jen-1
endif
if (ns(nx,ny).eq.ns(ixl,ny)) then
Jen=Jen+1
else
Jen=Jen-1
endif
if (ns(nx,ny).eq.ns(ixr,ny)) then
Jen=Jen+1
```

```
else
Jen=Jen-1
endif
if (ns(nx,ny).eq.ns(nx,nyu)) then
Jen=Jen+1
else
Jen=Jen-1
endif
Dh2=(2*EE*Jen)-ns(ix,iy)*E
if (Dh2.gt.0) then
pr2=exp(-B*Dh2)
r3=ran2(iseed)
If (r3.lt.pr2) then
iex=ns(ix,iy)
ns(ix,iy)=ns(nx,ny)
ns(nx,ny)=iex
endif
else
iex=ns(ix,iy)
ns(ix,iy)=ns(nx,ny)
ns(nx,ny)=iex
endif
endif
30 continue
```

```
return
end
cMEASURE ORDER PARAMETER
SUBROUTINE MEASURE(ns,lx,ly,S,S1)
implicit integer (i-n), real (a-h,o-z)
integer ns(20,20), nx, ny, iex
real EE,p,q
real S(0:6,0:6),S1(0:6,0:6),RE(0:6,0:6),
& rep(0:39),SR(0:6,0:6),SR1(0:6,0:6),IMAG(0:6,0:6),
& imp(0:39),FLC(0:6,0:6),rep2(0:39),imp2(0:39)
COMMON/params/ iseed
COMMON/temp/T
COMMON/el/E
COMMON/NN/ nr(20,20),nl(20,20),nu(20,20),nd(20,20)
lx=20
ly=20
A=lx*ly
B=1./T
EE=1./2.269
kxmax=6
kymax=6
do 30 l=1,2*A
Jen=0
r1=ran2(iseed)
```

```
m=INT(r1*3*A)
m1=(m+3-MOD(m,3))/3
iy=int((m1-1)/lx)+1
ix=MOD(m1,lx)
if (MOD(m1,lx).eq.0) ix=lx
nx=ix
ny=iy
if (MOD(m,3).eq.0) then
nx=nr(ix,iy)
else
ny=nu(ix,iy)
endif
cccCheck the occupation
if(ns(ix,iy).eq.ns(nx,ny)) goto 30
if (MOD(m,3).eq.0) then
ixl=nl(ix,iy)
iyu=nu(ix,iy)
iyd=nd(ix,iy)
nxr=nr(nx,ny)
if (ns(ix,iy).eq.ns(ixl,iy)) then
Jen=Jen+1
else
Jen=Jen-1
endif
```

```
if (ns(ix,iy).eq.ns(ix,iyu)) then
Jen=Jen+1
else
Jen=Jen-1
endif
if (ns(ix,iy).eq.ns(ix,iyd)) then
Jen=Jen+1
else
Jen=Jen-1
endif
if (ns(nx,ny).eq.ns(nx,iyu)) then
Jen=Jen+1
else
Jen=Jen-1
endif
if (ns(nx,ny).eq.ns(nx,iyd)) then
Jen=Jen+1
else
Jen=Jen-1
endif
if (ns(nx,ny).eq.ns(nxr,ny)) then
Jen=Jen+1
else
Jen=Jen-1
```

```
endif
Dh1=(2*EE*Jen)
if (Dh1.gt.0) then
pr1=exp(-B*Dh1)
r2=ran2(iseed)
If (r2.lt.pr1) then
iex=ns(ix,iy) ns(ix,iy)=ns(nx,ny)
ns(nx,ny)=iex
endif
else
iex=ns(ix,iy)
ns(ix,iy)=ns(nx,ny)
ns(nx,ny)=iex
endif
else
ixl=nl(ix,iy)
ixr=nr(ix,iy)
nyu=nu(nx,ny)
iyd=nd(ix,iy)
cccCalculate the bond energies
if (ns(ix,iy).eq.ns(ix,iyd)) then
Jen=Jen+1
else
Jen=Jen-1
```

```
endif
if (ns(ix,iy).eq.ns(ixl,iy)) then
Jen=Jen+1
else
Jen=Jen-1
endif
if (ns(ix,iy).eq.ns(ixr,iy)) then
Jen=Jen+1
else
Jen=Jen-1
endif
if (ns(nx,ny).eq.ns(ixl,ny)) then
Jen=Jen+1
else
Jen=Jen-1
endif
if (ns(nx,ny).eq.ns(ixr,ny)) then
Jen=Jen+1
else
Jen=Jen-1
endif
if (ns(nx,ny).eq.ns(nx,nyu)) then
Jen=Jen+1
else
```

```
Jen=Jen-1
endif
Dh2=(2*EE*Jen)-ns(ix,iy)*E
if (Dh2.gt.0) then
pr2=exp(-B*Dh2)
r3=ran2(iseed)
If (r3.lt.pr2) then
iex=ns(ix,iy)
ns(ix,iy)=ns(nx,ny)
ns(nx,ny)=iex
endif
else
iex=ns(ix,iy) ns(ix,iy)=ns(nx,ny)
ns(nx,ny)=iex
endif
endif
30 continue
pi=ACOS(-1.0)
edx=(pi*2.0)/lx
edy=(pi*2.0)/ly
do k1=0,(lx-1)
rep(k1)=cos(edx*k1)
imp(k1)=sin(edx*k1)
enddo
```

```
do k2=0,(ly-1)
rep2(k2)=cos(edy*k2)
imp2(k2)=sin(edy*k2)
enddo
do kx=0,kxmax
do ky=0,kymax
RE(kx,ky)=0
IMAG(kx,ky)=0
S(kx,ky)=0
enddo
enddo
do kx=0,kxmax
do ky=0,kymax
do ix=1,lx
do iy=1,ly
ik1=kx*ix
ik2=ky*iy
k1=ik1-(INT(ik1/lx)*lx)
k2=ik2-(INT(ik2/ly)*ly)
RE(kx,ky)=(rep(k1)*rep2(k2)-imp(k1)*imp2(k2))*ns(ix,iy)
& +RE(kx,ky) IMAG(kx,ky)=(rep(k1)*imp2(k2)+imp(k1)*rep2(k2))*ns(ix,iy)
& +IMAG(kx,ky)
enddo
enddo
```

```
S(kx,ky)=(((RE(kx,ky))**2.0)+((IMAG(kx,ky))**2.0))/A
S1(kx,ky)=((S(kx,ky))**2)
enddo
enddo
return
end
cRANDOM INITIAL CONFIGURATION
SUBROUTINE RANL(ns,lx,ly)
implicit integer (i-n), real (a-h,o-z)
integer ns(20,20)
COMMON/params/ iseed
NCPL=0
NPL=200
lx=20
ly=20 do j=1,lx
do k=1,ly ns(j,k)=-1
enddo
enddo
30 r1=ran2(iseed)
ix=INT(r1*lx)+1
r2=ran2(iseed) iy=INT(r2*ly)+1
if (ns(ix,iy).EQ.-1) then
ns(ix,iy)=1
NCPL=NCPL+1
```

```
endif
if (NPL.Gt.NCPL) goto 30
return
end
cRANDOM NUMBER GENERATOR
Function ran2(idum)
integer idum,IM1,IM2,IMM1,IA1,IA2,IQ1,IQ2,IR1,IR2,NTAB,NDIV
real ran2,AM,EPS,RNMX
parameter (IM1=2147483563,IM2=2147483399,AM=1.0/IM1,IMM1=IM1-1,
& IA1=40014,IA2=40692,IQ1=53668,IQ2=52774,IR1=12211,
& IR2=3791,NTAB=32,NDIV=1+IMM1/NTAB,EPS=1.2e-7,RNMX=1.0-EPS)
integer idum2,j,k,iv(NTAB),iy
save iv,iy,idum2
data idum2/123456789/, iv/NTAB*0/, iy/0/
If (idum .le. 0) then
idum = max(-idum,1)
idum2 = idum
Do j = NTAB+8, 1, -1
k = idum/IQ1
idum = IA1*(idum-k*IQ1)-k*IR1
if (idum.lt.0) idum = idum+IM1
if (j.le.NTAB) iv(j) = idum
End Do
iy = iv(1)
```

```
End If
k = idum/IQ1
idum = IA1*(idum-k*IQ1)-k*IR1
if (idum.lt.0) idum=idum+IM1
k = idum2/IQ2
idum2 = IA2*(idum2-k*IQ2)-k*IR2
if (idum2.lt.0) idum2=idum2+IM2
j = 1+iy/NDIV
iy = iv(j)-idum2
iv(j) = idum
if (iy.lt.1) iy=iy+IMM1
ran2 = min(AM*iy,RNMX)
return
End
```

Bibliography

[1] J. W. Gibbs *The Elementary Principles in Statistical Mechanics*, (Scribner, N.Y, 1902).

[2] L. Boltzmann *Lectures on Gas Theory*, english translation (Berkeley, California,1964).

[3] R. K. Pathria *Statistical Mechanics* 2nd ed (Butterworth-Heinemann, Oxford, 1996).

[4] D. Mukamel *Phase Transitions in Non-Equilibrium Systems*, Lecture notes of talks presented at the Nato School on Soft and Fragile Matter St. Andrews Scotland, July 1999.

[5] E. Ising *Z. Phys.* **31:**253 (1925).

[6] W. Lenz *Z. Phys.* **56:**778 (1929).

[7] S. Katz, J. L. Lebowitz and H. Spohn *Phys. Rev. B* **28**:1655 (1983); S. Katz, J. L. Lebowitz and H. Spohn *J. Stat. Phys.* **34**:497 (1984).

[8] M. B. Salamon *Physics of Superionic Conductors, Topics in Current Physics* Vol 15, Springer, Heidelberg (1979); *Fast Ionic Transport in Solids*, eds. J. B. Bates and G. C. Farrington (North Holland, N.Y., 1981).

[9] B. Schmittmann and R. K. P. Zia *Phase Transitions and Critical Phenomena* Vol 17, edited by C. Domb and J. L. Lebowitz (Academic, London, 1995).

[10] B. M. McCoy and T. T. Wu *The two dimensional Ising model (*Harvard Univ. Press, Cambridge, Mass., 1973).

[11] L. Onsager *Phys. Rev.* **65**:117 (1944).

[12] K. Kawasaki *Phys. Rev.* **148**:375 (1966).

[13] N. Metropolis, A. W. Rosenbluth, M. M. Rosenbluth, A. H. Teller and E. Teller *J. Chem. Phys.* **21**:1097 (1953).

[14] P. C. Hohenberg and B. I. Halperin *Rev. Mod. Phys.* **49**:435 (1977).

[15] R. K. P. Zia, L. B. Shaw, B. Schmittmann, and R. J. Astalos *Contrasts between Equilibrium and Non-equilibrium Steady states: Computer Aided Discoveries in Simple Lattice Gases*, Computer Physics Communications, Vol 127, No 1(May 2000).

[16] P. C. Martin, E. D. Siggia and H. H. Rose *Phys. Rev.* **A8**:423 (1973) ; H. K. Janssen, *Z. Phys.* **B23**:377 (1976); C. de Dominicis *J. Phys.* (Paris) Colloq. **37**:C247 (1976).

[17] H. K. Janssen and B. Schmittmann *Z.Phys* **B63**:517 (1986); *Z.Phys.* **B64**:503 (1986).

[18] K. -t. Leung and J. L. Cardy *J. Stat. Phys,* **44**:567 (1986) and **45**:1087 (Erratum).

[19] M. Q. Zhang, J. -S. Wang, J. L. Lebowitz, and J. L. Vallés *J.Stat.Phys.***52**:1461(1988).

[20] F. J. Alexander and G. L. Eyink *Phys. Rev.* **E57** : R6229 (1998).

[21] K. -t. Leung *Phys. Rev. Lett.* **66**:453 (1991) and *Int. J. Mod. Phys.* **C3**:367 (1992).

[22] K. -t. Leung , K. K. Mon, J. L. Vallés and R. K. P. Zia *Phys Rev Lett.* **61**:1744 (1988) and *Phys. Rev.* B **39:**9312 (1989).

[23] K. -t. Leung and R. K. P. Zia *J. Phys.*A **26:**L737 (1993).

[24] B. Schmittmann and R. K. P. Zia *Phys. Rev. Lett.* **66**: 357 (1991).

[25] H. van Beijeren and L. S. Schulman *Phys. Rev. Lett.* **53**:806 (1984).

[26] A. Achahbar, P.L. Garrido and J. Marro *Phys Lett.* A **172**:29 (1992).

[27] Z. Racz and R. K. P. Zia *Phys Rev. Lett. E*, **49**:139 (1994).

[28] K. Binder and D. W. Heermann *Monte Carlo Simulation in Statistical Physics* Springer, Berlin (1988); *Finite Size Scaling and Numerical Simulations of Statistical Physics*, ed. V. Privman (World Scientific, Singapore, 1990).

[29] C. Domb in *Phase Transitions and Critical Phenomena* Vol 3, edited by C. Domb and M. Green (Academic, London, 1972).

[30] C. C. Hill, R. K. P. Zia and B. Schmittmann *Phys.Rev. Lett* **77**:514 (1996).

[31] L. E. Ballentine *Physica* **30:**1231 (1964).

[32] K. Binder *Thin Solid Films* **20:**367 (1974).

[33] R. Merkel, E. Sackman and E. Evans *J Phys.* (Paris) **50**:1535 (1989).

[34] G. R. Carlow *Intercalation Channels in Staged Ag Intercalated* TiS_2. Ph.D Thesis, Simon Frasier University (1992).

[35] U. C. Täuber, B. Schmittmann, and R. K. P. Zia *J. Phys. A* **34:**L583 (2001).

[36] C. -P. Chng and J. -S. Wang *Unequal intra-layer coupling in a bilayer driven gas* (preprint).

[37] J. L. Vallés and J. Marro, *J.Stat.Phys.* **49**:89 (1987).

[38] P. L. Garrido, J. L. Lebowitz, C. Maes and H. Spohn *Phys Rev.* A **42**:1954 (1990).

[39] B. Schmittmann and R. K. P. Zia *J.Stat.Phys.* **91**:525 (1998).

[40] F. Spitzer *Adv. Math.* **5**:246, (1970).

[41] K. Hwang (1993) Unpublished.

[42] J. Krug, J. L. Lebowitz, H. Spohn and M. Q. Zhang *J. Stat. Phys.* **44**:535 (1986).

[43] J. Marro, J. L. Lebowitz, H. Spohn, M. H. Kalos *J. Stat. Phys.* **38**:725 (1985).

[44] B. Schmittmann, H. K. Janssen, U. C. Täuber, R. K. P. Zia, K. -t. Leung, J. L. Cardy *Phys. Rev. E* **61**:5977 (2000).

[45] K. Binder and J. -S. Wang *J. Stat. Phys.* **55**:87 (1989).

[46] J. -S. Wang *J. Stat. Phys.* **82**:1409 (1996).

[47] R. J. Glauber *J. Math. Phys.* **4**:294 (1963).

[48] F. Schmüser and B. Schmittmann *J. Phys. A***:** *Math. Gen***. 35:** 2569 (2002).

Vita

Personal data:

Date of Birth	January 11, 1973
Place of Birth	Iasi, Romania

Education:

B.S. Physics	Al. I. Cuza Univ., Iasi, Romania	1996
M.S. Physics	Virginia Tech	1998
Ph.D. Physics	Virginia Tech	2002

Experience:

Graduate Teaching Assistant	Virginia Tech	1997 - 2002